Investigating the effects of treatment in HIV disease models

by

Anden van der Berg

Thesis presented in partial fulfilment of the requirements for the degree of Master of Science (Biochemistry) in the Faculty of Science at Stellenbosch University

Supervisor: Dr. D. van Niekerk

Co-supervisor: Prof. J. L. Snoep

December 2021

Declaration

By submitting this thesis electronically, I declare that the entirety of the work contained therein is my own, original work, that I am the sole author thereof (save to the extent explicitly otherwise stated), that reproduction and publication thereof by Stellenbosch University will not infringe any third party rights and that I have not previously in its entirety or in part submitted it for obtaining any qualification.

Date: 2021/10/02 .....

Abstract

HIV/AIDS and disease response to antiretroviral (ARV) drugs are of major importance to the developing world, and the disease remains a burden on society, as viral replication still needs to be controlled continually in persons infected with HIV. The ever-increasing prevalence of drug-resistant viral strains and the latent reservoir which harbours dormant virus also remain barriers to a cure. To overcome these barriers, novel ways of treating the disease and new tools for effective and efficient drug development are required. The use of mathematical models of disease and drug treatment continues to grow and remains an essential tool in drug development and the search for a cure.

In this study, combined HIV disease-PKPD models are created and tested for their ability to simulate real world patient data. First, independent mathematical models of HIV disease dynamics and ARV pharmacology are reproduced from literature. The effect of patient variability on simulation results is tested using Monte Carlo simulations, in which parameters are varied within biologically relevant ranges. The HIV disease models are then linked to PK and PD models of the currently prescribed ARVs. Monte Carlo simulations are used to examine the effect that heterogeneity, model structure, and model assumptions have in the newly linked models. The viral load and $CD4^+$ T-cell count predictions made by the combined models are compared to clinical patient data from the Western Cape, South Africa. Analysis of the combined models show that model structure has to include latently infected cells and drug-resistant viral strains to be able to accurately predict the disease progression of HIV.

Models need to incorporate the mechanisms that affect disease outcome. In the context of HIV, this may include drug-resistant strains and the effect of long-lived latently infected cells. Model predictions can be improved by including these mechanisms which have an impact on disease outcome and by considering longitudinal patient datasets. Such continual improvements will aid in making models powerful diagnostic tools.

Samevatting

MIV/VIGS en siekterespons op antiretroviale medikasie is van uiterste belang vir die ontwikkelende wêreld; die virussiekte plaas druk op die samelewing aangesien virale replisering in 'n MIV-positiewe persoon deurlopend beheer moet word. Die immertoenemende algemeenheid van medikasiebestande virale stamme, sowel as die latente reservoir wat dormante virus huisves, bly steeds 'n hindernis vir genesing. Nuwe maniere om die virussiekte te behandel en nuwe instrumente vir die ontwikkeling van effektiewe en doeltreffende medikasie is broodnodig ten einde hierdie hindernisse te oorkom. Die gebruik van wiskundige modelle van siekteverloop en behandeling groei toenemend en bly 'n onontbeerlike instrument in die ontwikkeling van medikasie en soeke na 'n geneesmiddel.

Vir die doeleinde van hierdie studie is saamgestelde MIV PKPD-siektemodelle geskep en getoets vir hul vermoë om werklike pasiëntedata te simuleer. Eerstens is onafhanklike wiskundige modelle van MIV-siektedinamika en ARV-farmakologie uit vaklektuur geskep. Die invloed van pasiëntveranderlikheid op simulasies, waarin parameters binne biologiestoepaslike reikwydtes wissel, word deur Monte Carlo-simulering getoets. Die MIV-siektemodelle word dan aan PK- en PD-modelle van tansvoorgeskrewe ARVs gekoppel. Monte Carlo-simulering word gebruik om die invloed van heterogeniteit, modelstruktuur en modelaannames in die gekoppelde modelle te toets. Die gekombineerde modelle se virale lading- en $CD4^+$ T-seltelling-voorspellings word dan met kliniese pasiëntedata in die Wes-Kaap van Suid-Afrika vergelyk. Ontleding van die saamgestelde modelle toon dat modelstruktuur, latent-geïnfekteerde selle en medikasiebestande virusstamme moet insluit ten einde die siekteverloop van MIV presies te voorspel.

Modelle moet die meganismes wat siekte-uitkoms beïnvloed, bevat. In die geval van MIV kan dit medikasiebestande virusstamme en die invloed van langlewende latent-geïnfekteerde selle insluit. Modelvoorspellings kan verbeter word deur dié meganismes - wat 'n invloed op siekte-uitkoms het - sowel as longitudinale pasiëntdatastelle, in te sluit. Sulke deurlopende verbeteringe sal daartoe bydra om van modelle kragtige diagnostieke instrumente te maak.

Acknowledgements

Firstly, I would like to express my sincere gratitude to my supervisor, Dr. Dawie van Niekerk, for his support, encouragement and friendship throughout my time at university.

Thank you to my co-supervisor Prof Jacky Snoep and the whole Systems Biology lab at Stellenbosch University.

Thank you to Prof. M.F. Essop for access to the clinical data of the HAART to HEART study and his assistance with ethical approval.

Lastly, I want to thank my friends and family for always supporting and enabling me to achieve so much.

The financial assistance of the National Research Foundation (NRF) towards this research is hereby acknowledged. Opinions expressed and conclusions arrived at, are those of the author and are not necessarily to be attributed to the NRF.

Contents

List of Figures

List of Tables

Nomenclature

Abbreviations

ADME	Absorption Distribution Metabolism Excretion
AIDS	Acquired Immunodeficiency Syndrome
ARV	Antiretroviral
ART	Antiretroviral Therapy
cART	Combination Antiretroviral Therapy
CTL	Cytotoxic T Lymphocyte
DDIs	Drug-drug interactions
DNA	Deoxyribonucleic acid
HAART	Highly Active Antiretroviral Therapy
HIV	Human Immunodeficiency Virus
HIVDR	HIV drug resistance
IIV	Interindividual Variability
INSTI	Integrase strand transfer inhibitor
MC	Monte Carlo
NCA	Non-compartmental analysis
NNRTI	Non-nucleoside reverse transcriptase inhibitor

NRTI	Nucleoside reverse transcriptase inhibitor
ODE	Ordinary Differential Equation
ODEs	Ordinary Differential Equations
PCR	Polymerase Chain Reaction
PD	Pharmacodynamics
PI	Protease inhibitor
PK	Pharmacokinetics
PKPD	Pharmacokinetic-pharmacodynamic
RNA	Ribonucleic acid
RT	Reverse transcriptase

Model names

Rong1	HIV model by Rong et al. [1]
Kamboj1	HIV model by Kamboj et al. [2]
Wang1	HIV model by Wang et al. [3]
TDF	Tenofovir pharmacokinetic model by Duwal et al. [4]
DTG	Dolutegravir pharmacokinetic model by Duwal et al. [5]
LPV/r	Lopinavir/ritonavir pharmacokinetic model by Wang et al. [6]
FTC	Emtricitabine pharmacokinetic model by Valade et al. [7]

Chapter 1

General Introduction

Human Immunodeficiency Virus (HIV) was discovered more than 30 years ago and since then our ability to treat the disease has largely resulted in the effective suppression of viral replication [8]. HIV is no longer the death sentence it used to be. Current antiretroviral (ARV) drugs can maintain the viral load below detectable limits in patients if they follow the prescribed regimen [9]. Indeed, the 2019 UNAIDS report shows that the annual global number of new HIV infections continues to decline gradually [10]. The data shows that great progress has been made in Africa, where the reduction in new HIV infections in the eastern and southern regions between 2010 and 2018 was the strongest. However, new infections continue to take place and there are still 20.6 million people in eastern and southern Africa living with HIV who require continued ARV treatment. UNAIDS states that it is paramount that the drug treatment which persons living with HIV receive, is highly effective at suppressing viral replication and blocking the formation of new drug-resistant strains as part of the goal to end AIDS as a global public health threat.

Studying and understanding the dynamics of HIV infection is necessary for the creation of effective drugs that control viral replication in infected individuals and the spread of infection in populations. Mathematical models have helped researchers produce the highly effective ARVs that are being prescribed today. Mathematical models have been proven to be effective for the study of HIV and have increasingly been used to aid decision making in clinical medicine and public health [11, 12]. Models have been developed to describe various aspects of the disease, such as within-host infection and its epidemiology, as well as the effects of antiretroviral agents used for treatment. Modelling has been a valuable tool for fulfilling the demand for effective and efficient clinical trials by providing a system for integrating information gathered on new therapeutic agents [13]. Model simulations provide evidence that inform critical decision making regarding the

public health response to the HIV epidemic, optimise drug development, and enable clinicians to construct drug regimens which ensure maximum and durable suppression of HIV replication [14].

Nevertheless, several issues remain to be addressed. Firstly, the increasing emergence of drug resistance will lead to the current generation of ARVs becoming ineffective in controlling the spread of the virus. Secondly, finding a functional cure where a patient gains post-treatment control of the virus will lessen the burden on the public health system and also help further curb the spread of the virus. Lastly, the long-lived latently infected cells which harbour reservoirs of the virus remains a compelling possible target for a sterilising cure and eradicating the virus completely. Taking all of this into account, it is indisputable that there remains a clear need for continued research into HIV treatment and patient response.

Given the strengths and benefits of mathematical modelling and the existence of models that address various aspects of the disease in isolation, this study aims to answer the following research question: **Can combinations of existing HIV disease and ARV PKPD models give realistic predictions of drug response and treatment outcomes?**

The aim and objectives are as follows:

Aim: Construct combined PKPD-HIV models using independent models from literature and test their predictive ability against clinical data In this study, information from a variety of sources will be used to construct the models, including pharmacokinetic, clinical and biological studies.

Objectives:

1. Perform literature search for HIV, PK and PD models.
2. Code HIV, PK and PD models in Wolfram Mathematica [15].
3. Validate models against results in original publications.
4. Perform Monte Carlo simulations to quantify the effects of heterogeneity in individual models.
5. Combine models by linking HIV disease to PKPD models.

6. Perform Monte Carlo simulations on combined models to gauge the effect of heterogeneity on treatment response and outcomes.

7. Simulate clinical data using newly constructed combined models and compare.

A schematic summary of the research workflow is shown in Figure 1.1.

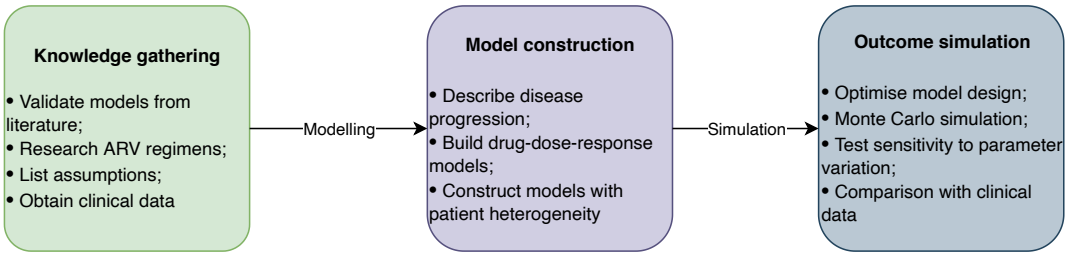

Figure 1.1: *Research work flow.* This figure provides a summary of the work flow during the research process. It can be divided into three simpler steps: knowledge gathering, model construction, and simulation of outcomes. Adapted from [16].

Chapter 2

Literature Review

This chapter provides information on the main research topics covered in this thesis, starting with the immune response to HIV infection and the establishment of the latent reservoir. The treatment and mathematical modelling of HIV infection is based on the basic building blocks of biology, and the understanding of that leads to greater insight of the pathogenesis of HIV. Subsequently the pharmacology of ARVs is discussed, covering how they interact with the body and how they are used to treat HIV infection. Relevant aspects of infectious disease modelling are then presented with specific focus on the mechanistic models used to simulate the viral dynamics of HIV disease progression. Lastly, pharmacological models of the drugs used to treat HIV infection are discussed, including how pharmacokinetic-pharmacodynamic models of ARVs are linked to HIV disease models to simulate drug therapy *in silico*.

2.1 HIV infection

The pathogenesis of disease caused by HIV is a complex problem of which all the stages are not yet fully understood [17]. The progression to acquired immunodeficiency syndrome (AIDS) happens as a result of the body's inability to control the viral replication cycle and subsequent destruction of the immune system's effector cells [18]. There are two viruses which are known to cause AIDS: HIV-1 and HIV-2 [19]. These two viruses have many shared characteristics, including the resulting clinical consequences of infection, but they are considered to originate from separate simian to human transmissions [20]. HIV-1 infections extend worldwide whereas HIV-2 remains largely confined to West Africa. Therefore, the research conducted here will pertain mainly to HIV-1.

The primary infection of cells take place at the site of infection in the blood and the mu-

cosal barrier. Within hours of HIV penetrating and infecting the mucosa, local amplification of initial founder viruses take place in a single focus of $CD4^+$ T cells [18]. It remains unclear why control of the virus eventually breaks down [21]. From the initial site of infection the virus is able to spread throughout the body to all lymphoid tissues [18]. A week later amplification in the draining lymph nodes is taking place and the infection is established in all lymphoid tissues, this includes the establishment of the HIV reservoir. The infection has now spread throughout the body and the viral load reaches its peak. Two to four weeks after the initial infection the host enters the acute primary infection phase indicated in Figure 2.1 as their immune system temporarily tries to control the acute infection but cannot prevent the establishment of chronic infection of cells in lymphoid tissues [18]. The innate antiviral host defence mechanism pathway against acute viral infections is exploited by the virus for its own dissemination. This signalling-mediated pathway is hijacked by the virus, which is then able to suppress global protein biosynthesis of the host cells and rather support its own replication [22]. Roughly nine weeks later, the host enters the clinical latency phase. There is a lowered production rate of virus but a continued progressive loss of $CD4^+$ T cells in lymphoid tissues, resulting in the destruction of the architecture of the lymphoid tissues [18]. Eventually when the $CD4^+$ T cell count falls below 200 cells per mm^3, patients are diagnosed as having AIDS. At this point the host is susceptible to opportunistic infections which can be lethal due to an impaired immune response. The perpetual viral replication taking place within the host's cells therefore depletes the body of T-cells and leads to the destruction and exhaustion of the immune system as a whole.

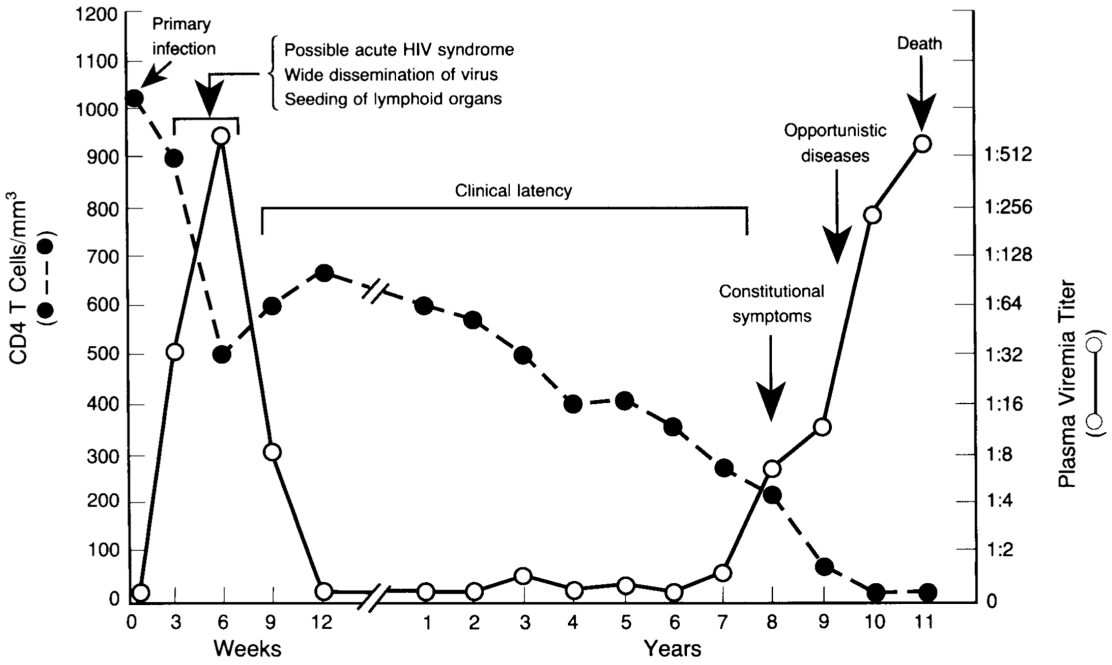

Figure 2.1: *Phases of HIV infection without treatment intervention.* During the primary infection phase, the T-cell count (black) decreases whilst there is a sharp increase in the viral load (white). If left untreated, during the latency phase the viral load steadily increases over a long period of time but eventually the virus overwhelms the immune system and the patient is diagnosed with AIDS. There is a gradual decline in T-cells during this time, leading to a compromised immune response and opportunistic diseases infecting the patient. Reproduced with permission from [23], Copyright Massachusetts Medical Society.

Viral load measurements are the standard for diagnosing and monitoring HIV diagnosis, as set out in the guidelines of the HIV Drug Resistance Report by the World Health Organisation [24]. Nucleic acid tests are the gold standard for viral load measurements, however these assays are not ideal for large-scale use due to their complexity, cost and duration to complete (8-10 h) [25]. Rather, RT-PCR (reverse transcriptase polymerase chain reaction) technologies have fulfilled the need for the increasing demand in viral load measurements. These technologies have proven to be robust, easier to use and many systems are fully automated. In South Africa, two often used systems include the Abbott m2000rt Real-Time HIV-1 assay (Abbott Molecular Inc., Germany) and GeneXpert®HIV-1 Quant Assay (Cepheid Innovations Pvt. Ltd., USA). Both have high sensitivity over the range of 50 to 10,000,000 copies/ml [25].

2.1.1 The viral replication cycle

The viral replication cycle of HIV can be divided into the following four sequential phases: (1) infection of cells; (2) production of viral DNA and its integration into the host genome; (3) expression of viral genes; and (4) production of viral particles [18] (see Figure 2.2).

(1) The first phase begins with the adhesion of virus to the host cell. The fusion and infection of a T-cell is dependent on an intricate series of protein-protein interactions that ultimately result in the delivery of the viral RNA. As detailed by Wilen et al. [26], the glycoprotein HIV Env attaches to the host cells, binding the CD4 cell receptor. HIV Env is comprised of the gp120 and gp41 subunits. The CD4 cell receptor normally functions to enhance T-cell receptor mediated signalling to other immune cells. The binding of Env and CD4 is absolutely required for virus entry into the host cell. The binding of Env causes a conformational change in the protein which allows for subsequent coreceptor binding. HIV strains can be broadly classified based on this coreceptor usage. The strains that use CXCR4 are classified as X4 HIV and those that use the CCR5 coreceptor are classified as R5 HIV [26]. After binding of the HIV envelope and host membrane, a fusion pore is formed and the virus is delivered into the host cell cytoplasm. Here the virus is uncoated by viral protease and its RNA is released along with the reverse transcriptase and integrase enzymes.

(2) This is followed by a process characteristic of all retroviruses: a viral enzyme called reverse transcriptase (RT) synthesises a DNA copy of the viral RNA [18]. The newly synthesised DNA can then move into the nucleus of the host cell, where another viral enzyme named integrase, integrates the viral DNA into the host cell's genomic DNA. The integrated viral DNA is now called a provirus.

(3) If an infected immune cell containing provirus is activated it responds by turning on the transcription of its own genes and subsequently it may also express the viral genes. Activation of the provirus results in the production of viral RNA and then biosynthesis of the viral proteins.

(4) From these proteins the assembly of the virion core structure can take place. The core structure migrates to the cell membrane where it acquires a lipid envelope from the host. Expression of the gp120 and gp41 glycoproteins take place on the cell surface from which mature viral particles can bud off, ready to infect another cell [18]. This viral replication

cycle results in the death of the infected cell when it bursts open, producing many virions, each capable of infecting nearby cells.

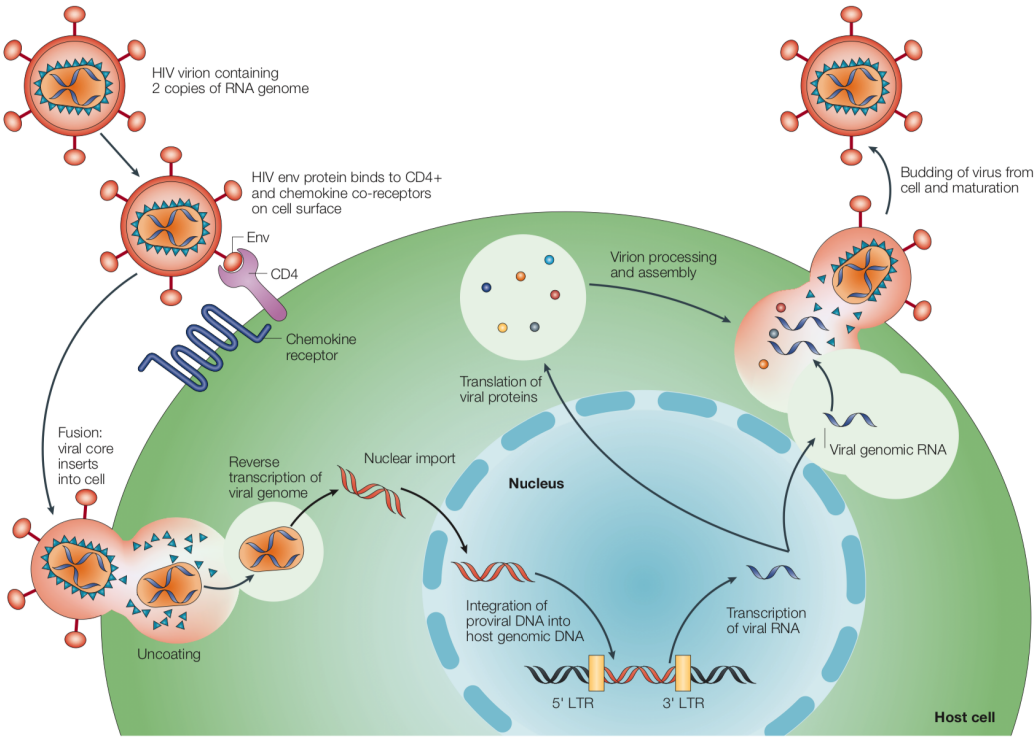

Figure 2.2: *The HIV life cycle is divided up in sequential phases.* Moving clockwise from the top left **(1) Infection of cells:** During this phase the virus infects the host cell by the binding of HIV Env to a CD4 receptor on the surface of the cell. This leads to the fusion of HIV to the cell and a pore is formed through which the virus is delivered into the cytoplasm. **(2) Production of viral DNA and its integration into the host genome:** RT synthesises a DNA copy of the viral RNA and integrase inserts this DNA into the nucleus. **(3) Expression of viral genes:** The activation and expression of these genes lead to the production of viral RNA and proteins required for assembly. **(4) Production of viral particles:** Viral particles are assembled and bud off from the cell membrane, ready to infect nearby cells. Image from [27] with copyright permission.

2.1.2 The mechanisms of CD4$^+$ T cell depletion

CD4$^+$ T-cell decline does not solely take place due to the death of infected cells. HIV-induced, bystander, CD4$^+$ T-cell killing is also recognised as central to immunodeficiency. Both infected and uninfected CD4$^+$ T-cells die during HIV infection by different cell-death pathways [28]. Some CD4$^+$ T-cell loss is due to direct destruction by the virus itself. The budding off of mature virions from the cell surface leads to disruption of the cell membrane. Furthermore, part of the innate immune response to viral infection is the killing of freshly infected cells through apoptosis [18]. However, a mechanism also exists in which apoptosis is resisted so that CD4$^+$ T-cells do not die directly after infection. This resistance of apoptosis promotes survival for long enough to ensure a productive infec-

tion and for the HIV reservoir to be established [28]. Further HIV-induced cytopathological effects result from the intracellular accumulation of viral RNA and unintegrated DNA [29]. This build up of viral DNA and RNA triggers cellular toxicity.

The depletion of $CD4^+$ T-cells also results in a defective immune response from cytotoxic T lymphocytes (CTL), even though HIV does not infect $CD8^+$ T-cells. This is likely because the $CD4^+$ helper T-cells are required for full $CD8^+$ CTL responses against many viral antigens [21]. Opportunistic infections thus often come from intracellular microbes, due to the impaired response from CTLs. The problem of the loss of control of viral replication remains complex. Wikramaratna et al. [21] further argue that the progressive loss of quality of $CD8^+$ T-cell responses is not the only cause of the breakdown of viral control. By taking into account the different lifespans of antibodies and $CD8^+$ T-cells, they created a framework for the infection dynamics of HIV which identify the cause as a loss of antibody induction [21]. This also comes as a consequence of the depletion of $CD4^+$ T-cells, due to the impaired helper T-cell dependent antibody responses to antigens.

2.1.3 The latent reservoir

A known remarkably stable major reservoir of latently infected cells is made up of resting-memory $CD4^+$ T-cells in which the proviral DNA is present but not actively expressed [30]. Latency occurs when a virus infects a $CD4^+$ T-cell but it does not progress beyond chromosomal integration of provirus [30]. Despite the efficacy of current cART in suppressing the viral replication of HIV, treatment must be continued for the lifetime of the patient. Furthermore, a timely diagnosis and initiation of cART before $CD4^+$ cell counts drop below 350 cells/μL is also crucial for achieving a normal level of $CD4^+$ T-cells [31]. If there is incomplete $CD4^+$ T-cell recovery the risk of both AIDS and non-AIDS related morbidity/mortality increases. In the vast majority of individuals if treatment is interrupted, it leads to the reestablishment of viremia and HIV disease progression [32]. Many studies have shown that this is due to the presence of a latent reservoir which remains during ARV therapy [30, 33–36].

There are indications that different tissue compartments contribute to this persistent viremia in patients receiving cART [37]. This led to the hypothesis that reseeding of viruses occurs from a reservoir which is established during the primary infection phase. A recent study [38] used ecological methods and existing data to show that the majority

of infected cells are members of clonal populations. By studying the genetic signatures of HIV persistence during cART, the study showed that identical HIV sequences in identical integration sites are carried by clonal populations of proliferating latently infected cells. This is in contrast to newly infected cells which are marked by novel HIV integration sites. Thus, the study by Reeves et al. [38] concludes that >99% of observed sequences originate from clonal cell populations. The survival mechanisms of the latent reservoir are thus ideal therapeutic targets for finding a functional or sterilising cure (see Figure 2.3).

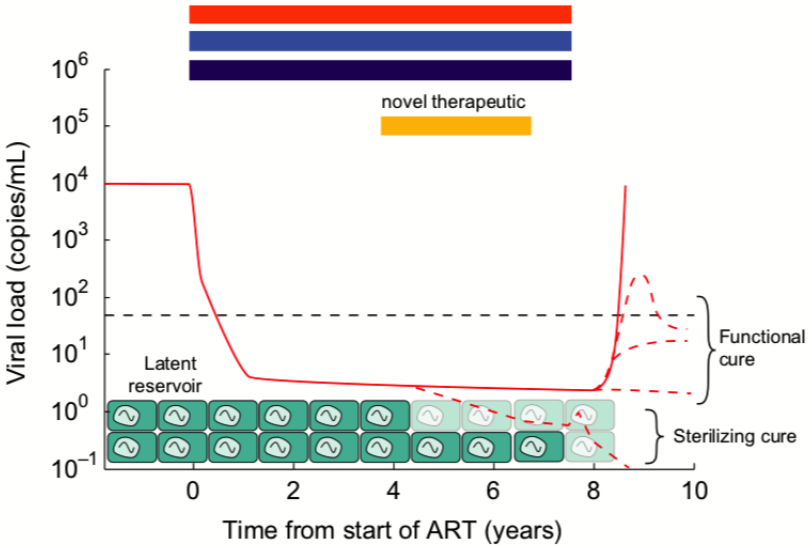

Figure 2.3: *The latent HIV reservoir and barriers to cure.* Combination ART (top red and blue bars) acts to effectively suppress viral replication over many years (solid red) to undetectable limits. However as seen at the bottom of the schematic, the latent HIV reservoir remains in place and if drug treatment is stopped the viral load rebounds (solid red). Only if a novel therapeutic, which targets this reservoir, is applied (yellow bar) could there be the possibility of cure scenarios (red dotted lines). A functional cure would mean that the patient's immune system becomes equipped to control infection without drug therapy. Image from [9] with copyright permission.

2.2 The pharmacology of ARVs

Understanding how ARVs work, what their mechanisms of action are and how they can be used to control viral replication is built on studying the basic HIV life cycle. Researchers have targeted key HIV enzymes and steps in this cycle to produce the highly effective medications used in HIV therapy. There are currently more than 30 antiretroviral medications available for the treatment of HIV [14], which interrupt the life cycle of HIV. These medications can target multiple specific points in this cycle [39]. There are different classes of medications used to treat HIV infection: fusion inhibitors, also referred to

as entry inhibitors; reverse transcriptase inhibitors; integrase strand transfer inhibitors; and protease inhibitors. Figure 2.4 shows where these classes of medication target the HIV life cycle. The emergence of drug resistance and ARV failure remains a major issue worldwide and continued research is necessary to develop new classes with different mechanisms of action to overcome these issues [40]. Current treatment guidelines by the Republic of South Africa's National Department of Health strongly recommend the use of triple-drug regimens comprising a combination of two reverse transcriptase inhibitors with either a protease inhibitor or an integrase strand transfer inhibitor [41]. This triple-drug regimen, also known as highly active antiretroviral therapy (HAART), is able to suppress the viral load to below 50 copies HIV-RNA/mL of blood. At this stage the patient is said to be undetectable as this is the detection limit using real-time RT-PCR [42]. The different classes and mechanisms of action will now be discussed.

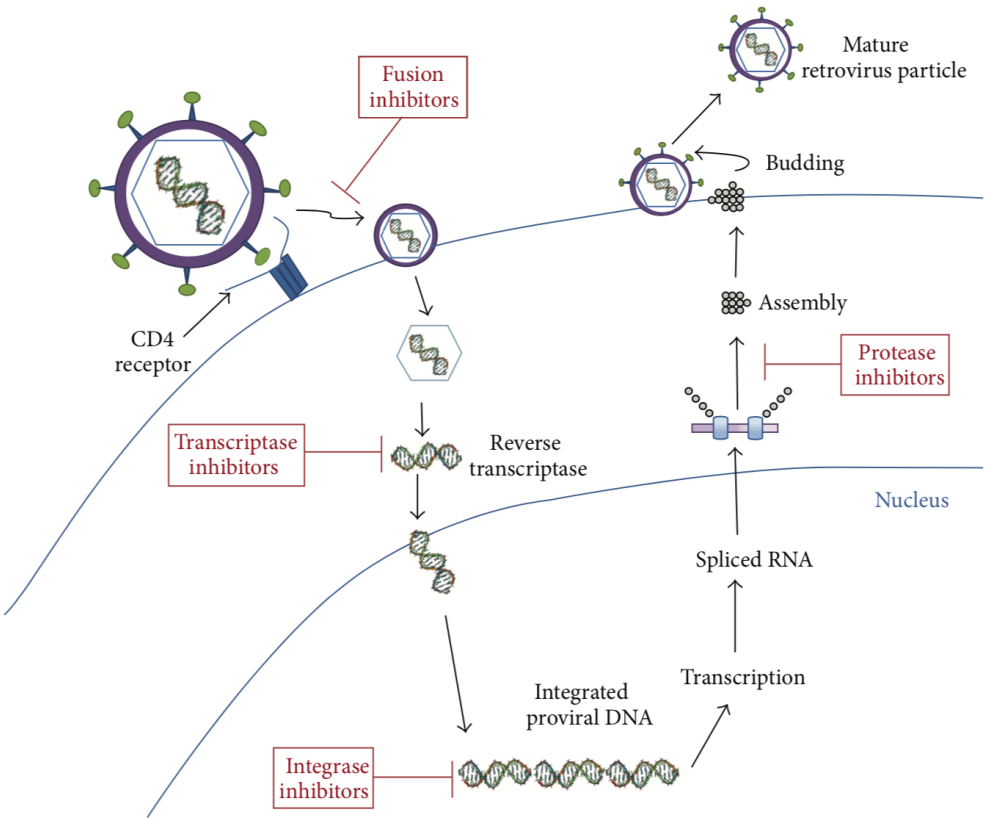

Figure 2.4: *ARV mechanisms of action.* Key enzymatic steps in the viral life cycle are targets for the inhibition of replication. The drug classes are shown in red boxes: fusion inhibitors; reverse transcriptase inhibitors; integrase inhibitors and protease inhibitors. Image from [43] with copyright permission (CC BY-ND 2.0).

HIV entry inhibitors HIV entry inhibitor drug molecules prevent the entry of HIV into the host's cells. This class of drugs is comprised of three subclasses, all of which have multiple mechanisms of action depending on the stage of the entry process at which they act [44]. These subclasses are: (1) CD4 attachment inhibitor, (2) CCR5 coreceptor antagonists, and (3) fusion inhibitors. **Attachment inhibitor:** This subclass is made up of compounds which prevent the entry of HIV by binding to the gp120 envelope protein of HIV. Upon binding to the protein on the surface of HIV, a conformational change of the protein is induced and stabilised which is not recognised by the CD4 receptor and therefore prevents the binding of the virus to the CD4 cell [40]. **CCR5 coreceptor antagonists:** CCR5 antagonists bind to the CCR5 coreceptor on the cell surface that are used by the virus to gain access to the cell. When CCR5 antagonists bind to the coreceptor, they cause a conformational change that prevents the normal interaction of HIV gp120 with the coreceptor and thus prevents HIV entry and fusion [45]. **Fusion inhibitor:** Following coreceptor binding, the HIV gp41 fusion peptide is inserted into the host membrane. HIV gp41 contains two heptad repeat regions named HR1 and HR2 which fold back on each other in the normal fusion process. A fusion pore is created when the host and viral membranes are brought into close proximity due to the interaction of the HR1 and HR2 domains of the gp41 fusion peptide [44]. The fusion inhibitor is a synthetic peptide with a sequence identical to part of the HR2 region. This inhibitor binds to the HR1 region, preventing the normal interaction of the fusion process.

Reverse transcriptase inhibitors The reverse transcriptase inhibitors function by interrupting the normal function of the RT enzyme which is responsible for the critical conversion of viral RNA to DNA. RT inhibitors can be further divided into two classes of medications: the nucleoside RT inhibitors (NRTIs) and the non-nucleoside RT inhibitors (NNRTIs) [46]. NRTIs and NNRTIs have two different mechanisms of action. The NRTIs act as host nucleotide decoys which cause termination of the elongating HIV DNA chain. They compete with human nucleotides for a spot in the elongating DNA chain but because they do not have a 3'-hydroxyl group, additional nucleotides cannot be linked and the chain is terminated. On the other hand, NNRTIs directly impede the function of the RT enzyme by binding in the active site of the enzyme. Upon binding in this pocket region, the molecule alters the active site by causing a conformational change in the enzyme and in doing so, blocks the process of the DNA polymerisation [46].

Integrase strand transfer inhibitors (INSTIs) Retroviruses must integrate their DNA, which was formed by the RT enzyme, into the host's DNA for them to be successfully replicated. The HIV enzyme integrase is responsible for performing two of the key catalytic reactions. This includes 3' processing of the HIV DNA and strand transfer of the HIV DNA into the host DNA [47]. There are many potential steps in the integration process which can be targeted by medications. Currently available medications utilise multiple mechanisms to interrupt the integrase strand transfer step. INSTI medications function by blocking the virus from integrating its DNA into the host cells' genomes. The drug molecules inhibit this step by binding in the active site of HIV integrase after the enzyme has attached to the viral DNA. This displaces the DNA and interrupts the integration process [47].

Protease inhibitors (PIs) HIV protein processing is also targeted by ARV medications. HIV protease plays a key role in the post-transcriptional processing of some viral polyproteins by acting as molecular scissors. A sequential sequence of polyprotein cleavage events results in the release of mature infectious particles [48]. It was this fundamental role of the protease enzyme in the release of infectious particles which made it an ideal target for therapeutic intervention. PIs are molecules that bind in the active site and inhibit the enzymatic function of HIV protease. This causes the arrest of the normal maturation process by inhibiting post-transcriptional processing [48].

Currently at least 3 ARVs must typically be provided to promote treatment effectiveness and help prevent the development of drug resistance. In the South African market currently available as the first-line of treatment includes two NRTIs, emtricitabine and tenofovir, with one integrase inhibitor, dolutegravir or efavirenz. If therapy fails a patient may be switched to the second-line regimen which includes the two NRTIs, emtricitabine and tenofovir, with one protease inhibitor, lopinavir or atazanavir. Switching to the PI-based regimen includes testing for drug resistance before a final decision can be made on switching. These are according to the ART clinical guidelines published by the Republic of South Africa National Department of Health for the management of HIV [41].

2.2.1 The mechanisms of the currently prescribed ARVs

Tenofovir Tenofovir disoproxil fumerate (TDF) is an antiretroviral drug, belonging to the class of nucleoside reverse transcriptase inhibitors (NRTIs) used for the treatment of

HIV-1 and hepatitis B [4]. After first pass of TDF through the liver, tenofovir (TFV), an analogue of the endogenous deoxyadenosine monophosphate (dAMP) is formed. Upon enzymatic uptake into HIV target cells, TFV becomes sequentially phosphorylated by a phosphodiesterase to form tenofovir diphosphate (TFV-DP). The active form, TFV-DP, is an analog of endogenous deoxyadenosine triphosphate (dATP) [49]. TFV-DP subsequently competes with endogenous dATP in the cell for incorporation into nascent viral DNA during reverse transcription. It prevents further DNA polymerisation during reverse transcription, once it becomes incorporated. TFV-DP thus prevents the production of proviral DNA, which is required for stable host cell infection and viral replication.

Emtricitabine Emtricitabine is also a drug in the class of NRTIs used for the treatment of HIV-1. Emtricitabine is phosphorylated by intracellular kinases to its active metabolite, emtricitabine 5'-triphosphate, which inhibits the activity of HIV reverse transcriptase by competing with the endogenous substrate for incorporation into the HIV DNA chain [50]. Emtricitabine 5'-triphosphate lacks a hydroxyl group in the 3' position of the sugar moiety and its incorporation into the HIV DNA chain results in chain termination.

Dolutegravir For replications, retroviruses must integrate the linear, double-stranded HIV DNA formed by reverse transcription into the host DNA. This integration event is a multistep process and the HIV enzyme integrase performs the key catalytic reactions [47]. Dolutegravir inhibits this HIV DNA integration process by blocking the integrase strand transfer step and thus forms part of the INSTI class of ARVs [5]. DTG inhibits the integrase enzyme through the binding of oxygen atoms on the drug molecule to divalent metal ions in the active site of the enzyme which results in no formation of integrated proviral DNA [51].

Lopinavir/ritonavir Lopinavir is a PI which was originally developed from, and is structurally related to, ritonavir [52]. The two drugs have the same mechanism of action for inhibiting the HIV protease enzyme. Within the highly potent molecule, a hydroxyethylene bond makes the drug a nonhydrolysable substrate for HIV protease. This stops the production of mature, infectious viral particles by inhibiting the post-translational processing of viral polyprotein products into functional core proteins and viral enzymes [52]. Lopinavir has an approximately tenfold higher *in vitro* activity against HIV proteases than ritonavir, however, its *in vivo* activity is greatly attenuated by a high first-

pass hepatic metabolism. The low-dose ritonavir coadministered with lopinavir inhibits metabolic inactivation of lopinavir and acts only as an enhancer [6].

2.2.2 The metabolism of ARVs

Pharmacokinetics (PK) is the study of the time course of the absorption, distribution, metabolism and excretion (ADME) of a drug after its administration to the body [53]. PK describes the movement of a compound within the body after their administration, whereas the pharmacodynamics (PD) is the study of the relationship between the concentration of a compound at its site of action and the magnitude of the response [53]. Without the knowledge of a drug's PK properties, its *in vivo* properties cannot be fully described. Shortcomings in the understanding of a compound's PK properties can lead to confusion in data interpretation and result in experimental outcomes that are invalid. As Hodgson has noted [54] – "A chemical cannot be a drug, no matter how active nor how specific its action, unless it is also taken appropriately into the body (absorption), distributed to the right parts of the body, metabolised in a way that does not instantly remove its activity, and eliminated in a suitable manner – a compound must get in, move about, hang around, and then get out."

The ADME of a compound are the four fundamental processes which influence its *in vivo* PK properties. They are distinct but also interrelated processes which occur between the administration and elimination of a compound from the body [53]. Firstly, a drug can be absorbed across the intestinal lumen in the gastrointestinal tract following the oral administration of a drug. Otherwise, a drug can also be injected intravenously where arterial circulation will distribute the compound to the various tissues and organs. Secondly, the extent of the distribution of a compound in the body due to systemic circulation will have an effect on the concentration of the drug in the blood or plasma. Distribution is often defined in terms of the volume of distribution and is influenced by factors such as blood flow, solubility, the size of the compound and its extent of plasma protein and tissue binding. Thirdly, the drug is metabolised, mainly by the liver but other extrahepatic tissues may also play a significant role. Metabolic reactions may first have to convert the inactive drug into its active form before it can then illicit its effect. Lastly, the compound is eliminated from the body through two major excretory routes: renal and biliary excretion [53].

2.3 The modelling of infectious diseases

Mathematical models of infectious diseases have been shown to be effective and useful tools in understanding the mechanisms governing host-pathogen interaction [55]. Mathematical models are often used to integrate information gathered on new therapeutic agents with information from models of disease progression [13]. Model results can then be used to inform clinical and public health decision making. Disease progression models, together with biological data, can also provide researchers with valuable information regarding the dynamics of the immune response to a disease. This ranges from chronic infections, with pathogens such as HIV [1, 2, 56], hepatitis B [57], hepatitis C [57, 58] and tuberculosis [59]; to acute infections such as influenza [60], dengue [61] and malaria [62].

Important biological parameters, such as the in-host basic reproduction number (R_0), can easily be quantified with the numerical investigation and data fitting of in-host models [55]. R_0 is the number of secondary infections which one infection would produce in a completely susceptible population [63]. In the case of HIV within-host/disease models, it specifically measures how many cells a single infected cell will infect when there is no target cell limitation [64]. Many other important biological parameters such as the pathogen and infected cell half-lives and the daily pathogen production values can be uncovered [55]. These parameters are usually estimated indirectly by fitting mathematical models to viral load data since they can rarely be determined directly [65]. Disease outcome predictions can also be made since the strength of the immune response and the efficacy of different drug therapies can be estimated. Due to the fact that model parameters are often estimates obtained from viral load data, certain assumptions may have to be made in modelling the virus life cycle. Therefore, it is important that one remains aware of the limitations of what can be learnt by fitting mathematical models to infectious disease data and statistical techniques must be employed to express the uncertainty in the estimates obtained using any particular model.

Models are published with population mean parameter values. These wild-type models, which are unaltered from their published form, can therefore simulate one parameter set equating to one average individual in the population. To more accurately represent the natural variation present in populations, parameters can be varied within certain biologically relevant ranges. The variation in these parameters are implemented though

the use of built-in functions in Wolfram Mathematica [15]. Firstly, the parameter values are modelled by using a distribution function which represents a statistical distribution between a given minimum and maximum value. For simulations, parameter values are sampled from their associated statistical distributions of which the ranges were obtained from the original publications. This is done for all the varied parameters, allowing for numerous sets of parameters to be generated.

All infectious diseases models start off with including certain characteristics that are 'basic' to that specific disease's dynamics in the host. Firstly, for example, the population of infectious particles within the host's body. Secondly, the host cells that the pathogen infects. Thirdly, the time-scale of the infection of the host. Some pathogens have a short-lived, acute infection while others result in a long-lived, persistent (chronic) infection. Lastly, for this example of a basic model, it may include the mechanisms and dynamics of the life cycle of the pathogen. This would define how the pathogen is able to produce progeny. Interestingly, this type of 'basic' model can be applicable to many different types of pathogens and may only vary in a few respects. This basic model format remains similar for many pathogen types such as viruses, bacteria and parasites [55].

2.3.1 Viral dynamics models of HIV

One of the earliest HIV disease models was published by Perelson et al. [66]. Initial models describing viral dynamics within the host attempted to explain viral load measurements in patients chronically infected with HIV. Their pioneering work showed that a mathematical model could be used to simply explain quantitative features of HIV infection. Their simple model of chronic viral infection is a one-stage viral infection model as it includes a single stage of infected-cells in their scheme and describes the interaction of HIV with $CD4^+$ T-cells. It considers the following three populations: uninfected T-cells, actively infected T-cells and free virus, all of which are represented by the ordinary differential equations (ODE) below and shown in Figure 2.5. Uninfected T-cells (TU) are produced by the body at rate λ_{TU} and die at rate δ_{TU}. The TU target cells are infected by free viruses (V) with a reaction rate constant of β resulting in an infected T-cell population (T^*). These productively infected T-cells can then release new viruses with a rate constant N, which are either cleared with a rate constant CL or re-infect the uninfected target cells. The infected T-cells die at a constant rate, specified by δ_{T*}. The model is

mathematically specified by the following system of coupled ODEs:

$$\frac{d}{dt}TU = \lambda_{TU} \cdot TU(t) - \delta_{TU} \cdot TU(t) - \beta \cdot V(t) \cdot TU(t) \tag{2.3.1}$$

$$\frac{d}{dt}T^* = \beta \cdot V(t) \cdot TU(t) - \delta_{T^*} \cdot T^*(t) \tag{2.3.2}$$

$$\frac{d}{dt}V = N \cdot T^*(t) - CL \cdot V(t) - \beta \cdot V(t) \cdot TU(t) \tag{2.3.3}$$

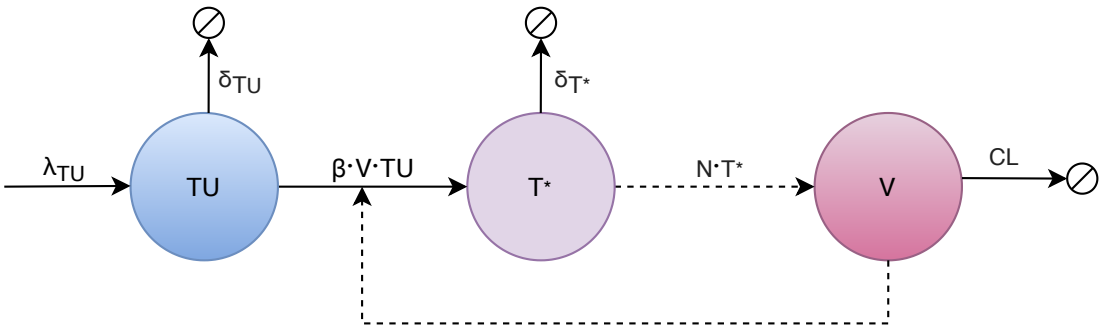

Figure 2.5: *Structure of a basic HIV model.* A schematic representation of the HIV model by Perelson et al. The three compartment model includes uninfected T-cells (TU), infected T-cells (T^*) and virus (V). Uninfected T-cells are born at rate λ_{TU} and become infected at rate β. Infected T-cells die at rate δ_{T*} and produce more virus with burst size N. Virus die at rate CL

Many within-host viral dynamic models consider a single infection stage during infection, i.e., the productively infected stage of cells that can produce virions. However, in reality the HIV life cycle consists of a number of processes and antiretroviral drugs have been developed to act at specific stages. Two-stage viral dynamics models revealed more details on how the nature of the different stages of the viral life cycle are inhibited due to the distinct mechanisms of action of different classes of ARV drugs [67]. This was prompted after puzzling discrepancies were noted between the *in silico* outcome of disease treatment in early one-stage models and the actual measured *in vivo* efficacy of drugs as assessed by viral load measurements [68]. Thus, two-stage models represent the infected target cells with two populations of T-cells: pre-RT infected T-cells and post-RT infected T-cells [3]. Additionally, over the two decades of progress made in the modelling of infectious diseases, more pools of target cells were added to HIV disease models. This includes the latent reservoir of infection, attributed to resting $CD4^+$ memory T-cells which explains further phases of viral decay [56]. Other populations of target cells often added to HIV disease models are those of macrophages and CTLs, which when

included can give further insight into the interaction between the virus and immune system. These cells are long-lived since they are less susceptible to viral cytopathic effects than are $CD4^+$ T-cells and may have an influence on the viral production rate [69].

2.3.2 Modelling drug action within disease models

As ARVs suppress the viral replication process by inhibiting the formation of new viral particles, similarly drug action is implemented in disease models. Continuing from the example HIV model described above, discussed below is how drug action effects are incorporated in this model through the introduction of drug effect parameters:

A **protease inhibitor** drug, which could block viral protease activity by 100% would result in no new viruses produced. In the model mentioned above, that would imply N = 0. However, drugs are not 100% effective in reality, in which case N would be altered by a factor (1 - η_{PI}) and 0.0 $\leq \eta_{PI} \leq$ 1.0, where η_{PI} is the PI drug efficacy. The equation representing the change in viral load over time would now be written as:

$$\frac{d}{dt}V = (1 - \eta_{PI}) \cdot N \cdot T^*(t) - CL \cdot V(t) - \beta \cdot V(t) \cdot TU(t) \tag{2.3.4}$$

Reverse transcriptase inhibitors block the enzymatic function of RT and prevents the synthesis of viral DNA from HIV RNA. Thus, RTIs can be assumed to reduce the viral infection rate β by a factor of (1 - η_{RTI}) and 0.0 $\leq \eta_{RTI} \leq$ 1.0, where η_{RTI} is the drug efficacy. Here, for example, the change of the infected and uninfected T-cell population over time would now be written as:

$$\frac{d}{dt}TU = \lambda_{TU} \cdot TU(t) - \delta_{TU} \cdot TU(t) - (1 - \eta_{RTI}) \cdot \beta \cdot V(t) \cdot TU(t) \tag{2.3.5}$$

$$\frac{d}{dt}T^* = (1 - \eta_{RTI}) \cdot \beta \cdot V(t) \cdot TU(t) - \delta_{T^*} \cdot T^*(t) \tag{2.3.6}$$

Integrase strand transfer inhibitors block integrase, the enzyme HIV uses to integrate the viral DNA produced by RT into the host cell. Two-stage HIV models have an additional parameter on which the reduction in viral reproductivity by an INSTI can be modelled [3]. The rate k_1 is the transition rate of infected cells from pre-RT (T_1) to post-RT (T_2) cells. In post-RT cells the viral DNA has been integrated into the host genome. Thus, we assume that the transition rate k_1 is reduced by a factor (1 - η_{INI}) in the presence of an INSTI due to the non-completion of the DNA integration step and the model

equations can be adapted as follows:

$$\frac{d}{dt}T_1 = \beta \cdot V(t) \cdot TU(t) - \delta_{T_1} \cdot T_1(t) - (1 - \eta_{INI}) \cdot k_1 \cdot T_1(t) \tag{2.3.7}$$

$$\frac{d}{dt}T_2 = (1 - \eta_{INI}) \cdot k_1 \cdot T_1(t) - \delta_{T_2} \cdot T_2(t) \tag{2.3.8}$$

$$T^* = T_1 + T_2 \tag{2.3.9}$$

Clearly, viral decay dynamics during antiretroviral drug therapy depend on the inhibited stages of the viral replication cycle [3]. Therefore, when researching the HIV disease models to be used in this study, models were chosen which allow for the meaningful implementation of each individual drug's effect on different stages of the viral life cycle.

2.4 Pharmacological modelling

The drug development process has been revolutionised through the use of mathematical modelling that construct, validate, and utilise disease models, drug dose-response models, and pharmacometric models to facilitate drug development [16]. Mathematical models provide a system for integrating all information gathered on new therapeutic agents [13]. Data from mathematical models provide evidence to enable critical decision making and to optimise drug development. In the context of HIV, for example, model-based drug development enables clinicians to produce drugs and drug regimens which enable maximum and lasting suppression of HIV replication [14], essential to controlling the spread of the disease, improving patients' lives and minimising drug side-effects.

The modelling of the PK of a drug alone does not provide a complete picture of drug action. The PK assessment of a drug is relevant only to the extent that drug concentration or exposure can be related to the drug actions of interest. Likewise, PD analysis of a drug has limited utility unless it can be related to the concentration over time and total exposure profile of the drug in the recipient [70]. As shown in Figure 2.6, a PD model can be linked to a PK model using drug concentration (C). Pharmacodynamics thus describes the relationship between the compound concentration at the site of action and the effect produced by the compound, including its time course and the intensity of therapeutic and adverse effects [70]. The incorporation of a PD model of a drug allows us to predict a measure of drug effect [13] and can be used study the effect of drug therapy on disease progression.

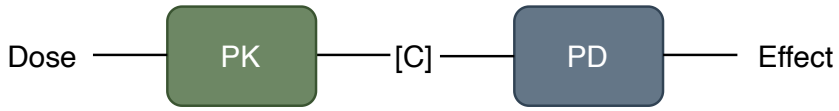

Figure 2.6: *Schematic representation of a basic linked PKPD model.* The dose-effect relationship can be illustrated using this representation of a linked pharmacokinetic (PK) and pharmacodynamic (PD) model. C = drug concentration.

A major goal of model-based drug development is the quantitative prediction of drug effects and the field of pharmacokinetic-pharmacodynamic (PKPD) modelling has made many advances in this regard [71]. The basic concept of the dose-response relationship has now been extended to complex mechanistic-based models. By combining the common feature which PK and PD models share, the drug concentration, it allows us to describe the overall dose-effect relationship. This provides a basis for understanding the time-course of drug exposure and the response after the administration of different doses or formulations [13]. In the context of HIV, linking the PKPD models of antiretroviral drugs to models of HIV disease progression allows us to then study the effect of drug therapy on variables such as the viral load and $CD4^+$ T cell counts.

2.4.1 Pharmacokinetic models

In clinical trials, the assessment of PK parameters happen through the use of PK models, which describe the relationship between drug concentration and time [13]. PK models make use of compartments that represent a group of tissues with similar rates of drug distribution, in which the drug is well mixed and kinetically homogenous. Compartmental models are fundamentally based on the four basic phases of drug pharmacokinetics as discussed above: absorption, distribution, metabolism and excretion. Complex physiological systems can be easily described with simple models using compartments, allowing for the ADME processes to be combined in a logical and straightforward manner [72]. Compartmental analyses are also useful for the characterisation of drug effect at the effect site in relation to the drug concentration. Non-compartmental analyses (NCA) are model-independent and do not rely upon assumptions about body compartments but rather relies almost exclusively on algebraic equations to estimate PK parameters, making them less complex, faster to use and more cost-efficient [72]. Deciding between NCA and compartmental analyses depends upon the purpose of the analysis as both provide different insights. Whereas NCAs are useful for analysing PK within a single study,

here we prefer to make use of more complex compartmental analyses as it allows for characterising PK across multiple studies and for exploring PK variability due to patient heterogeneity.

A major goal of pharmacokinetic modelling is gaining understanding of and resolving the factors determining drug access to target sites, known as biophase distribution [73]. When a drug is administered orally as an extravascular dose, it undergoes an absorptive phase prior to being taken into the plasma. Once in plasma, the drug is distributed to various organs and tissues and is then metabolised by an organ such as the liver or kidney. Finally, the drug is excreted in urine or faeces. Compartmental models assume that the body is made up of "compartments" through which the drug passes prior to being excreted. Each compartment forms part of a system of differential equations which are derived based on the law of conservation of mass [74]. By the law of conservation of mass, the change in the amount of drug versus time is equal to the sum of the contributing mass flow rates for each compartment. For example, a pharmacokinetic model with two compartments plus an oral dosing compartment is schematically shown in Figure 2.7:

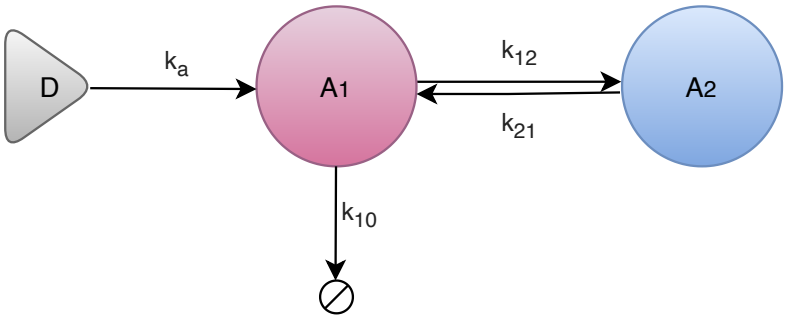

Figure 2.7: *The structure of a two-compartment pharmacokinetic model.* This example PK model makes use of two main compartments: A_1 could represent the amount of drug present in the central plasma compartment and A_2 represents the peripheral tissue compartment. D is the oral dosing compartment with k_a the absorption rate constant. Drug flows between the plasma and peripheral compartments with rate constants k_{12} and k_{21}. The drug is excreted from the blood plasma compartment at rate k_{10}

The model is represented by the following differential equations:

$$\frac{d}{dt}D = -k_a \cdot A_1(t) \tag{2.4.1}$$

$$\frac{d}{dt}A_1 = k_a \cdot A_1(t) + k_{21} \cdot A_2(t) - k_{12} \cdot A_2(t) - k_{10} \cdot A_2(t) \tag{2.4.2}$$

$$\frac{d}{dt}A_2 = k_{12} \cdot A_2(t) - k_{21} \cdot A_2(t) \tag{2.4.3}$$

where D represents the amount of drug present in the dosing compartment and k_a the absorption rate constant. A_1 represents the amount of drug present in the central plasma compartment and A_2 represents the poorly diffused peripheral tissue compartment. Here, drug flows between the plasma and peripheral compartments with rate constants k_{12} and k_{21}. The drug is excreted from the plasma compartment at rate k_{10}. The rate constants are defined according to the following parameters:

$$k_{12} = \frac{(Q/F)}{(Vc/F)} \tag{2.4.4}$$

$$k_{21} = \frac{(Q/F)}{(Vp/F)} \tag{2.4.5}$$

$$k_{10} = \frac{(CL/F)}{(Vc/F)} \tag{2.4.6}$$

with bioavailability-adjusted intercompartmental clearance (Q/F), central volume of distribution (Vc/F) and peripheral volume of distribution (Vp/F) and apparent elimination clearance (CL/F) all adjusted for bioavailability. Bioavailability is defined as the fraction of the active form of a drug that reaches systemic circulation unaltered. However, bioavailability is difficult to measure *in vivo*. PK equations are formulated so that it remains accounted for without the need to specifically calculate it. Under normal circumstances the bioavailability factor remains constant and does not change with dose [72]. Here the same assumption is made for all ARV models.

The parameters of a PK model are determined experimentally during clinical trails following well-defined protocols. The plasma drug concentrations are determined at various times after the dose has been administered to a group of individuals taking part in the clinical trail [72]. Several blood samples are drawn from each individual during this time, especially around the peak, to ensure that the drug-concentration profile is characterised adequately. The PK parameters are then determined for each individual through

analysis of the data generated during the trial. Each parameter can be averaged across the group to calculate the mean and standard deviation or be represented using a suitable probability distribution.

2.4.2 Pharmacodynamic models

In most pharmacodynamic scenarios, biophase distribution is extremely rapid and drug effects can be directly related to drug concentrations in plasma. For the modelling of drug pharmacodynamics, the variable of interest is the concentration of drug in the blood plasma compartment or the concentration of drug in the intracellular compartment. The direct action of a drug on the body is usually modelled using the E_{max} or sigmoidal E_{max} model and the concentration that produces 50% maximum response would be defined as EC_{50} [72]. For ARVs, of which the effect is the inhibition of viral replication, the effect is differentiated and categorised as inhibition (I) and thus we make use of the I_{max} model with IC_{50} being the concentration that results in 50% inhibition of viral replication. With a decrease in the value of IC_{50}, the potency of the drug increases [72]. The direct drug effect can be modelled over the whole range of concentrations using the I_{max} equation:

$$\epsilon_D(t) = \frac{D_t^m}{IC_{50}^m + D_t^m} \tag{2.4.7}$$

where ϵ_D(t) is the inhibition effect $0.0 \leq \epsilon_D \leq 1.0$ and D(t) is the target site concentration of the drug at time t. The term IC_{50} denotes the drug concentration at which the targeted process is inhibited by 50% and m denotes a Hill coefficient [75]. In the context of the viral dynamics model, the drug effect will be used to model how it inhibits the reproduction of viral particles. This can be achieved by linking its inhibition effect to certain parameters in the disease model such as the clearance of viral particles and the viral infection rate, as described in the subsection above for the viral dynamics of HIV models. To simulate combination therapy with two drugs from a single class, as in the case for HIV therapy, a pharmacodynamic model can be used which determines the net drug efficacy. The Bliss independence model [76] quantifies this net drug efficacy:

$$\epsilon_{D(a+b)}(t) = 1 - (1 - \epsilon_{Da}(t)) \cdot (1 - \epsilon_{Db}(t)) \tag{2.4.8}$$

where $\epsilon_{D(a+b)}$(t) is the new net drug efficacy with ϵ_{Da}(t) and ϵ_{Db}(t) being the efficacies of drug A and drug B respectively. The parameters of a PD model are determined through *in vitro* studies or the fitting of disease-PKPD models to patient data. With *in vitro* studies, whole cell lines are used and a range of concentrations of drug is applied [77]. This

generates a curve from which the inhibitory constant can be calculated. Determining the dose-response relationship of PD models are inherently more difficult due to the inability of measuring the drug concentration directly at the site of action. The processes associated with the PD phase of drug response are more varied and complex. They often include processes that need to be taken into account such as receptor binding, sensitivity and specificity of response and the efficacy of the response [72]. Figure 2.8 summarises the parameters which characterise the compartments in the PK and PD models presented, which is a progression from Figure 2.6 above.

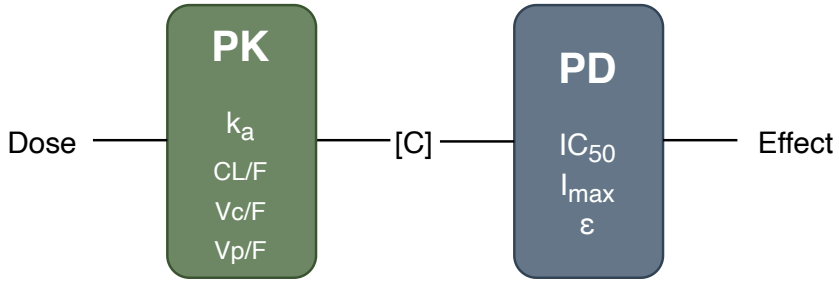

Figure 2.8: *Schematic representation of ARV PKPD model.* The dose-effect relationship can be illustrated using this representation of a linked pharmacokinetic (PK) and pharmacodynamic (PD) model. C = drug concentration. The PK model of each ARV are parameterised by k_a, CL/F, Vc/F and Vp/F, whereas the PD models are parameterised by IC_{50}, I_{max} and ϵ.

PK and PD models are usually published with population mean parameter values. These wild-type models therefore simulate one parameter set equating to one average individual in the population. Biological variation is present in all populations which affect the prognosis of infected individuals. Therefore it is necessary to consider this distribution in the parameter values to more accurately determine the effects of the population's biological variation. This variation is often referred to as patient heterogeneity and it is important to account for this in model simulations. To this end, parameters can be varied within relevant biologically ranges. by sampling their values from their associated probability distributions. Interindividual variability (IIV) is often characterised using a log-normal distribution and the mean and %CV (coefficient of variation) is reported where [4]

$$\%\text{CV} = 100\sqrt{e^{\sigma^2} - 1} \tag{2.4.9}$$

with σ^2 the variance of the associated normal distribution.

2.5 Previous studies using combined PKPD-HIV models

In a study by Jacqmin et al. [78], a combined model was used to demonstrate the derivation of a Reproduction Minimum Inhibitory Concentration (RMIC) of an antiretroviral compound. They used an E_{max} model to decrease the infection rate and to described the effect of antiretroviral compounds. This could also be used in a model in which two different classes of ARVs are administered which act on different stages of the viral life cycle, each having its own independent drug efficacy parameter [79].

The study by Wu et al. [80] parametrised a combined model using viral load data from a clinical trial of ARVs in HIV-infected individuals who had previously failed protease inhibitor–containing ARV therapies. They concluded that viral rebound may occur because of drug resistance, non-adherence and other factors. By combining PKPD and HIV models, a drug efficacy threshold can be calculated for each patient to assess whether an ARV regimen is potent enough to suppress HIV viruses in the individual. The combined models provide a framework to be able to inform decision-making on the individual level and to predict response to treatment for each patient.

Rosario et al. [81] employed a combined pharmacokinetic-pharmacodynamic disease model to predict the *in vivo* antiviral activity of a CCR5 receptor antagonist. The same author extended the work by including receptor theory in the combined PKPD-disease model to determine whether quantifying receptor occupancy by the antiviral compound could help to better predict the *in vivo* efficacy of the drug [82].

The review by Hill et al. [9] shows that basic viral dynamic models can be adapted and combined with a drug dose-response model to assess the effect treatment has on viral infection. It is demonstrated how an inhibitory model can be used to calculate a drug efficacy factor of the drug concentration relative to the IC_{50} value. The inhibitory sigmoidal E_{max} model is widely used, effective and simple to implement in an HIV disease model as will also be shown in the present study.

In the following chapter each model will be described, along with the variation in certain parameters. Models of HIV disease progression will be discussed as well as PKPD models of ARVs. The chapter will also show how the combined PKPD-HIV models are constructed by linking PKPD models to the HIV disease models. In contrast to previous

work where models are often singular PK/PD/HIV models or limited combinations, and are parametrised on singular cohorts in well controlled clinical trials, we start by considering models from independent studies focusing on disease or pharmacology. We then create linked PKPD-disease models from all combinations that are relevant for the South African context. We also do not refit parameters but evaluate the models' predictive abilities by varying the previously determined parameters within their known ranges.

Chapter 3

Constructing the combined HIV-pharmacokinetic-pharmacodynamic models

The mathematical models that were reproduced are described in this chapter. Models were reproduced using Wolfram Mathematica v 12 [15]. The models will first be described as originally published, whereafter it will be discussed how each model was adapted for linking to PKPD models of the ARVs. First to be described will be **Kamboj1**, then **Wang1** and lastly the most complex model which includes the evolution of drug resistance, **Rong1**. These three models with differing levels of complexity in terms of the variable types they include, were chosen based on their specific characteristics to cover important aspects of infection: **Kamboj1** provides a basic overview of infection; **Wang1** goes one step further and provides insight into the effect that latency has on disease outcome; lastly, **Rong1** adds the effect that drug-resistance has on treatment efficacy. These models were chosen as they help to understand the two barriers to a cure stated in Chapter 1: the latent reservoir and drug-resistance. Further motivation will be given for why each model was chosen as they are discussed below.

3.1 Models of HIV infection and treatment

3.1.1 Multidrug therapy for HIV infection: Dynamics of immune system model by Kamboj, D. & Sharma, M.D. [2]

This model [2] allows for the studying of the effect of inhibition on specific steps in the viral life cycle, which plays an important role in the study of HIV. This two-stage model

describes the *in vivo* efficacy of RTI and PI treatment assessed by viral load measurements. The model and parameter values are well substantiated and drawn from authors whose work in the field are often referenced, such as Perelson et al. [83]. However this model also improves on the work done by Perelson et al. by including a compartment for the effect of CTLs. T-cells are identified as uninfected $CD4^+$ (T), pre-RT infected (T_1) and post-RT infected (T_2) cells. The viral load is represented by V and the response of the immune cell population of CTLs is represented by E. The logistic expression rT(1-$\frac{T}{T_{max}}$) accounts for those T-cells in the process of growth of the T-cell population that are maintained as T-cells in the presence of infection. ARV drug efficacy is modelled with ϵ_{RT} and ϵ_{PI} representing the ARV efficacy of reverse transcriptase inhibitors and protease inhibitors respectively. These two parameters inhibit the viral replication capacity with a factor ranging from 0-1. The reverting rate of infected to uninfected cell due to non-completion of reverse transcription is defined by bT_1. The mathematical model is defined by the following system of five ODEs:

$$\frac{d}{dt}T = s - \mu T(t) + rT(t)(1 - \frac{T(t)}{T_{max}}) - kV(t)T(t) + bT_1(t) + \epsilon_{RT}\alpha T_1 \tag{3.1.1}$$

$$\frac{d}{dt}T_1 = kV(t)T(t) - \mu_1 T_1(t) - \alpha T_1(t) - bT_1(t) \tag{3.1.2}$$

$$\frac{d}{dt}T_2 = (1 - \epsilon_{RT})\alpha T_1(t) - \delta T_2(t) - d_x E(t)T_2(t) \tag{3.1.3}$$

$$\frac{d}{dt}V = (1 - \epsilon_{PI})\delta N T_2(t) - \mu_v V(t) \tag{3.1.4}$$

$$\frac{d}{dt}E = pT_2(t) - d_E E(t) \tag{3.1.5}$$

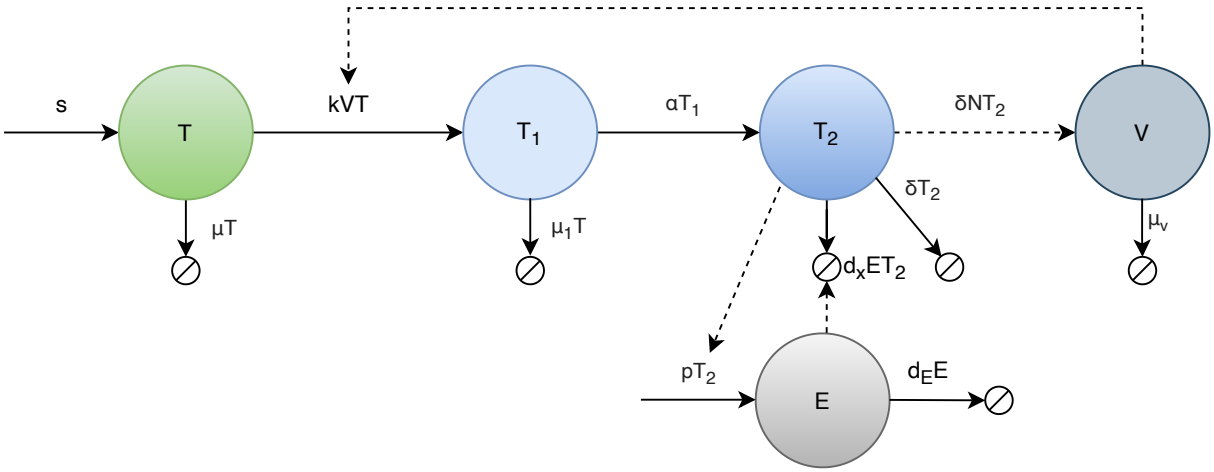

Figure 3.1: *Schematic diagram of Kamboj HIV model.* T = uninfected T-cells; T_1 = pre-RT infected T-cells; T_2 = post-RT infected T-cells; V = virus; E = CTLs.

Figure 3.1 above shows a schema representing the model compartments and model parameters are defined in Table 3.1. At the onset of infection, all the infected cells will form part of the pre-RT class (T_1). A fraction ($\alpha\, T_1$) of these cells leaves the pre-RT class to join the productively infected post-RT class (T_2). The presence of a RT inhibitor is assumed to revert a fraction of the pre-RT cells ($\epsilon_{RT}\alpha T_1$) back to the uninfected class, where $0.0 \leq \epsilon_{RT} \leq 1.0$ and ϵ_{RT} is the drug efficacy. The remaining cells in the pre-RT class (1 - ϵ_{RT})αT_1 become productively infected and proceeds on to become T_2 cells. Furthermore, combination therapy with a protease inhibitor results in a decreased number of viral particles being produced (1- ϵ_{PI}) N, where $0.0 \leq \epsilon_{PI} \leq 1.0$ and ϵ_{PI} is the drug efficacy. The immune response of CTLs present in the body is incorporated in the model by including its attack on post-RT cells. Due to the nature of the immune system, pre-RT cells which do not express HIV cannot illicit a response by CTLs, therefore, the intensity of the response only depends on the concentration of T_2 cells. The full list of fixed and varied parameters for the kamboj1 model can be found in Table 3.1.

Table 3.1: Parameter values for HIV disease model by Kamboj et al.

Parameter	Definition	Value	Unit	Parameter variation	Distribution	Reference
s	Rate at which new T-cells are created	10	$mm^{-3}day^{-1}$	4.2-13.8	Uniform	[83]
k	Rate constant for $CD4^+$ cells becoming infected	0.000024	mm^3day^{-1}	$1.2x10^{-5}$-$3.6x10^{-5}$	Uniform	[83]
Nv	Average number of viral particles produced by an infected cell	1000	-	400-1200	Uniform	[83]
T_{max}	Maximum $CD4^+$ cell population level	1500	mm^{-3}	-	-	[83]
β	Reverting rate of infected cells to uninfected class due to the non-completion of reverse transcription	0.05	day^{-1}	-	-	[2]
α	Transition rate from pre-RT class to post-RT infected class	0.4	day^{-1}	-	-	[2]
δ	Death rate of productively infected cells (T_2)	0.24	day^{-1}	-	-	[83]
r	Rate of growth for the $CD4^+$ cell population	0.03	day^{-1}	-	-	[83]
μ	Death rate of uninfected cells	0.01	day^{-1}	0.005-0.016	Triangular	[2]
μ_1	Death rate of infected cells	0.015	day^{-1}	-	-	[2]
μ_v	Clearance rate of virus	2.4	day^{-1}	0.91-3.6	Triangular	[83]
p	Proliferation rate of CTLs	1.02	day^{-1}	0.05-3.0	Uniform	[2]
d_x	Rate of clearance of infected cells (T_2) by CTLs	0.01	$mm^3\ day^{-1}$	0.005-0.1	Uniform	[2]
d_E	Death rate of CTLs	0.1	day^{-1}	-	-	[2]
ϵ_{RT}	Efficacy of RT inhibitor	0 - 1	-	-	-	See text
ϵ_{PI}	Efficacy of protease inhibitor	0 - 1	-	-	-	See text

3.1.2 Modelling the slow CD4$^+$ T-cell decline in HIV-infected individuals by Wang et al. [56]

The authors of this paper state that they developed the model to study the time scale of long term CD4$^+$ T-cell decline during HIV infection. This model expands on previous models such as Perelson et al. [83] by including latently infected cells and CD8$^+$ T-cells. It also includes the effect that cytokines have on inflammation and disease progression. The one compartment model also includes the CD8$^+$ T-cell response to the decline in CD4$^+$ T-cells, as this response plays a major role in the immune dynamics of HIV infection [56]. Uninfected CD4$^+$ T-cells are represented by the variable (T) and are generated at the rate λ. Inflammatory cytokines (C) enhance the infection rate adding to the population of productively infected T-cells (T*). T-cells can also be abortively infected (M*), however virus (V) is only produced by productively infected T-cells (T*). In the original publication, by including the effect of drug treatment the viral infection rate (k) is reduced by a factor $(1-\epsilon)$ where ϵ is the overall drug efficacy of the treatment. CD8$^+$ T-cells (E) are modelled to kill infected T-cells at a rate αET*. Latently infected T-cells (L) are produced with a fraction (μ) during HIV-1 infection. The adaptive immune response by CD8$^+$ T-cells depends on the level of infected cells and CD4$^+$ T-cells play an important role in the activation the adaptive immune response. This influence by CD4$^+$ and CD8$^+$ T-cells is accounted for using the saturation function $p_E(\frac{T^*}{T^*+\theta})(\frac{T}{T+\eta})$. Latently infected cells can also be maintained by proliferation which is assumed to rely on the cytokine level $(1+\phi$C). The carrying capacity of latently infected cells is maintained with $(1-\frac{L}{L_{max}})$. Certain parameters remain fixed during simulations and others are varied to represent the natural biological variation present in populations. The varied and constant parameters are defined in Table 3.2, Figure 3.2 is a schematic representation and the

model is defined by the following system of ODEs:

$$\frac{d}{dt}T = \lambda - (1-\epsilon)k(1+\gamma_i C(t))V(t)T(t) - d_1 T(t) \tag{3.1.6}$$

$$\begin{aligned}\frac{d}{dt}T^* &= (1-f)(1-\mu)(1-\epsilon)k(1+\gamma_i C(t))V(t)T(t) \\ &\quad - \alpha E(t)T^*(t) - d_2 T^*(t)\end{aligned} \tag{3.1.7}$$

$$\frac{d}{dt}M^* = f(1-\epsilon)k(1+\gamma_i C(t))V(t)T(t) - d_3 M^*(t) \tag{3.1.8}$$

$$\frac{d}{dt}V = p_v T^*(t) - d_4 V(t) \tag{3.1.9}$$

$$\frac{d}{dt}C = N_c d_3 M^*(t) - d_5 C(t) \tag{3.1.10}$$

$$\frac{d}{dt}E = p_E\left(\frac{T^*(t)}{T^*(t)+\theta}\right)\left(\frac{T(t)}{T(t)+\eta}\right) - d_E E(t) \tag{3.1.11}$$

$$\begin{aligned}\frac{d}{dt}L &= \mu(1-f)(1-\epsilon)k(1+\gamma_i C(t))V(t)T(t) \\ &\quad + p_L(1+\phi C(t))L(t)\left(1-\frac{L(t)}{L_{max}}\right) - d_L L(t)\end{aligned} \tag{3.1.12}$$

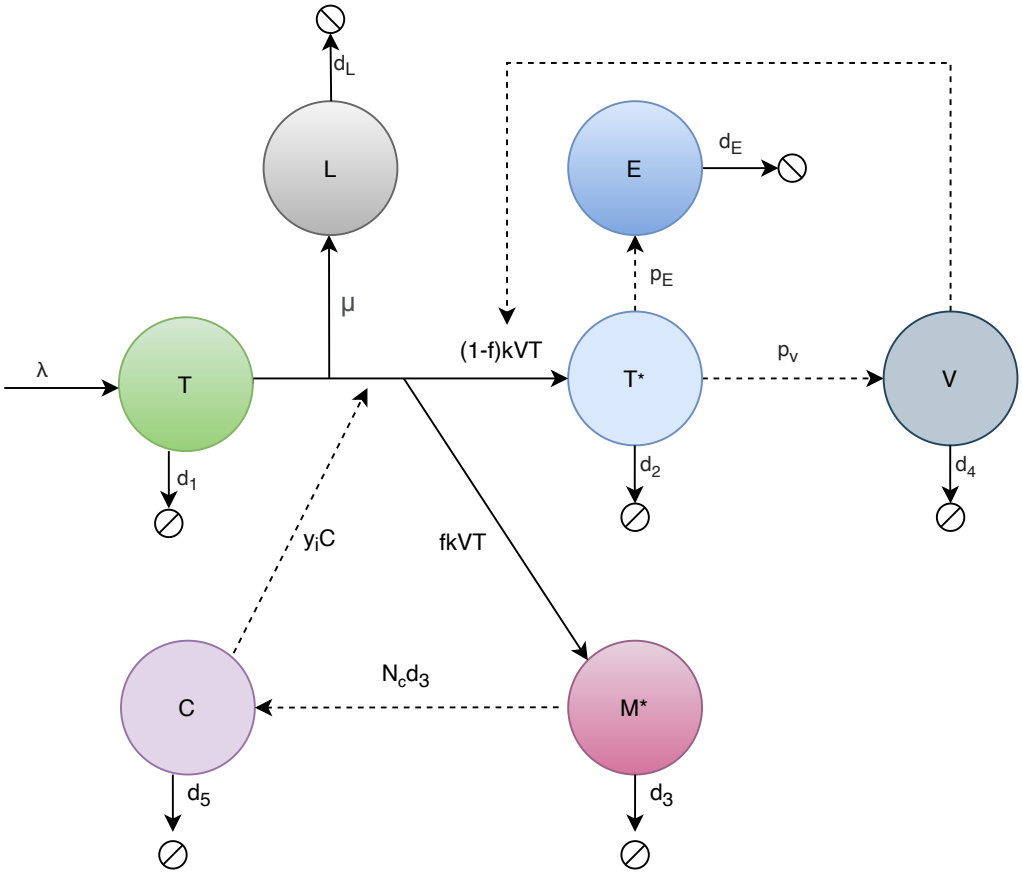

Figure 3.2: *Schematic diagram of Wang HIV model.* T = uninfected T-cells; T* = infected T-cells; V = virus; M* = abortively infected T-cells; C = inflammatory cytokines; E = $CD8^+$ T-cells; L = latently infected T-cells.

Table 3.2: Parameter values for the one-compartment HIV model by Wang et al.

Parameter	Definition	Value	Unit	Parameter variation	Distribution	Reference
λ	CD4+ T-cell generation rate	10^4	$ml^{-1}\ day^{-1}$	6000-14000	Uniform	[3]
k	Infection rate of target cells	$2.4x10^{-8}$	$ml\ day^{-1}$	$1.44x10^{-8}$-$3.36x10^{-8}$	Uniform	[3]
d_1	Death rate of uninfected $CD4^+$ T-cells	0.01	day^{-1}	-	-	[3]
d_2	Death rate of infected $CD4^+$ T-cells	1	day^{-1}	-	-	[3]
d_3	Death rate of abortively infected cells	0.001	day^{-1}	0.0006-0.0014	Uniform	[3]
d_4	Viral clearance rate	23	day^{-1}	-	-	[3]
d_5	Death rate of cytokines	6.6	day^{-1}	3.96-9.24	Uniform	[3]
y_i	Effectiveness of cytokines on infection	$2x10^{-4}$	$ml\ molecule^{-1}$	$1.2x10^{-4}$-$2.8x10^{-4}$	Uniform	[3]
f	Fraction of abortive infection	0.95	-	0.931-0.969	Uniform	[3]
p_v	Viral production rate	$2.5x10^4$	$virions\ cell^{-1}\ day^{-1}$	15 000-35 000	Uniform	[3]
N_c	Burst size of cytokines	15	molecule	9-21	Uniform	[3]
ρ	Hill coefficient in exponential function	$2x10^{-4}$	$ml\ molecule^{-1}$	-	-	[3]
α	Killing rate of $CD8^+$ T-cells	0.01	$ml\ cell^{-1}\ day^{-1}$	-	-	[3]
p_E	Max activation rate of $CD8^+$ T-cells	100	$cells\ ml^{-1}\ day^{-1}$	-	-	[3]
η	Effect of $CD4^+$ T-cells on $CD8^+$ activation	500	$cells\ ul^{-1}$	-	-	[3]
d_E	Death rate of $CD8^+$ T-cells	0.06	day^{-1}	-	-	[3]
μ	Fraction of latent infection	0.001	-	-	-	[3]
p_L	Proliferation rate of latently infected T-cells	0.001	day^{-1}	-	-	[3]
ϕ	Effect of cytokines on latent proliferation	10^{-2}	$ml\ molecule^{-1}$	0.006-0.014	Uniform	[3]
L_{max}	Carrying capacity of latently infected cells	100	$cells\ ml^{-1}$	-	-	[3]
d_L	Death rate of latently infected T-cells	0.001	day^{-1}	-	-	[3]
ϵ	Efficacy of combined drug therapy	0-1	-	-	-	See text

3.1.3 Emergence of HIV-1 drug resistance during antiretroviral treatment model by Rong et al. [1]

This model includes infection with two viral strains: wild-type and drug-resistant. It allows for a strain to mutate and become drug-resistant during the process of reverse transcription. The mutation rate (μ) from drug sensitive to resistant strain is based on the frequency of single point mutations. This then results in a level of resistance (α) that the drug resistant strain has toward the ARV efficacy ranging from 0-1. ARV drug efficacy is modelled with ϵ_{RT} and ϵ_{PI} representing the ARV efficacy of reverse transcriptase inhibitors and protease inhibitors respectively. These two parameters inhibit the viral replication capacity with a factor ranging from 0-1. In the model there are five variables defined in concentration: uninfected T-cells (T); productively infected by drug sensitive virus (T_{sen}); productively infected by drug resistant virus (T_{res}); V_{sen} and V_{res} represent the concentrations of drug sensitive and drug resistant virus respectively. The parameters are defined in Table 3.3, a schematic representation of the model is shown in Figure 3.3 and the model is described by the following system of ODEs:

$$\frac{d}{dt}T = \lambda - dT(t) - (1-\epsilon_{RT})k_s V_{sen}(t)T(t) - (1-\alpha\epsilon_{RT})k_r V_{res}(t)T(t) \tag{3.1.13}$$

$$\frac{d}{dt}T_{sen} = (1-\epsilon_{RT})(1-u)k_s V_{sen}(t)T(t) - \delta T_{sen}(t) \tag{3.1.14}$$

$$\frac{d}{dt}V_{sen} = (1-\epsilon_{PI})N_s \delta T_{sen}(t) - cV_{sen}(t) \tag{3.1.15}$$

$$\frac{d}{dt}T_{res} = (1-\epsilon_{RT})uk_s V_{sen}(t)T(t) + (1-\alpha\epsilon_{RT})k_r V_{res}(t)T(t) - \delta T_{res}(t) \tag{3.1.16}$$

$$\frac{d}{dt}V_{res} = (1-\alpha\epsilon_{PI})N_r \delta T_{res}(t) - cV_{res}(t) \tag{3.1.17}$$

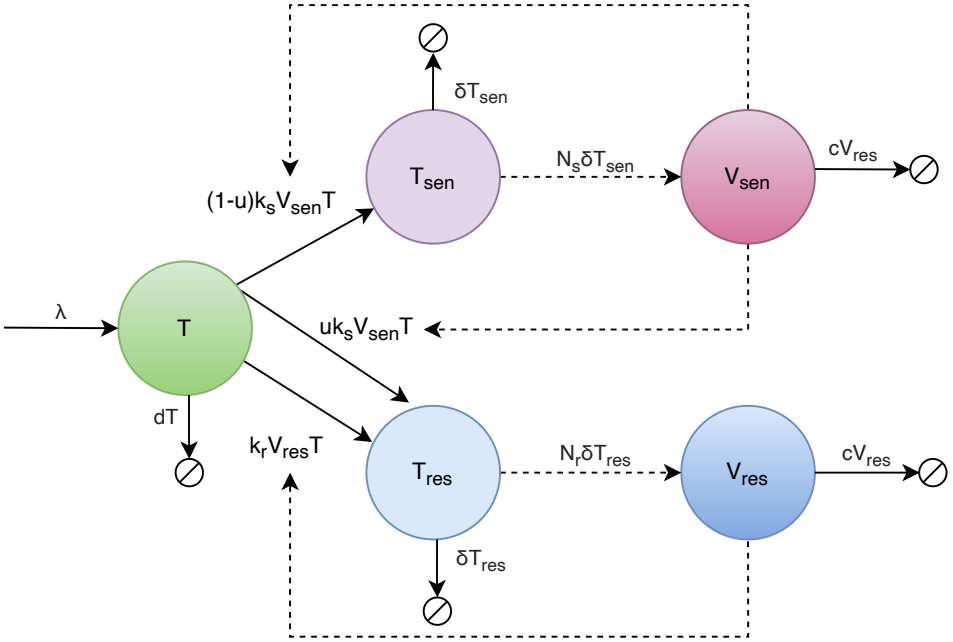

Figure 3.3: *Schematic diagram of Rong HIV model.* T = uninfected T-cells; T_{sen} = drug sensitive infected T-cells; T_{res} = drug resistant infected T-cells; V_{sen} = drug sensitive virus and V_{res} = drug resistant virus.

The model by Rong et al. [1] describes infection with two viral strains: wild-type and drug-resistant. During the process of reverse transcription, the model allows for the viral strain to mutate and become drug-resistant. It is this implementation of the evolution of drug resistance which sets this model apart from others, since it includes some complexity which may lead to more realistic model simulations and outcomes. A parameter that remains constant in the model is the mutation rate (u) as it is based on the frequency of single point mutations. The recruitment rate of uninfected T-cells (λ) also remains constant. However, the parameters with known variation include: the death rate of uninfected cells (d); infection rate of target cells by wild-type (k_s) and drug-resistant (k_r) strains; death rate of infected cells (δ); burst size of drug-sensitive (N_s) and drug-resistant (N_r) strains; and the clearance rate of free virus (c).

Table 3.3: Parameter values for HIV disease model by Rong et al.

Parameter	Definition	Value	Unit	Parameter variation	Distribution	Reference
λ	Recruitment rate of uninfected cells	10^4	ml^{-1} day^{-1}	-	-	[1]
d	Death rate of uninfected cells	0.01	day^{-1}	0.005-0.016	Triangular	[1]
k_s	Infection rate of target cells by wild-type virus	$2.4x10^{-8}$	ml day^{-1}	$1.2x10^{-8}$-$3.6x10^{-8}$	Uniform	[83]
k_r	Infection rate of target cells by drug-resistant virus	$2.0x10^{-8}$	ml day^{-1}	$0.8x10^{-8}$-$3.2x10^{-8}$	Uniform	[1]
μ	Mutation rate from sensitive strain to resistant strain	$3x10^{-5}$	-	-	-	[1]
δ	Death rate of infected cells	1	day^{-1}	0.5-1.4	Uniform	[1]
N_s	Burst size of drug-sensitive strain	3000	-	2000-4000	Uniform	[1]
N_r	Burst size of drug-resistant strain	2000	-	1000-3000	Uniform	[1]
c	Clearance rate of free virus	23	day^{-1}	9.1-36	Triangular	[1]
α	Resistance level of mutant strain	0-1	-	-	-	[1]
ϵ_{RT}	Efficacy of RT inhibitor	0-1	-	-	-	See text
ϵ_{PI}	Efficacy of protease inhibitor	0-1	-	-	-	See text

3.2 Pharmacokinetic models

Drug pharmacokinetics are important for ARV drug development and clinical therapy. Pharmacokinetics refers to the relationship between drug input (dose, dosing interval, dosage form, etc.) and the concentration attained in the body over time. In the context of HIV therapy, viral suppression is impacted by time-dependent changes in drug concentration. The research of the PK models presented here can be broadly divided into two stages. The first stage focuses on the selection of an appropriate structural model (e.g., two-compartment model with blood plasma and cellular compartments), which includes the implementation of a dose regimen. The second stage involves characterising the PK parameters of interest and their relationship to the subsequent modelling of drug efficacy in pharmacodynamics. The mathematical framework are presented for the models that enabled us to implement key PK characteristics related to the present-day drugs used for HIV treatment as defined by the 2019 ART clinical guidelines [41], published by the Republic of South Africa's National Department of Health and in the 2019 HIV treatment policy published by the World Health Organisation [24]. The current state of first-line ART has been revised to include a formulation of the daily fixed dose combination of two reverse transcriptase inhibitors (tenofovir disoproxil fumerate (TDF) + emtricitabine (FTC)) and one integrase inhibitor (dolutegravir (DTG)). However, when a patient receiving first-line regimen treatment experiences virological failure, they may be switched to second-line treatment. Virological failure can happen if the virus with which the patient is infected develops resistance during first-line treatment. Second-line treatment includes a combination of two RTIs (tenofovir disoproxil fumerate (TDF) + emtricitabine (FTC)) and one protease inhibitor which is a co-fomulation of lopinavir/ritonavir (LPV/r) twice daily.

3.2.1 Dolutegravir

A study by Duwal et al. [5] employed a two-compartment model with an oral dosing compartment. Their pharmacokinetic model is mathematically specified by a system of coupled ODEs and constitutes three compartments: $C_D(t)$ denotes the amount of drug in the dosing compartment, $C_p(t)$ is the concentration of DTG in the peripheral compartment and $C_c(t)$ is the concentration in our compartment of interest, the central blood plasma compartment, shown in Figure 3.4. Notably, DTG is active in its administered

form (does not require biotransformation) and has physicochemical attributes that allow the unbound drug to rapidly cross the cellular membrane [5]. Parameter values are defined in Table 3.4 and the model is described by the following system of coupled ODEs:

$$\frac{d}{dt}C_D = -k_a \cdot C_D(t) \tag{3.2.1}$$

$$\frac{d}{dt}C_c = \frac{k_a}{V_c} \cdot C_D(t) - \frac{CL}{V_c} \cdot C_c(t) - \frac{Q}{V_c} \cdot C_c(t) + \frac{Q}{V_p} \cdot C_p(t) \tag{3.2.2}$$

$$\frac{d}{dt}C_p = \frac{Q}{V_c} \cdot C_c(t) - \frac{Q}{V_p} \cdot C_p(t) \tag{3.2.3}$$

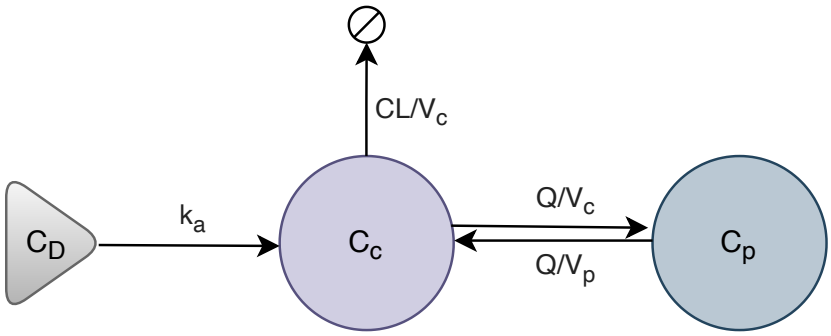

Figure 3.4: *Schematic diagram of Dolutegravir pharmacokinetic model.* C_D = dosing compartment; C_c = central blood plasma compartment; C_p = peripheral tissue compartment. Adapted from [5].

Table 3.4: Final pharmacokinetic parameter estimates of model for dolutegravir (DTG). Note that due to the fractions in the model equations above (also indicated in Figure 3.4) the unknown bioavailibility F disappears.

Parameter	Definition	Value	Unit	CV [%]	Distribution	Reference
k_a	Absorption rate constant	2.24	h^{-1}	-	-	[5]
CL/F	Apparent total clearance of the drug	0.85	liter·h^{-1}	16.9	Log normal	[5]
Vc/F	Apparent volume of central compartment	17.7	liter	16.4	Log normal	[5]
Vp/F	Apparent volume of peripheral compartment	0.73	liter	-	-	[5]
Q/F	Intercompartmental clearance	0.0082	liter·h^{-1}	-	-	[5]

3.2.2 Emtricitabine

The study by Valade et al. [7] aimed to describe blood plasma and seminal plasma pharmacokinetics of emtricitabine resulted in the development of a three-compartment model (plus a dosing compartment). Their final model also included an additional compartment which described the FTC concentration in the seminal plasma. However, for the purpose

of this study we were primarily interested in the central blood plasma compartment. The final pharmacokinetic model is mathematically specified by a system of coupled ODEs and thus constitutes four compartments: A_1 is the quantity of drug in the dosing compartment. A_2 is the quantity of drug in the central compartment, A_3 is the quantity of drug in the peripheral compartment and A_4 is the concentration of drug in the seminal compartment. The concentration of the drug can be calculated by dividing by the volume of the compartment e.g. A_4 is divided by Vc in this model. Parameter values are defined in Table 3.5, Figure 3.5 a schematic representation and the model is described by the following system of coupled ODEs:

$$\frac{d}{dt}A_1 = -k_a \cdot A_1(t) \tag{3.2.4}$$

$$\frac{d}{dt}A_2 = k_a \cdot A_1(t) + k_{21} \cdot A_3(t) - k_{12} \cdot A_2(t) - k_{10} \cdot A_2(t) \tag{3.2.5}$$

$$\frac{d}{dt}A_3 = k_{12} \cdot A_2(t) - k_{21} \cdot A_3(t) \tag{3.2.6}$$

$$\frac{d}{dt}A_4 = k_{1e} \cdot \frac{A_2(t)}{V_c} - k_{e1} \cdot A_4(t) \tag{3.2.7}$$

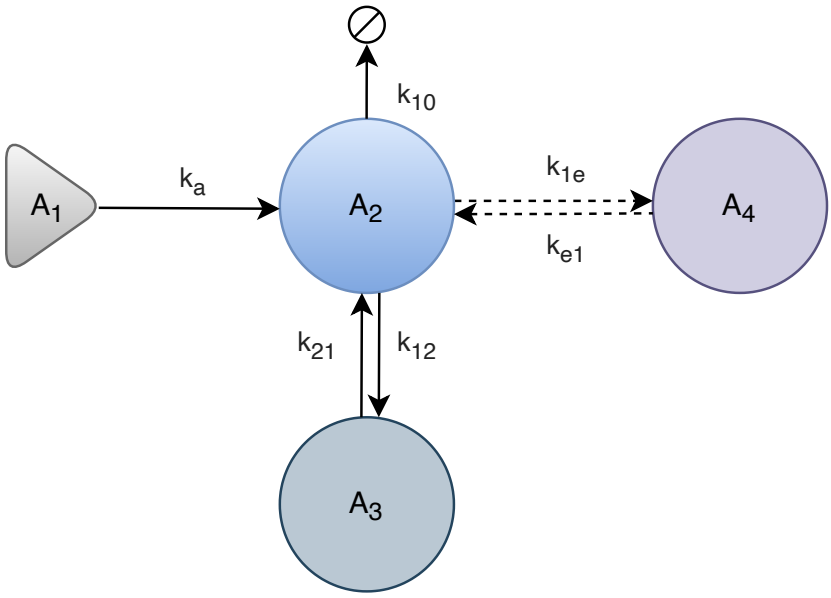

Figure 3.5: *Schematic diagram of Emtricitabine pharmacokinetic model.* A_1 = dosing compartment; A_2 = central blood plasma compartment; A_3 = peripheral tissue compartment; A_4 = seminal compartment. The drug concentration in each compartment can be calculated by dividing by the volume of each compartment. Adapted from [7].

Table 3.5: Final pharmacokinetic parameter estimates of model for Emtricitabine (FTC)

Parameter	Definition	Value	Unit	ω IVV estimate	Distribution	Reference
k_a	Absorption rate constant	0.53	$hour^{-1}$	-	-	[7]
CL/F	Apparent total clearance of the drug	14.8	$liter \cdot h^{-1}$	0.255	Log normal	[7]
Vc/F	Apparent volume of central compartment	51.6	liter	-	-	[7]
Vp/F	Apparent volume of peripheral compartment	106	liter	-	-	[7]
Q/F	Intercompartmental clearance	8.19	$liter \cdot h^{-1}$	-	-	[7]
k_{1e}	Blood plasma to seminal plasma transfer rate constant	0.341	$hour^{-1}$	0.533	Log normal	[7]
k_{e1}	Seminal plasma elimination rate constant	0.113	$hour^{-1}$	-	-	[7]
k_{12}	$\frac{Q/F}{Vc/F}$	-	-	-	-	[7]
k_{21}	$\frac{Q/F}{Vp/F}$	-	-	-	-	[7]
k_{10}	$\frac{CL/F}{Vc/F}$	-	-	-	-	[7]

3.2.3 Tenofovir disoproxil fumerate

The model developed by Duwal et al. [4] is employed to simulate the pharmacokinetic profile of TDF. The researchers found that TDF plasma pharmacokinetics are best described by a two-compartment model (plus a dosing compartment). They extended this model to also include an intracellular compartment which models the PK of TFV-DP, the active form of the drug. The final pharmacokinetic model is mathematically specified by a system of ODEs and thus constitutes four compartments: C_T represents the mass of tenofovir in the dosing reservoir. C_1 is the central compartment, which represents the plasma concentration of TFV. The second compartment C_2 represents the poorly perfused (peripheral) tissues and the cellular compartment C_{cell} resembles the concentrations of TFV-DP in the biophase. Parameter values are defined in Table 3.6, Figure 3.6 a schematic representation and the model is described by the following system of coupled ODEs:

$$\frac{d}{dt}C_T = -k_a \cdot C_T(t) \tag{3.2.8}$$

$$\frac{d}{dt}C_1 = \frac{F_{bio} \cdot k_a \cdot C_T(t)}{V_1} - C_1(t) \cdot k_e - k_{12} \cdot C_1(t) + k_{21} \cdot C_2(t) \tag{3.2.9}$$

$$\frac{d}{dt}C_2 = k_{12} \cdot C_1(t) - k_{21} \cdot C_2(t) \tag{3.2.10}$$

$$\frac{d}{dt}C_{cell} = \frac{V_{max} \cdot C_1(t)}{K_m + C_1(t)} - C_{cell}(t) \cdot k_{out} \tag{3.2.11}$$

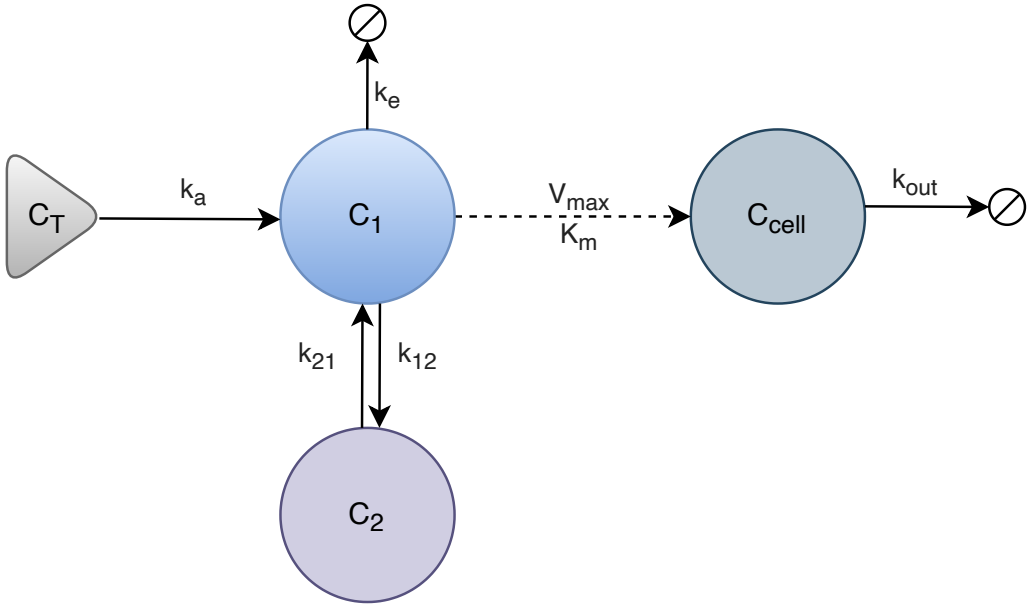

Figure 3.6: *Schematic diagram of Tenofovir pharmacokinetic model.* C_T = dosing compartment; C_1 = central blood plasma compartment; C_2 = peripheral tissue compartment; C_{cell} = cellular compartment. Adapted from [4].

Table 3.6: Final pharmacokinetic parameter estimates of model for Tenofovir (TDF)

Parameter	Definition	Value	Unit	Parameter range	Distribution	Reference
k_a	Absorption rate constant	1	h^{-1}	-	-	[4]
k_e	Elimination rate constant	0.12	h^{-1}	-	-	[4]
k_{12}	Influx rate constant to peripheral compartment	0.2926	h^{-1}	-	-	[4]
k_{21}	Outflux rate constant from peripheral compartment	0.1537	h^{-1}	-	-	[4]
K_m	Michaelis–Menten constant giving half V_{max}	29.3	$\mu g\, L^{-1}$	-	-	[4]
V_1	Apparent volume of compartment 1	244	L	-	-	[4]
k_{out}	Rate of elimination of TFV-DP	0.006	h^{-1}	0.01-0.06324	Log Normal	[4]
F_{bio}	Bioavailability constant	0.32	-	-	-	[4]
V_{max}	Max rate of TFV-uptake and conversion to TFV-DP	1.44	$\mu g\, L^{-1}\, h^{-1}$	6.845-24	Log Normal	[4]

3.2.4 Lopinavir/ritonavir

A lopinavir (LPV) population pharmacokinetic model was developed by Wang et al. [6] to investigate the impact of alpha-1-acid glycoprotein (AAG) drug-binding on total (LPV_t) and free (LPV_f) lopinavir concentrations. Protease inhibitors bind with high affinity primarily to AAG which has an influence on the free plasma concentrations of the drugs. As ritonavir (RTV) is a co-formulation with lopinavir, the pharmacokinetic

model consists of four compartments with an independent analysis relating AAG and LPV_t with LPV_f. The initially separate models for LPV_t and RTV were linked through the effect that the concentration of RTV has on LPVt and LPVt clearance (CL_{LPVt}) and the final linked model simultaneously represents the relationship between RTV concentrations and CL_{LPVt}. Parameter values are defined in Table 3.7 and Figure 3.7 a schematic representation of the model. The following four equations represent the joint model for both drugs, including an exponential term for the effect of RTV concentration on LPV_t clearance:

$$\frac{d}{dt}B_1 = -\frac{CL_{LPVt} \cdot e^{[-c_1 \cdot (C_{RTV}-299)]}}{V_t} \cdot B_1(t) + k_{aLPVt} \cdot B_2(t) \tag{3.2.12}$$

$$\frac{d}{dt}B_2 = -k_{aLPVt} \cdot B_2(t) \tag{3.2.13}$$

$$\frac{d}{dt}B_3 = -\frac{CL_{RTV}}{V_{RTV}} \cdot B_3(t) + k_{aRTV} \cdot B_4(t) \tag{3.2.14}$$

$$\frac{d}{dt}B_4 = -k_{aRTV} \cdot B_4(t) \tag{3.2.15}$$

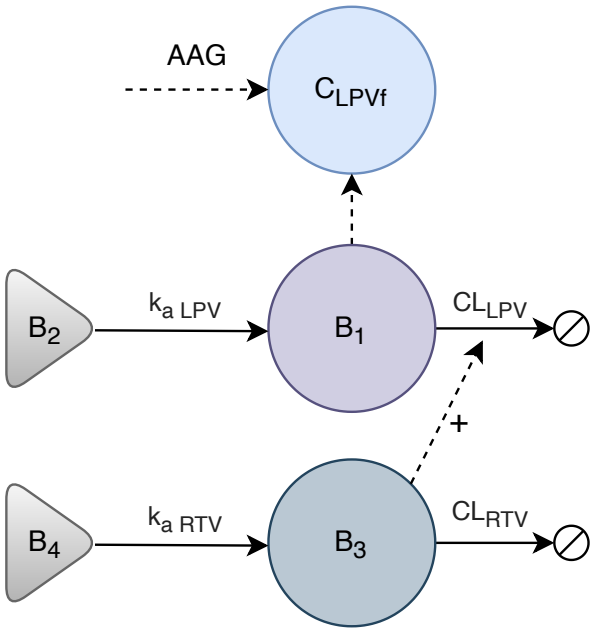

Figure 3.7: *Schematic diagram of Lopinavir/ritonavir pharmacokinetic model.* B_1 = LPV central blood plasma compartment; B_2 = LPV dosing absorption compartment; B_3 = RTV central blood plasma compartment; B_4 = RTV dosing absorption compartment; C_{LPVf} = free LPV in relation to AAG. Adapted from [6].

B_1 and B_2 are the amount of LPV_t in the measured blood plasma (central) and absorption compartments, respectively. B_3 and B_4 represent the amounts of RTV in the measured and absorption compartments, respectively. The impact of alpha-1-acid glycoprotein (AAG) drug-binding on LPV_t and LPV_f lopinavir concentrations were quantified using an enzyme-linked immunosorbent assay (ELISA). The data from these assays were pooled and a model of AAG binding was selected by the authors of this publication to calculate LPV_f. The concentration of LPV_f in relation to AAG can be determined according to:

$$C_{LPVf} = [fu_0 - p_1 \cdot (AAG - 91.8)] \cdot B_1(t) \tag{3.2.16}$$

Table 3.7: Final pharmacokinetic parameter estimates of model for co-formulated Lopinavir Ritonavir (LPV/RTV)

Parameter	Definition	Value	Unit	CV [%]	Distribution	Reference
CL_{LPVt}	Total clearance of LPV	4.73	$L{\cdot}h^{-1}$	-	-	[6]
c_1	Coefficient of the RTV effect	6.24×10^{-4}	-	28.3	Log normal	[6]
V_{LPVt}	Total volume of distribution for LPV_t	55.7	L	55.2	Log normal	[6]
k_{aLPVt}	Absorption rate constant for LPV_t	0.325	$L{\cdot}h^{-1}$	-	-	[6]
CL_{RTV}	Clearance rate of RTV	22.0	$L{\cdot}h^{-1}$	50.5	Log normal	[6]
p_1	Slope for AAG	1.13×10^{-5}	-	103.0	Log normal	[6]
$f\mu_0$	Fraction of unbound drug with median AAG	0.0093	$L{\cdot}h^{-1}$	23.4	Log normal	[6]
V_{RTV}	Total volume of distribution for RTV	117.0	L	61.7	Log normal	[6]
k_{aRTV}	Absorption rate constant for RTV	0.740	$L{\cdot}h^{-1}$	107	Log normal	[6]
$IC_{50}(LPV)$	Concentration of the drug producing 50% inhibition	5.84	$ng{\cdot}mL^{-1}$	53.1	Log normal	[6]
γ_{LPV}	Hill coefficient of LPV	1.88	-	19.2	Log normal	[6]
τ_{LPV}	Mean transit time of LPV	3.22	h	41.6	Log normal	[6]
AAG	Unbound concentration of LPV at the median AAG	91.8	$mg{\cdot}dL^{-1}$	-	-	[6]

3.3 Pharmacodynamic models

Determining the appropriate metric for assessing the adequacy of a patient's response to therapy is an important part of producing accurate models with meaningful results. Studying the biological effect of each drug requires linking of the dose-concentration profile described by its PK properties to the drug's pharmacodynamic model. Due to extremely rapid receptor binding and biophase distribution, most drug effects can be

related with reasonable accuracy directly to the drug concentration in the effect compartment [73]. The I_{max} equation for the inhibition of viral replication as described in the previous chapter was used to implement the concentration-effect relationship for each drug. The drug efficacy term (ϵ) described below for each of the ARVs can be implemented in the HIV disease models as inhibiting the viral reproductive capacity by a factor ranging between 0 - 1.

$$\epsilon = 1 - \frac{IC_{50}^{h}}{IC_{50}^{h} + C^{h}} \tag{3.3.1}$$

where ϵ is the drug efficacy with $0.0 \leq \epsilon \leq 1.0$, IC_{50} is the concentration of the drug which inhibits infection by 50%, h the Hill coefficient and C is the drug concentration.

Dolutegravir The I_{max} model [72] for the dose-effect relationship of dolutegravir was implemented as:

$$\epsilon_{DTG} = 1 - \frac{IC_{50\cdot DTG}^{h}}{IC_{50\cdot DTG}^{h} + C_c(t)^{h}} \tag{3.3.2}$$

Where $IC_{50\cdot DTG}$ (Table 3.8) denotes the drug concentration which inhibits cell infection by 50%, C_c(t) the drug concentration in the effect compartment and h is the slope parameter (Hill coefficient) [5]. ϵ_{DTG} is the efficacy of the drug treatment and $0.0 \leq \epsilon_{DTG} \leq 1.0$, IC_{50}.

Emtricitabine The I_{max} model [72] for the dose-effect relationship of emtricitabine was implemented as:

$$\epsilon_{FTC} = 1 - \frac{IC_{50\cdot FTC}}{IC_{50\cdot FTC} + A_2(t)} \tag{3.3.3}$$

Where $IC_{50\cdot FTC}$ (Table 3.8) denotes the drug concentration which inhibits cell infection by 50% and A_2(t) the drug concentration in the effect compartment [7]. ϵ_{FTC} is the efficacy of the drug treatment and $0.0 \leq \epsilon_{FTC} \leq 1.0$.

Tenofovir disoproxil fumerate The I_{max} model [72] for the dose-effect relationship of tenofovir was implemented as:

$$\epsilon_{TDF} = 1 - \frac{IC_{50\cdot TDF}}{IC_{50\cdot TDF} + C_{cell}(t)} \tag{3.3.4}$$

Where $IC_{50\cdot TDF}$ (Table 3.8) denotes the drug concentration which inhibits cell infection by 50% and C_{cell}(t) the drug concentration in the effect compartment [4]. ϵ_{TDF} is the efficacy of the drug treatment and $0.0 \leq \epsilon_{TDF} \leq 1.0$.

Lopinavir/ritonavir The I_{max} model [72] for the dose-effect relationship of lopinavir was implemented according to the following, where several transit delay compartments were used to account for the delay between the initiation of therapy and the observed decrease in viral load:

$$\frac{d}{dt}D_1 = \frac{1}{\tau_{LPV}} \cdot \left[\frac{I_{max} \cdot C^h_{LPVf}}{IC^h_{50 \cdot LPV} + C^h_{LPVf}} - D_1(t) \right] \tag{3.3.5}$$

$$\frac{d}{dt}D_2 = \frac{1}{\tau_{LPV}} \cdot [D_1(t) - D_2(t)] \tag{3.3.6}$$

$$\frac{d}{dt}\epsilon_{LPV} = \frac{1}{\tau_{LPV}} \cdot [D_2(t) - \eta_{LPV}(t)] \tag{3.3.7}$$

Where $IC_{50 \cdot LPV}$ (Table 3.8) denotes the drug concentration which inhibits cell infection by 50%, C_{LPV_f} is the free drug concentration in the effect compartment and I_{max} is the maximum inhibition effect of LPV_f (fixed at 1 assuming no escaping virus routes) [6]. ϵ_{LPV}(t) is the efficacy of the drug treatment and $0.0 \leq \epsilon_{LPV} \leq 1.0$.

Table 3.8: Pharmacodynamic parameters of the relevant ARVs.

ARV	IC_{50}	Unit	Hill coefficient	Reference
Dolutegravir (DTG)	0.089	nM	1.3	[5]
Emtricitabine (FTC)	0.012	$mg{\cdot}L^{-1}$	-	[7]
Tenofovir disoproxil fumerate (TDF)	0.076	$mg{\cdot}L^{-1}$	-	[4]
Lopinavir/ritonavir (LPVr)	5.84	$ng{\cdot}mL^{-1}$	-	[6]

Combination drug therapy pharmacodynamics Simulating ARV combination therapy with multiple drugs required modelling the net efficacy of jointly acting drugs from a single class. Two classes of ARVs are prescribed in a single drug regimen at a time, with first-line treatment including one INSTI and two RTIs and second-line treatment including one PI and the two RTIs. In both cases, due to the different mechanisms of action of the two classes of drugs involved, each class can be implemented separately in the viral dynamics model. The Bliss independence model enables us to jointly simulate the two RTI drugs which inhibit the same biological process [76]:

$$\epsilon_{RTI} = 1 - [(1 - \epsilon_{FTC}) \cdot (1 - \epsilon_{TDF})] \tag{3.3.8}$$

where ϵ_{FTC} and ϵ_{TDF} are the drug efficacies of emtricitabine and tenofovir, respectively. ϵ_{RTI} becomes the new pharmacodynamic drug efficacy of the two drugs to be implemented in the viral dynamics models and $0.0 \leq \epsilon_{RTI} \leq 1.0$.

3.4 Model simulation and implementation

3.4.1 HIV models

During model simulation, certain parameters are varied to represent the biological variation present in populations, also known as patient heterogeneity. Patient heterogeneity results in differing responses to infection due to biological variation and thus has an impact on disease outcome. The variation in HIV model parameters are implemented though the use of built-in functions in Wolfram Mathematica [15]. Parameter values are sampled from probability distributions (specified or determined by the authors of the original models) as shown in Tables 3.1, 3.2 and 3.3. This is done for all the varied parameters, allowing for numerous sets of parameters to be generated, each representing a unique individual in the population.

3.4.2 PKPD models

After each PKPD model was reproduced, the prescribed drug regimens were implemented using daily or bi-daily dosing events. Dosing events are modelled as impulse inputs, with

$$d_{C_D,t} = d_{C_D,t} + dose_k \tag{3.4.1}$$

whenever the current simulation time t coincided with a dosing event τk. C_D is the amount of the drug in the dosing compartment and $dose_k$ is the dosing input.

Similarly to the HIV disease models, certain parameters are varied to represent the natural biological variation present in populations. The variable pharmacology of patients has an impact on the amount of drug available at the target site and thus will have an impact on the efficacy of the administered dose. Parameter values are sampled from probability distributions (specified or determined by the authors of the original models) as shown in in Table 3.4, 3.5, 3.6 and 3.7. Just as certain parameters are varied within a population, so can certain treatment scenarios exist which vary from patient to patient, e.g. the specific combination of drugs which the patient is currently receiving, how adherent a patient is to taking their medication daily, and for how long the individual was infected before receiving treatment. Each of scenarios can have an effect on the effectiveness of the treatment and thus the prognosis of each patient. Simulations can be used to model each of these scenarios and were implemented accordingly.

3.5 Summary

In this chapter, the different types models were introduced which include existing pharmacokinetic and pharmacodynamic models of ARVs and disease progression models of HIV. The methods of simulation and implementation as described above were used to generate the results in Chapter 4, including Monte Carlo simulations to study the impact of heterogeneity in populations. In addition, irregular treatment adherence and variation in treatment initiation time after infection were simulated and compared to clinical patient data.

The clinical data was obtained from the Cape Winelands HAART to HEART study (Worcester Community Day Centre, Cape Town, South Africa) [84]. This study complies with the Declaration of Helsinki, and ethical approval was obtained from the Human Research Ethics Committee of Stellenbosch University (reference number: N12/12/086) and the Department of Health of the Western Cape Government of South Africa (reference number: RP090/2013). Before the study, all participants were informed about procedures and consent forms were signed by all.

Chapter 4

Results and discussion

The first section of this chapter shows initial validations and reproductions from literature. The subsequent sections examine the analyses of these models in more detail, first using the individual models and then the combined PKPD-disease models. Throughout, Monte Carlo simulations are used to examine the impact of population heterogeneity. Finally, simulation results are compared to patient clinical data to study how well the models selected here are able to predict the drug response and treatment outcomes.

4.1 Reproduced HIV disease model simulations

4.1.1 HIV model with two-stages of T-cell infection

The mathematical model developed by Kamboj et al. [2] is considered to illustrate the dynamics of the immune system. This model was successfully coded in Wolfram Mathematica [15] and reproduced the time-course dynamics in the original article seen in Figure 4.1. Transient oscillations can be seen in the time-course plots before steady state is reached. This includes the $CD4^+$ T-cell population and the viral load, both with and without immune response. From the initial values of T(0)= 300 μL^{-1}, $T_1(0) = T_2(0) = V(0)$ = 10 μL^{-1}, E(0) = 1 μL^{-1}, with an immune response, the T-cell count rebounds to a steady state value of 640 μL^{-1} and the viral load increases to a value of 1000 μL^{-1}. Whereas without an immune response, the T-cell count reaches a steady state value of 116 μL^{-1} and the viral load increases to a steady state value of 4840 μL^{-1}.

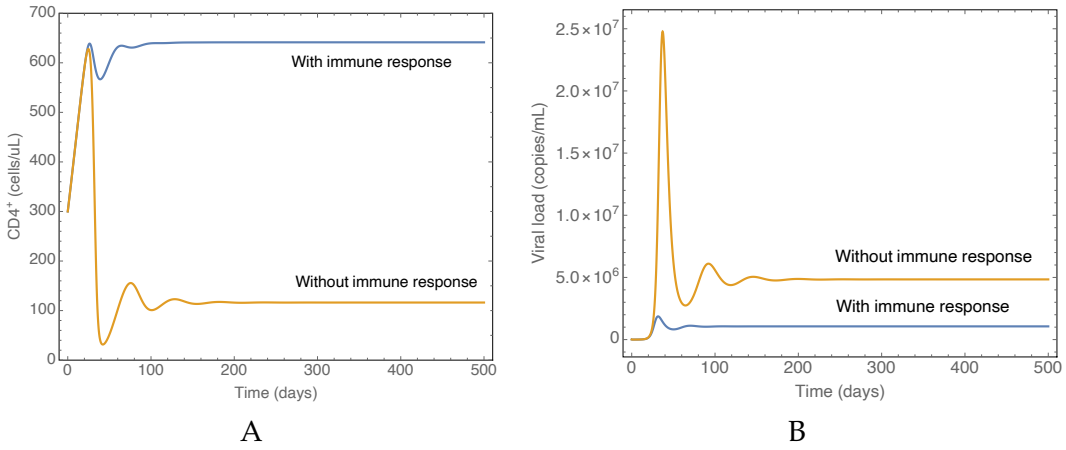

Figure 4.1: *Validation of the Kamboj1 model [2].* The Kamboj1 model was reproduced and simulated for 500 days. The figure shows the steady state time courses of (A) uninfected $CD4^+$ T-cells and (B) the viral load. The simulations were performed with (blue) and without (orange) an immune response.

4.1.2 HIV model with latently infected T-cells

The mathematical model created by Wang et al. [3] illustrates the long-term dynamics of the immune system. This model was successfully coded in Wolfram Mathematica [15] and reproduced the time-course dynamics in the original article. Transient oscillations can be seen in the time-course plots before steady state is reached. Initial values were implemented as V(0) = 10^{-3} RNA copies/mL, T(0) = 1000 μL^{-1}, T$\star$(0) = M(0) = C(0) = 0. The simulation results are consistent with the long term depletion of T cells during HIV infection. With chronic inflammation, the T-cell count declines from the initial 1000 cells/μL to about 200 cells/μL after some years of infection as shown in Figure 4.2. The viral load increases sharply during the first year of chronic infection before reaching a steady state of $\pm$400 000 RNA copies/mL.

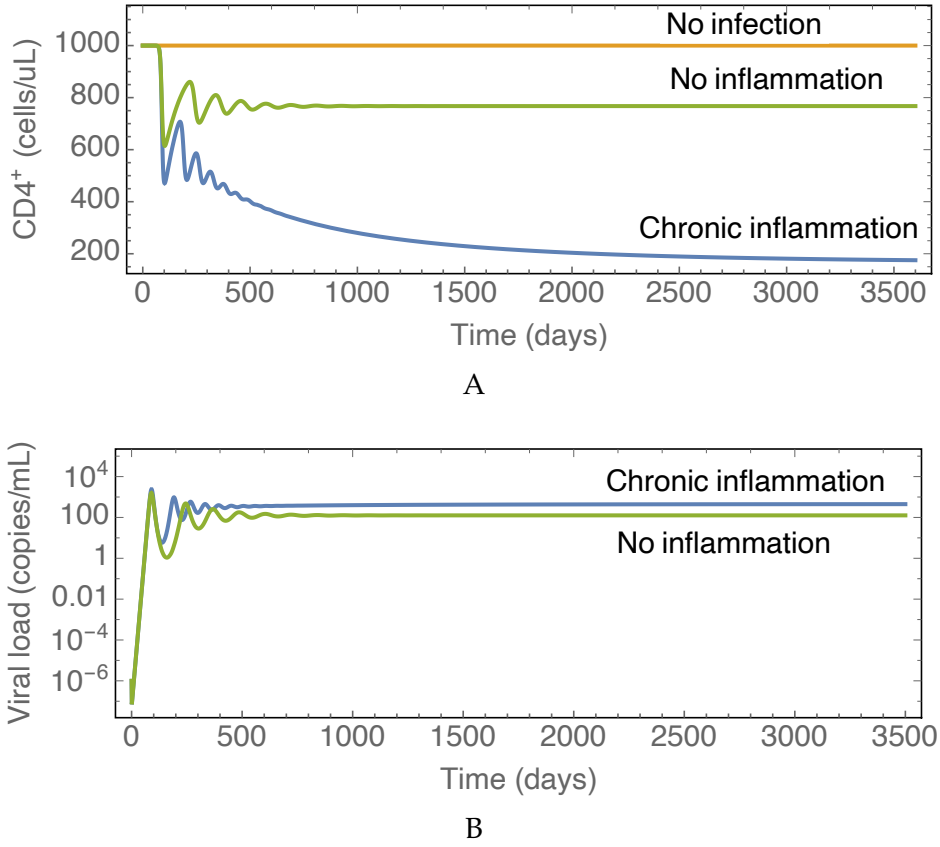

Figure 4.2: *Validation of the Wang1 model [3].* The Wang1 model was reproduced and simulated for 3500 days. The figure shows the steady state time courses of (A) $CD4^+$ T-cells and (B) the viral load.

4.1.3 HIV model with drug resistance

The HIV disease model developed by Rong et al. [1] was successfully coded in Wolfram Mathematica [15] and reproduced the time-course dynamics in the original article seen in Figure 4.3. Transient oscillations can be seen in the time-course plots before steady state is reached. In Figure 4.3 A, the uninfected state, the density of $CD4^+$ T-cells is in equilibrium at 1000 uninfected cells/μL. In the pretreatment steady state, the uninfected cell count drops to ±320 cells/μL and the total viral load amounts to 880,000 RNA copies/mL from an initial value of 10^{-6} copies/mL. These lie within the normal expected biological range values of a person who is infected with HIV and not receiving treatment [85].

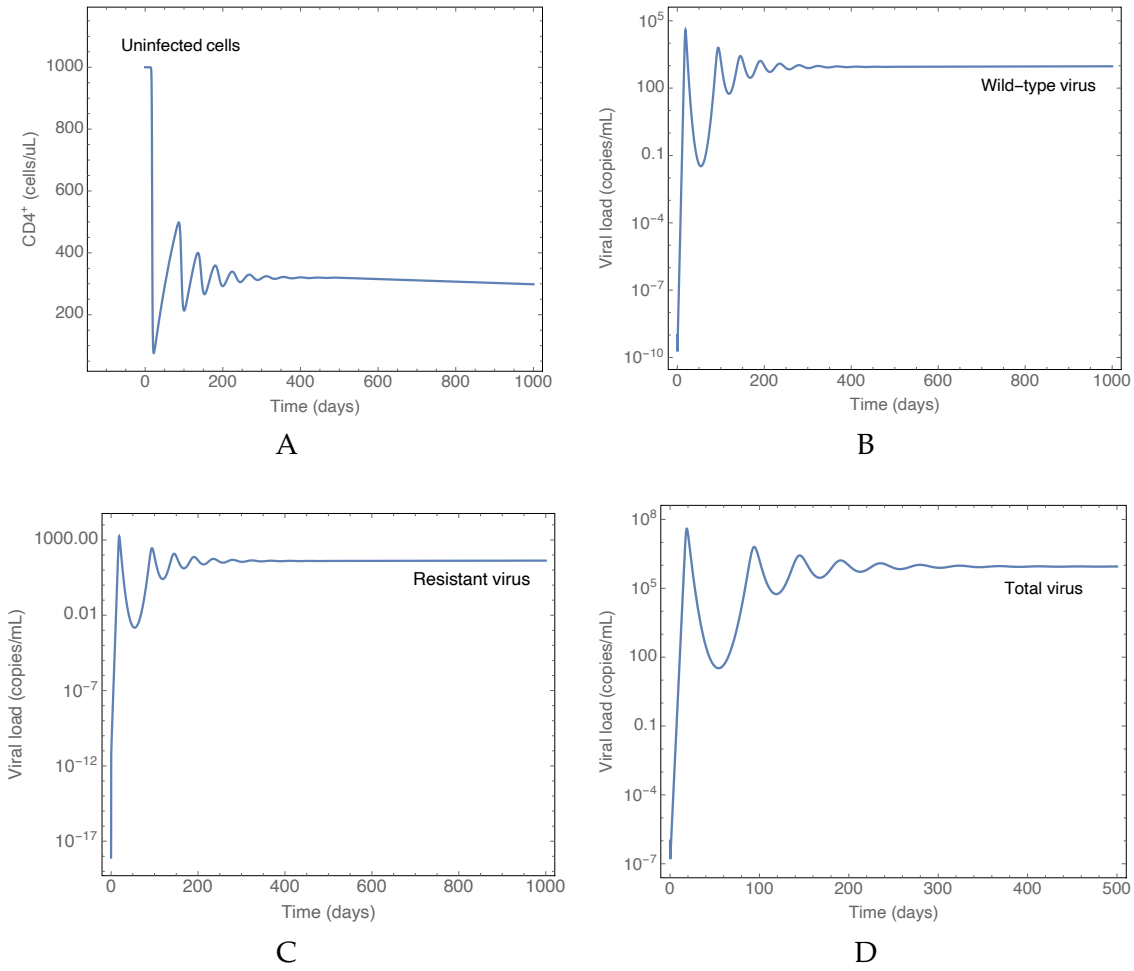

Figure 4.3: *Validation of the Rong1 model [1].* The Rong1 model was reproduced, coded in Wolfram Mathematica and simulated for 500 days. The figure shows the untreated steady state time courses of: (A) uninfected $CD4^+$ T-cells, (B) drug-sensitive virus, (C) drug-resistant virus and (D) total viral load.

4.1.4 Viral load range comparison

Following initial validation and reproduction, Monte Carlo (MC) simulations were used to predict the impact of parameter variation on model performance. Firstly, the parameter values are modelled by using a distribution function which represents a statistical distribution between a given minimum and maximum value. These values for the HIV models can be found in Table 3.3, 3.1 and 3.2. For simulations, parameter values are sampled from their associated statistical distributions of which the ranges were obtained from the original publications. This was done for all the varied parameters, allowing for numerous sets of parameters to be generated. In Figure 4.4 and 4.5, these parameter sets (N=100 000) were used to examine the spread in the viral load and T-cell counts obtained in the untreated steady state.

Comparing the spread in the viral load for these three models, the results show that Rong1 and Wang1 have a slightly higher median value than Kamboj1 in Figure 4.4. This is accompanied by a lower T-cell count for Rong1 and Wang1 in Figure 4.5. This is to be expected as Wang1 includes the infection of latently infected T-cells which act as a reservoir for virus and Rong1 has drug resistant virus which are harder to treat with drug therapy. Apart from parameter effects, steady state viral load and T-cell count values will thus be different for each of the models because factors like latency and drug resistance have an impact on disease progression. However, these results compare well between models and the viral load ranges largely overlap between models. The results are also within the normal expected biological range values of a person who is infected with HIV and not receiving treatment: low (<10 000 copies/mL), medium (10 000 - 99 999 copies/mL) and high (>100 000 copies/mL) for the viral load, and low (<200x10^6/L), medium (200 - 349x10^6/L) and high ($\geq$350x10^6/L) for the $CD4^+$ T-cell count [85].

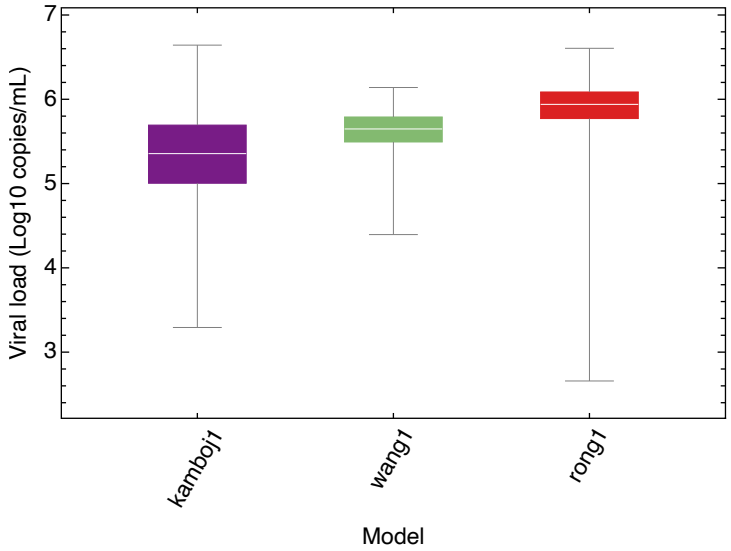

Figure 4.4: *Monte Carlo simulation viral load comparison of HIV models.* Parameter values for each model were varied by sampling from their associated statistical distributions. The simulation generated a range of untreated viral loads for each model. Steady state values are used in the box-and-whisker plot. The box includes 25%-75% of the simulated population viral loads with the lines extending towards the min and max values plotted. Medians of the model predictions are 226 588 copies/mL (kamboj1), 444 539 copies/mL (wang1) and 870 488 copies/mL (rong1) and a Kruskal-Wallace test with Dunn's multiple comparisons indicated these to be significantly different with p<0.0001.

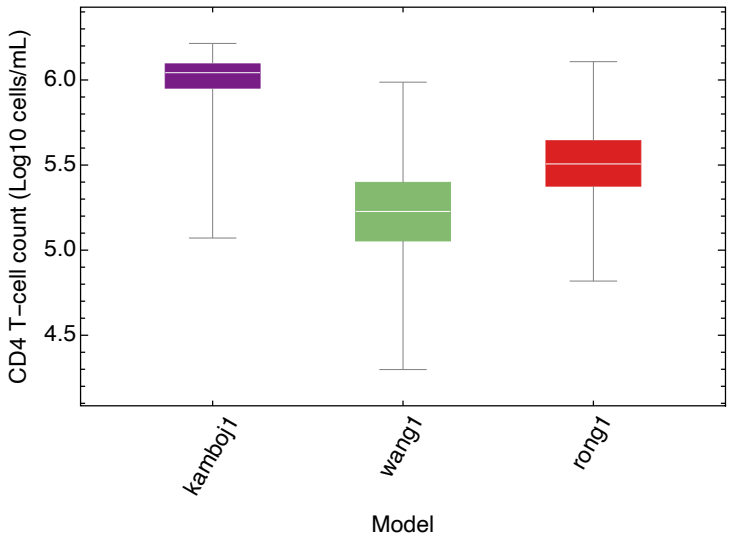

Figure 4.5: *Monte Carlo simulation CD4$^+$ T-cell count comparison of HIV models.* Parameter values for each model were varied by sampling from their associated statistical distributions. The simulation generated a range of untreated CD4$^+$ T-cell counts for each model. Steady state values are used in the box-and-whisker plot. The box includes 25%-75% of the simulated population T-cells counts with the lines extending towards the min and max values plotted. Medians of the model predictions are 1 103 283 cells/mL (kamboj1), 168 862 copies/mL (wang1) and 321 162 cells/mL (rong1) and a Kruskal-Wallace test with Dunn's multiple comparisons indicated these to be significantly different with p<0.0001.

4.1.5 Required drug efficacy

The following simulations were performed on all three HIV models. A drug efficacy scan was performed with Monte Carlo simulations to determine the drug efficacy required to bring the viral load count to below the detectable limit of 50 copies/mL of blood. Each generated parameter set (N=100 000) is scanned starting from 0 up to 1 for the drug efficacy parameter (ϵ). For these simulations ϵ was implemented as in the originally published articles by the authors.

Wang1 In Figure 4.6 on the x-axis, the RTI drug efficacy parameter is a value ranging from 0 - 1, where 0 means no inhibition and 1 means complete inhibition of viral replication. The simulation was performed for N=100 000 patients in the Wang1 HIV disease model. There is a spread across the required efficacy with a tendency towards higher drug efficacy requirements to bring the viral load to below the detectable limit, and a mean value of approximately 0.55. This model predicts that in a population, all individuals will have an undetectable viral load if the efficacy is high enough. For a substantial part of the population, however, high efficacy might be over treating them raising concerns about side effects.

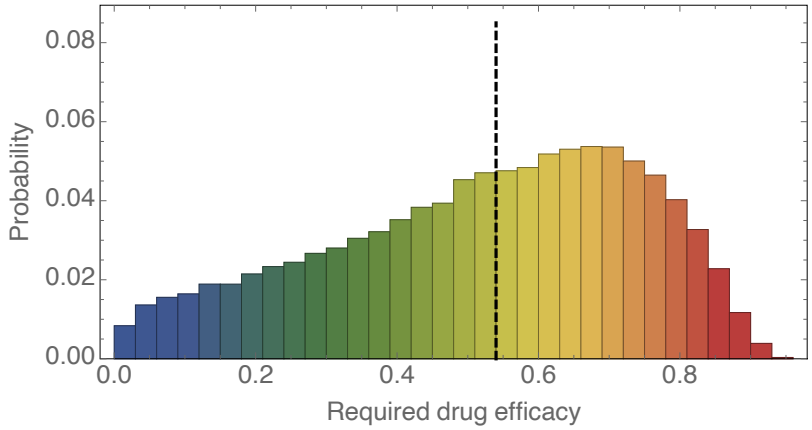

Figure 4.6: *Required drug efficacy scan of Wang1.* A model simulation was performed using the Wang1 model by sampling values from parameter probability distributions (Table 3.2), generating 100,000 unique parameter sets. Treatment was then simulated with an increasing drug efficacy value until the required value was found to bring the viral load to below detectable limit (<50 copies/mL) for each parameter set. On the x-axis, the drug efficacy ranges from 0-1 with the mean value indicated by the dotted black line.

Rong1 The simulation was also performed for the Rong1 model and as indicated by the black dotted line representing the mean, a relatively high drug efficacy is required to suppress viral replication effectively. This high drug efficacy value is likely due to the presence of a drug-resistant viral population in the model. This result adds to the evidence that highly effective and continuous drug therapy is required to fully suppress viral replication and to block the emergence of drug-resistant strains. In addition, for a very small fraction, 100% efficacy is required which might not be feasible.

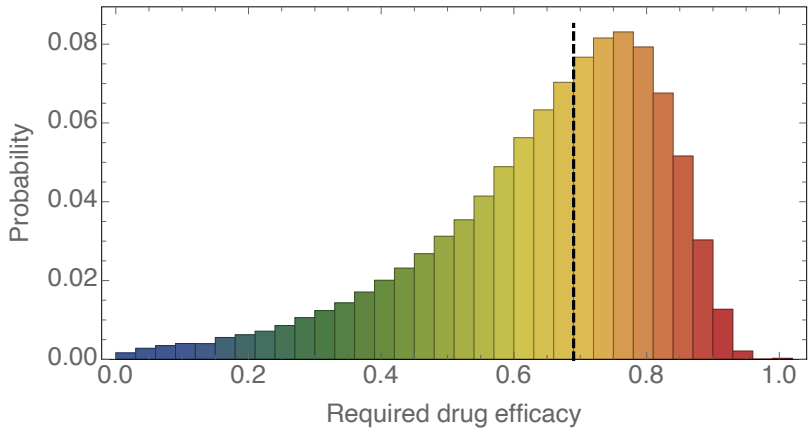

Figure 4.7: *Required drug efficacy scan of Rong1.* A model simulation was performed using the Rong1 model by sampling values from parameter probability distributions (Table 3.3), generating 100,000 unique parameter sets. Treatment was then simulated with an increasing drug efficacy value until the required value was found to bring the viral load to below detectable limit (<50 copies/mL) for each parameter set. On the x-axis, the drug efficacy ranges from 0-1 with the mean value indicated by the dotted black line.

Kamboj1 is an HIV disease model which allows for multiple drug types to be modelled independently as they act on different stages of the HIV life cycle. In this simulation drug treatment is with RTIs and PI. The results are shown in Figure 4.8, where a parameter scan was done (N = 100 000) for two types of ARVs acting at the same time, a protease inhibitor and two reverse transcriptase inhibitors. Different classes of ARVs have differing mechanisms of action, with different stages of the viral life cycle being targeted. This can be seen here in the result of the simulation. On the PI axis, which is a class of drug that is more effective overall as it acts later in the life cycle. In comparison, RTIs seem to have a slightly lower efficacy than PIs and thus more individuals require a higher drug efficacy to bring the viral load to below detectable limits.

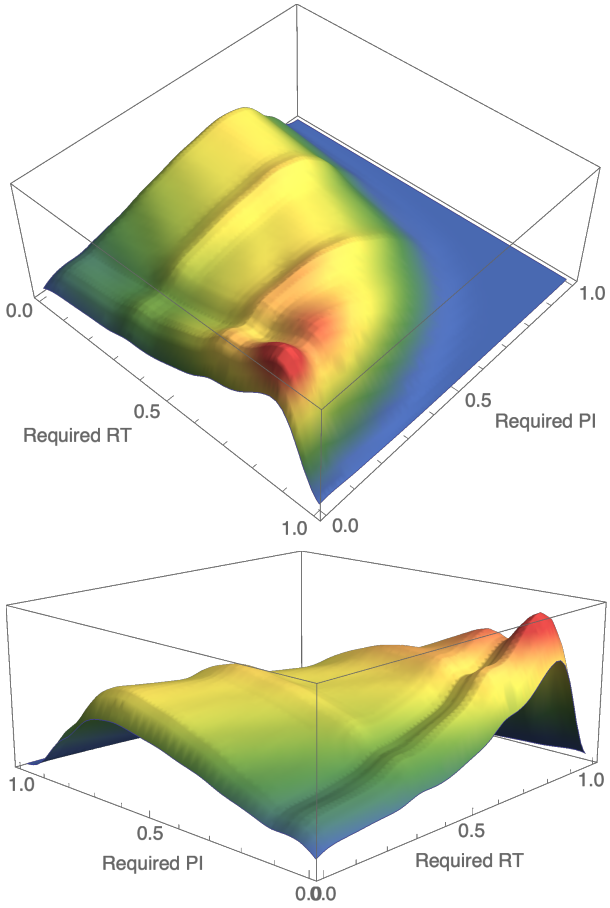

Figure 4.8: *Required drug efficacy scan of Kamboj1.* A model simulation was performed using the Kamboj1 model by sampling values from parameter probability distributions (Table 3.1), generating 100,000 unique parameter sets. Treatment was then simulated with an increasing drug efficacy value until the required value was found to bring the viral load to below detectable limit (<50 copies/mL) for each parameter set. On the x-axis, the drug efficacy ranges from 0-1 for RTIs and on the y-axis for PIs.

4.2 Pharmacokinetic-pharmacodynamic models

The quantitative prediction of drug effect is a major goal of clinical pharmacology. Drug-body interactions can be studied through the characterisation of a drug's pharmacokinetic and pharmacodynamic properties. Pharmacokinetics is the study of the movement of a compound within the body after its administration, whereas pharmacodynamics is the study of the relationship between the concentration of a compound at its site of action and the magnitude of the drug effect [53]. Firstly, pharmacokinetic models were used to study the time course of the absorption, distribution, metabolism and excretion of the currently prescribed antiretroviral drugs.

4.2.1 Dolutegravir

A model of the pharmacokinetics of Dolutegravir (DTG) was constructed by Duwal et al. [4] and in the previous chapter. A two compartment model with oral absorption best described the pharmacokinetics of the drug. Figure 3.4 shows a schematic representation of the model. This model was successfully reproduced in Wolfram Mathematica [15] and the drug plasma concentration plots were visually similar to those published in the article. Model simulations were performed to predict the change in DTG drug plasma concentration. The simulated dosage administered once daily was 50 mg DTG. In Figure 4.9 the pharmacokinetic model is used to predict the plasma drug concentration for the first four days after initiation of a once daily 50 mg oral regimen. The simulation result shows the peak concentration reached ±2 hours after every dose and the daily fluctuation in the drug plasma concentration. Fluctuations are expected because as soon as the drug has been absorbed, the body starts working to distribute, metabolise and excrete it (ADME). These four mechanisms all influence the drug levels and kinetics of drug exposure.

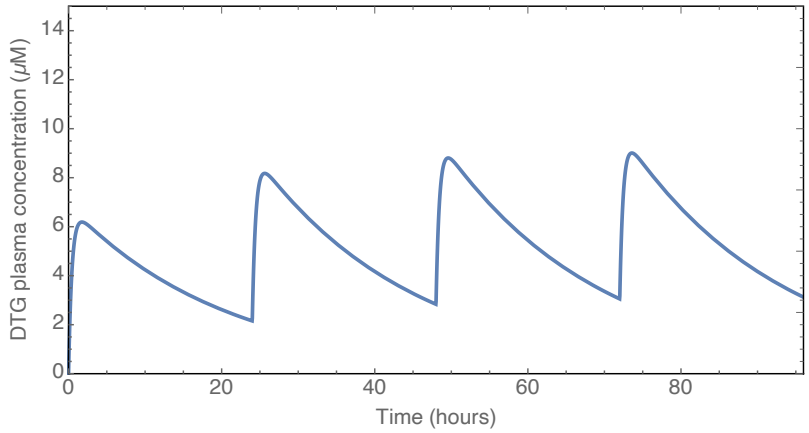

Figure 4.9: *Validation of DTG pharmacokinetic model.* The two compartment model used to simulate drug therapy with dolutegravir is coded and validated. DTG is taken daily (50 mg). Plotted is the simulated drug concentration in the blood plasma over time for the first four days after initiation of treatment.

Heterogeneity in the population leads to biological variation and thus variation in how each individual responds to drug therapy. In terms of pharmacokinetics, there will be differences in how each individual absorbs, distributes, metabolises and excretes the drug. This will result in the time-drug concentration profile being slightly different for each patient. Along with the population PK parameter estimates, the authors of the DTG model reported data for interindividual variability on drug clearance (CL/F_{bio}) and the volume of distribution (V_c/F_{bio}), which can be found in Table 3.4. This data can be used to simulate patient heterogeneity by sampling parameter values from their associated distributions. This allows for numerous sets of parameters to be generated, each representing a unique individual in the population. 1000 parameter sets were generated (N=1000 virtual patients) with a simulated dosage of daily 50 mg DTG of the first four days. The results of the variation in the predicted plasma concentration time profiles are shown in Figure 4.10 below, where the white line depicts the median concentration, dark grey areas represent the interquartile range and light grey the remainder between min and max values. This result compares well to the VPC the authors performed in the original publication.

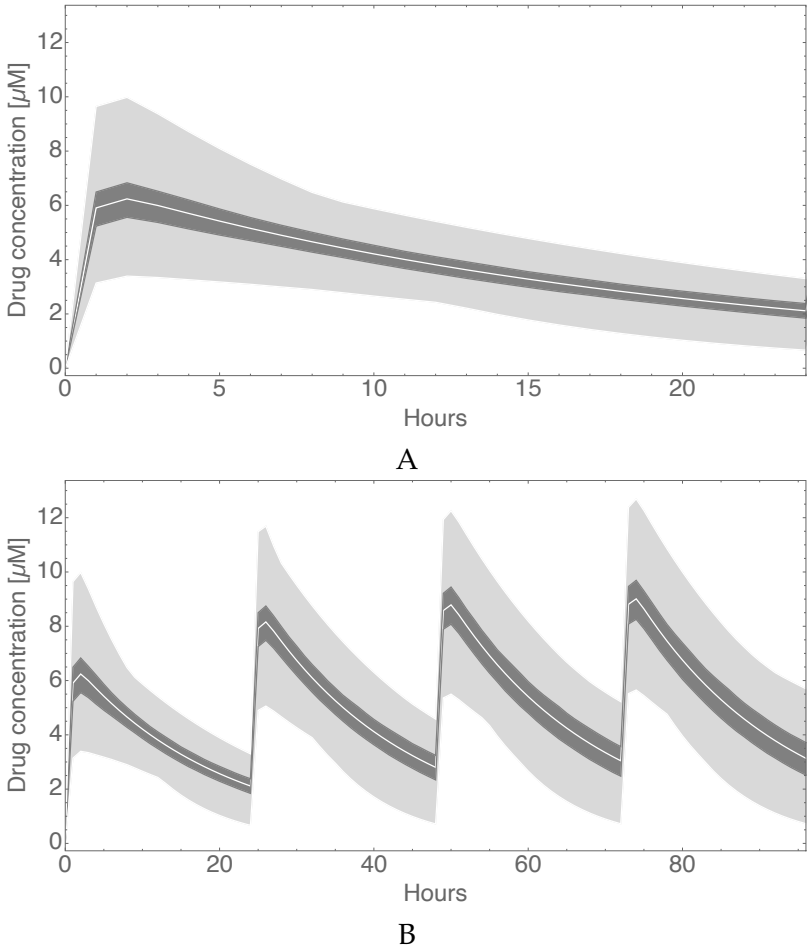

Figure 4.10: *Monte Carlo simulation of DTG model.* Model simulations were performed using 1000 parameter sets generated from Table 3.4. The variation in these parameter sets represent the patient heterogeneity which result in a variation in the drug concentration profiles of different individuals following drug administration. This is the change in drug concentration over time for a single day (A) and four days (B), where the white line depicts the median concentration, dark grey areas represent the interquartile range and light grey the remainder between min and max values.

Pharmacokinetic models are not useful on their own when drug effect needs to be fully described. Through the incorporation of pharmacodynamics, a measure of drug effect on disease progression can be predicted. Drug effect can be related to the concentration over time and drug profile as described in its PK. Since biophase distribution is extremely rapid, drug effects can often be directly related to drug concentrations in the blood plasma. The effect of DTG was modelled with the I_{max}-equation where the drug concentration efficacy is determined by using the IC_{50} value for DTG. This equation was used to calculate the drug efficacy over time in Figure 4.11, where the Y-axis is the drug efficacy ranging from 0 - 1. The efficacy fluctuates as the drug concentration fluctuates

in between doses. However, the efficacy never falls below 0.98, indicating that it is unlikely that drug-sensitive viral replication will be able take place at any time during the day. The drug regimen of 50mg DTG daily is sufficient to suppress the viral life cycle and the likelihood of resistant strains emerging if the patient remains 100% adherent to their prescribed drug therapy.

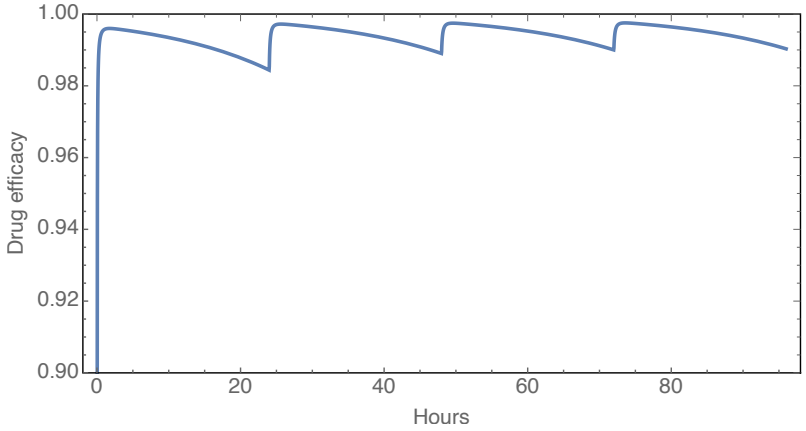

Figure 4.11: *Drug efficacy of DTG.* By using a pharmacodynamic model linked to the drug concentration profile of DTG, a prediction can be made in terms of the efficacy of the drug over time. The PD model makes use of the IC_{50} value for the drug to calculate the drug efficacy at a given drug concentration. Drug efficacy ranges from 0-1, where 0 means no inhibition and 1 means complete inhibition of viral production. The graph indicates the efficacy of DTG for four days following daily administration and fluctuates over time as the drug concentration does.

4.2.2 Lopinavir/Ritonavir

A model of Lopinavir co-formulated with Ritonavir (LPV/RTV) was created by Wang et al. [6]. A four compartment model best described the pharmacokinetics of the drugs of which a schematic representation is shown in the previous chapter in Figure 3.7. This four compartment model consists of linked models, one for LPV and one for RTV. This model was successfully reproduced in Wolfram Mathematica [15] and the drug plasma concentration plots were similar to those published in the article. Model simulations were performed to predict the change in total (LPV_t) and free (LPV_f) drug plasma concentration over a 12 hour period during the second week of treatment. The simulated dosage administered at t=192 (day 8) was 400/100 mg LPV/RTV. In Figure 4.12 the pharmacokinetic model is used to predict the change in drug concentration after an oral dose for 12 hours. Four hours after administration, the drug has been absorbed and reaches peak concentration in the in the blood plasma. In Figure 4.13 this is extended for multiple days with a twice daily oral administration of the drug. During the first 8 dosages there

is a gradual accumulation of the free form LPV$_f$ whereafter it plateaus. The simulation result shows the peak concentration is reached 4 hours after administration and the daily fluctuation in the drug plasma concentration. Fluctuations are expected because as soon as the drug has been absorbed, the body starts working to distribute, metabolise and excrete it (ADME). These four mechanisms all influence the drug levels and kinetics of drug exposure.

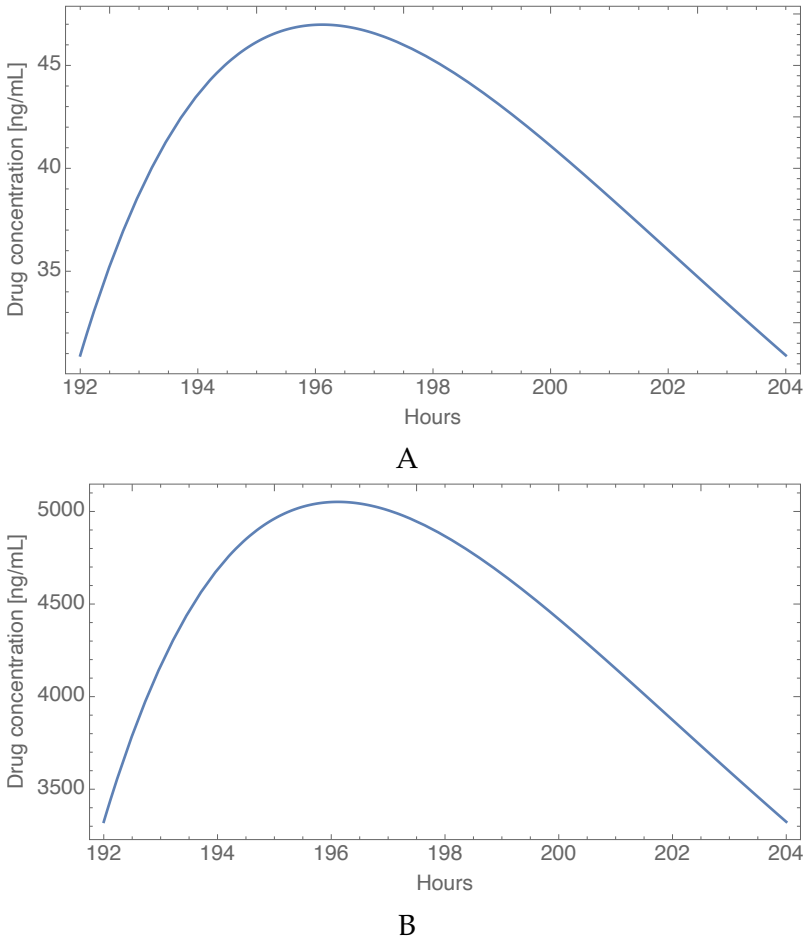

Figure 4.12: *Validation of the LPV/r pharmacokinetic model.* The pharmacokinetic model for LPV/r is coded and validated. Co-formulated bi-daily lopinavir/ritonavir is administered orally with a dosage of 400/100mg. The plots are similar to those published in the original article and show the first dose of week two (day 8). Shown here is (A) LPV$_{free}$ and (B) LPV$_{total}$.

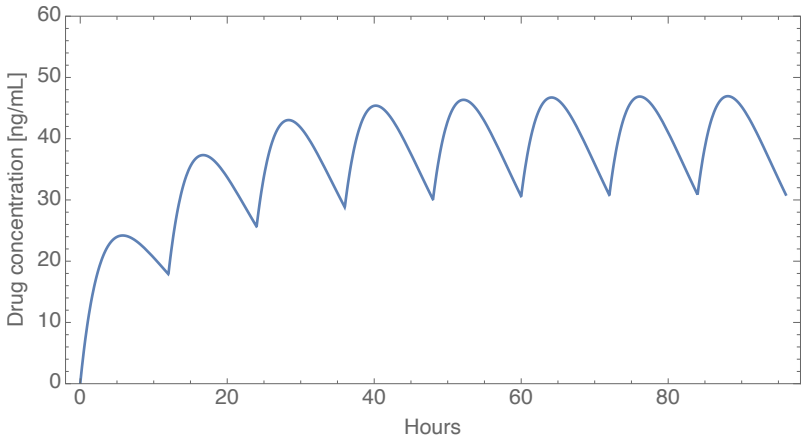

Figure 4.13: *Multiple dose drug concentration profile of LPV.* LPV/RTV is administered orally bi-daily with a dosage of 400/100mg. The drug reaches peak concentration 4 hours after the dose is given. Plotted above is LPV_f, the free form of the drug, where during the first 8 dosages there is a gradual accumulation of LPV_f.

Along with the population PK parameter estimates, the authors of the LPV/RTV model reported data for interindividual variability on a large number of parameters, which can be found in Table 3.7. This data can be used to simulate patient heterogeneity by sampling parameter values from their associated distributions. This allows for numerous sets of parameters to be generated, each representing a unique individual in the population. 1000 parameter sets were generated (N=1000 virtual patients) with a simulated dosage of 400/100 mg LPV/RTV. The results of the variation in the predicted plasma concentration time profiles are shown in Figure 4.14 below, where the white line depicts the median concentration, dark grey areas represent the interquartile range and light grey the remainder between min and max values. In this result, drug concentration profiles can vary dramatically in the population due to patient heterogeneity.

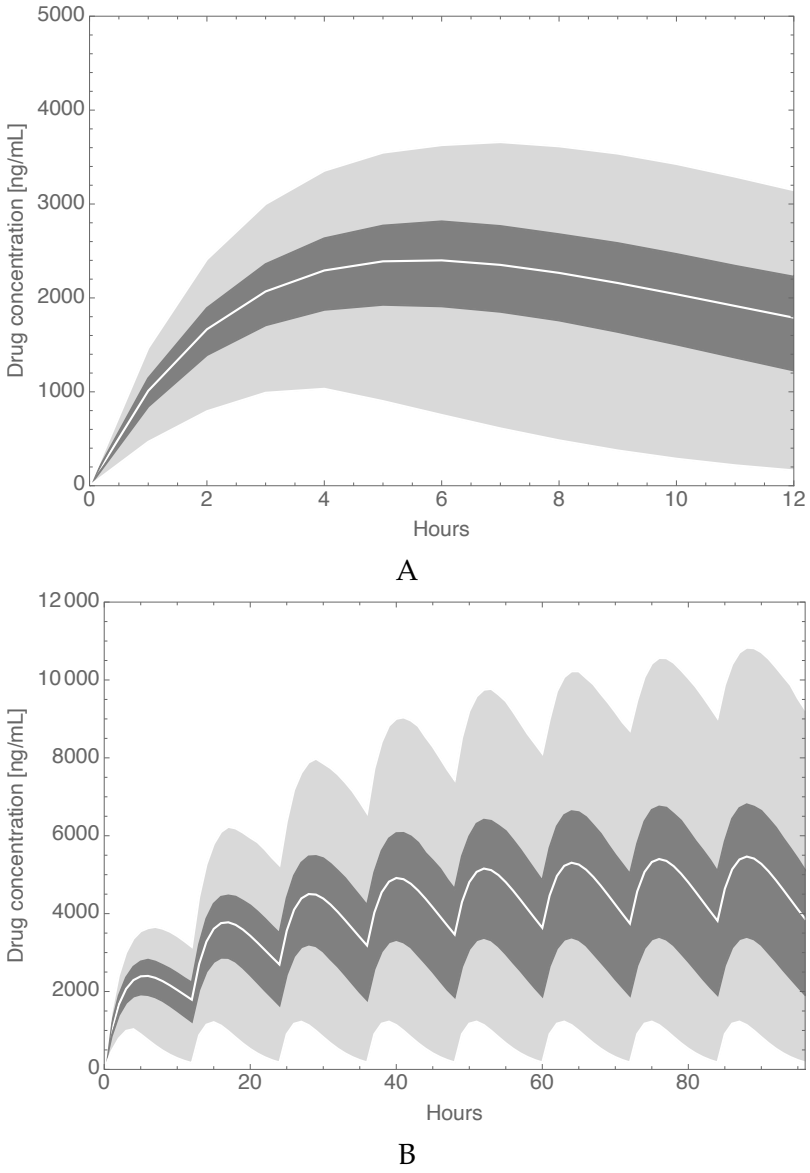

Figure 4.14: *Monte Carlo simulation of LPV/RTV model.* Model simulations were performed using 1000 parameter sets generated from Table 3.7. The variation in these parameter sets represent the patient heterogeneity which result in a variation in the drug concentration profiles of different individuals following drug administration. This is the change in drug concentration over time for a single day (A) and four days (B), where the white line depicts the median concentration, dark grey areas represent the interquartile range and light grey the remainder between min and max values.

The effect of LPV/RTV was modelled with the I_{max}-equation where the drug concentration efficacy is determined by using the IC_{50} value for LPV. This equation was used to calculate the drug efficacy over time as shown in Figure 4.15, where the Y-axis is the drug efficacy ranging from 0 - 1. The increase in efficacy over the first few days can be seen as there is a gradual accumulation of the drug in the body and the efficacy fluctuates slightly

as the drug concentration fluctuates in between doses. However, the efficacy never falls below 0.7, indicating that it is unlikely that viral replication will be able take place at any time during the day.

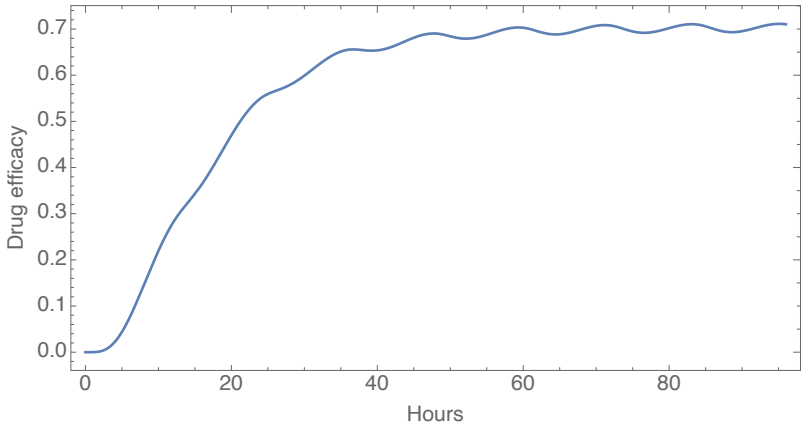

Figure 4.15: *Drug efficacy of LPV/r.* By using a pharmacodynamic model linked to the drug concentration profile of LPV, a prediction can be made in terms of the efficacy of the drug over time. The PD model makes use of the IC_{50} value for the drug to calculate the drug efficacy at a given drug concentration. Drug efficacy ranges from 0-1, where 0 means no inhibition and 1 means complete inhibition of viral reproduction. The graph indicates the efficacy of LPV for four days following bi-daily administration and fluctuates over time as the drug concentration does.

4.2.3 Tenofovir

A model of Tenofovir was developed by Duwal et al. [4], who found that a two compartment model best described the TFV plasma pharmacokinetics and of which a schematic can be seen in the previous chapter in Figure 3.6. This model was successfully reproduced in Wolfram Mathematica [15] and the drug plasma concentration plots were similar to those published in the article. Model simulations were performed to predict the change in TFV plasma concentration over a 24 hour period. The simulated dosages administered at t=0 were 75, 150, 300 and 600 mg of TDF respectively. Figure 4.17 shows the drug concentration profile for 24 hours after a single dose. Two hours after administration the drug reaches peak concentration in the in the blood plasma. Daily fluctuations in the drug plasma concentration can also be noted in the simulation result in Figure 4.18. Fluctuations are expected because as soon as the drug has been absorbed, the body starts working to distribute, metabolise and excrete it (ADME). These four mechanisms all influence the drug levels and kinetics of drug exposure.

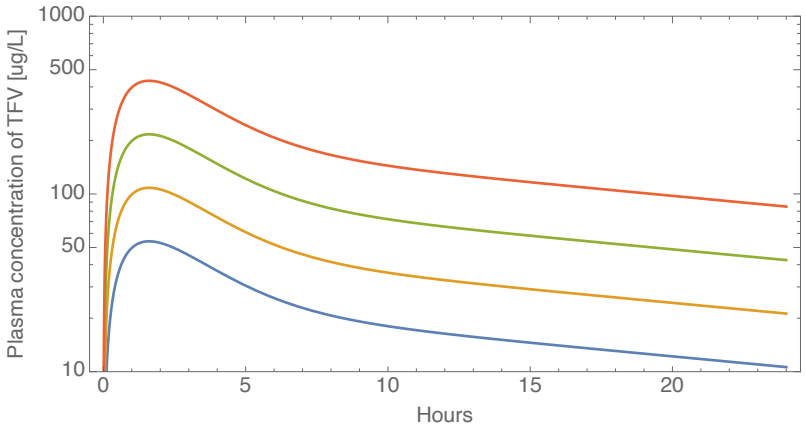

Figure 4.16: Validation of TDF model

Figure 4.17: *Validation of the TDF pharmacokinetic model.* The model used to simulate drug therapy with tenofovir is coded and validated. Plotted is the simulated drug concentration in the blood plasma over time for a single dose after initiation of treatment. The simulated dosages administered at t=0 were 75 (blue), 150 (yellow), 300 (green) and 600 (red) mg of TDF respectively. Peak plasma drug concentration is reached two hours after administration.

This model includes a cellular compartment (C_{cell}) which represents the concentration of TFV-DP in peripheral blood mononuclear cells (PBMCs). In Figure 4.18 the model prediction shows that there is a gradual accumulation of the intracellular active form TFV-DP in the cells whereafter it starts to approach a plateau. This plateau level is reached after about approximately 21 dosing events on average.

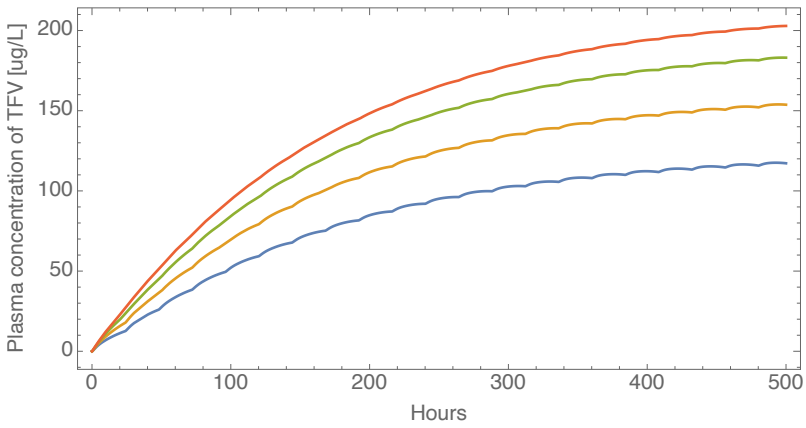

Figure 4.18: *Accumulation of TFV-DP in PBMCs.* The model used to simulate drug therapy with tenofovir includes a cellular compartment, where the drug has entered peripheral blood mononuclear cells. In this compartment the drug accumulates over the first 21 days of treatment before a plateau is reached. The daily simulated dosages administered were 75 (blue), 150 (yellow), 300 (green) and 600 (red) mg of TDF respectively.

The authors included variability estimates for two parameters: (V_{max}) and (k_{out}). These

values along with the rest of the parameters can be found in Table 3.6. As described above, this data can be used to simulate patient heterogeneity by generating parameter sets, each representing a unique individual in the population. Parameter sets were generated (N=1000 virtual patients) and the results of the variation in the predicted plasma concentration time profiles are shown in Figure 4.19 below, where the white line depicts the median concentration, dark grey areas represent the interquartile range and light grey the remainder between min and max values. Patient heterogeneity results in the drug concentration profile showing dramatic variation and impacts the model's predictive capability.

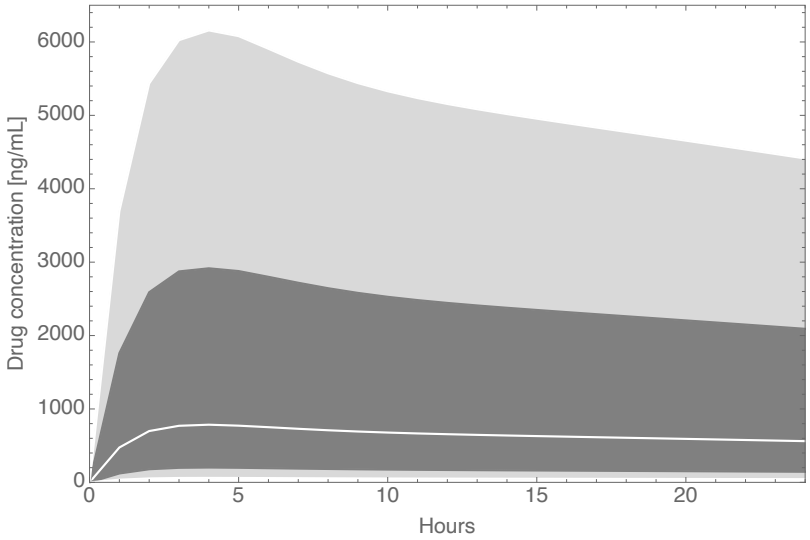

Figure 4.19: *Monte Carlo simulation of TDF model (single dose).* Model simulations were performed using 1000 parameter sets generated from Table 3.6. The variation in these parameter sets represent the patient heterogeneity which result in a variation in the drug concentration profiles of different individuals following drug administration. This is the change in drug concentration over time (24 hours) following a single dose, where the white line depicts the median concentration, dark grey areas represent the interquartile range and light grey the remainder between min and max values.

The effect of TDF was modelled with the I_{max}-equation where the drug concentration efficacy is determined by using the IC_{50} value for TDF. For this drug, the PD model prediction of drug efficacy is based on the cellular drug concentration. This equation was used to calculate the drug efficacy over time as shown in Figure 4.20, where the Y-axis is the drug efficacy ranging from 0 - 1. The increase in efficacy over the first three weeks can be seen as there is a gradual accumulation of the drug in the body. The efficacy

starts to approach a plateau at approximately 0.7, indicating that it is unlikely that viral replication will be able take place.

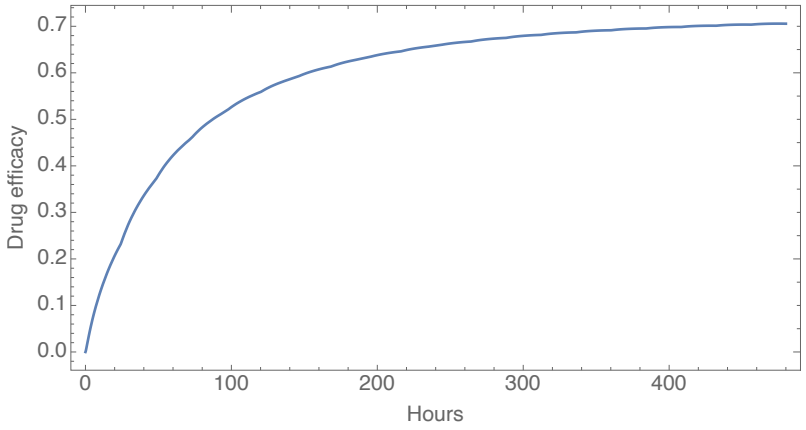

Figure 4.20: *Drug efficacy of TDF.* By using a pharmacodynamic model linked to the drug concentration profile of TDF, a prediction can be made in terms of the efficacy of the drug over time. The PD model makes use of the IC_{50} value for the drug to calculate the drug efficacy at a given drug concentration. Drug efficacy ranges from 0-1, where 0 means no inhibition and 1 means complete inhibition of viral reproduction. The graph indicates the efficacy of TDF over three weeks following daily administration.

4.2.4 Emtricitabine

A model of Emtricitabine (FTC) was created by Valade et al. [7], who found that a two compartment model best described the FTC plasma pharmacokinetics as shown the previous chapter in Figure 3.5. This model was successfully reproduced in Wolfram Mathematica [15] and the drug plasma concentration plots were similar to those published in the article. Model simulations were performed to predict the change in TFV plasma concentration over a 24 hour period. The simulated dosage is 200 mg once daily and the result of this simulation can be seen below in Figure 4.21. The drug in the central blood plasma compartment reaches its peak concentration two hours after oral administration. Two compartments are included in this model, the blood plasma compartment and a seminal plasma compartment. Our compartment of interest remains the compartment representing the blood plasma drug concentration.

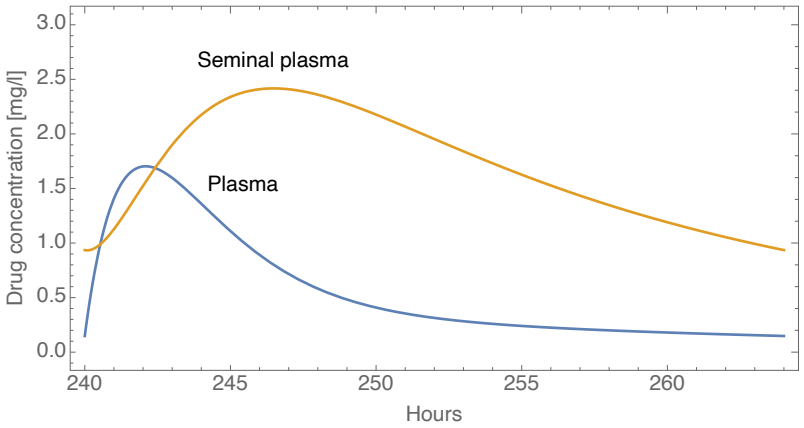

Figure 4.21: *Validation of the FTC pharmacokinetic model.* The model used to simulate drug therapy with emtricitabine is coded and validated. Plotted is the simulated drug concentration in the blood plasma over time for a single dose at day 10. The blue line indicates the drug concentration in the blood plasma and the orange line indicates the change in drug concentration in the seminal compartment.

The authors included interindividual variability estimates for the two parameters: apparent elimination clearance (CL/F) and blood plasma to seminal plasma transfer rate constant (k_{1e}). These values along with the rest of the parameters can be found in Table 3.5. As described above, this data can be used to simulate patient heterogeneity by generating parameter sets, each representing a unique individual in the population. 1000 parameter sets were generated (N=1000 virtual patients) with a simulated dosage of 200 mg FTC daily for four days. The results of the variation in the predicted plasma concentration time profiles are shown in Figure 4.22 below, where the white line depicts the median concentration, dark grey areas represent the interquartile range and light grey the remainder between min and max values. Patient heterogeneity results in variation in the drug concentration profile for different individuals, however this model performs better than the previous TDF model to more realistically represent this even if the TDF model had fewer varied parameters.

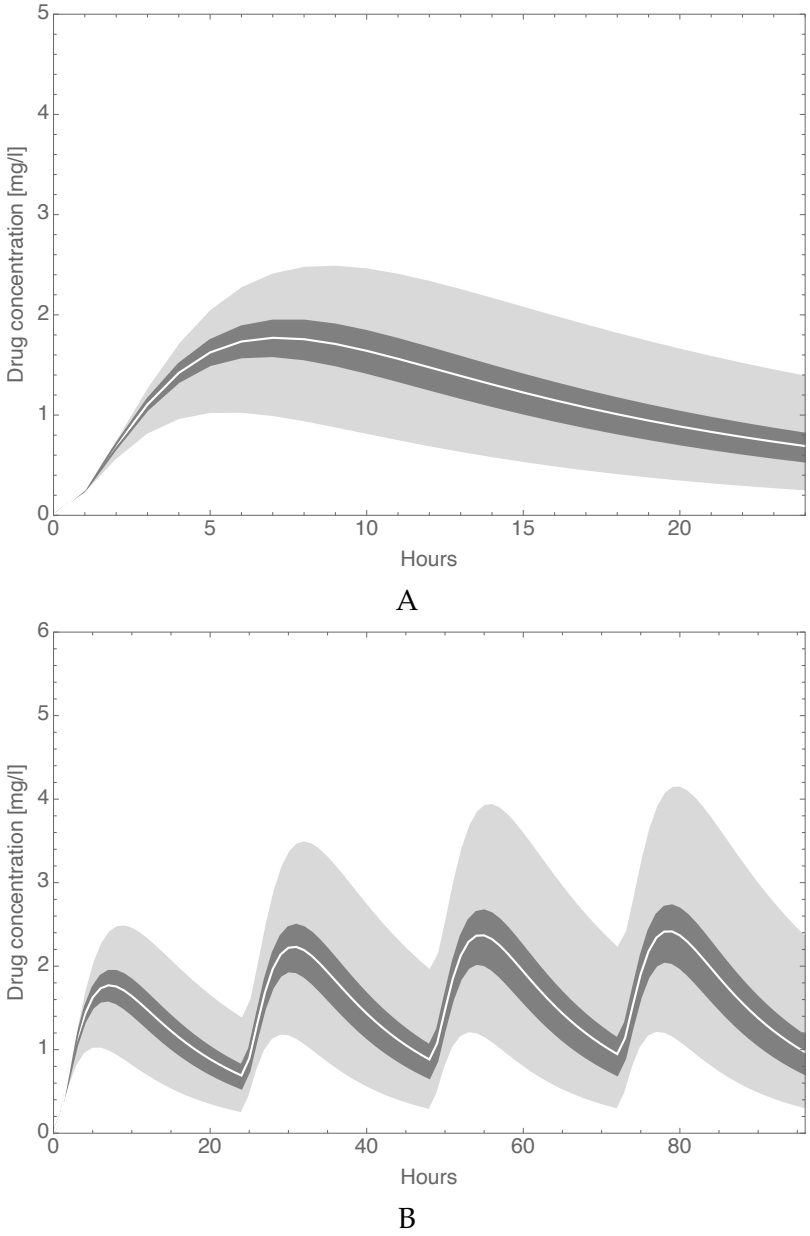

Figure 4.22: *Monte Carlo simulation of FTC model.* Model simulations were performed using 1000 parameter sets generated from Table 3.5. The variation in these parameter sets represent the patient heterogeneity which result in a variation in the drug concentration profiles of different individuals following drug administration. This is the change in drug concentration over time for a single day (A) and four days (B), where the white line depicts the median concentration, dark grey areas represent the interquartile range and light grey the remainder between min and max values.

The effect of FTC was modelled with the I_{max}-equation where the drug concentration efficacy is determined by using the IC_{50} value for FTC. This equation was used to calculate the drug efficacy over time as shown in Figure 4.23, where the Y-axis is the drug efficacy ranging from 0 - 1. The efficacy fluctuates slightly as the drug concentration fluctuates

in between doses. However, the efficacy never decreases sharply, indicating that it is unlikely that viral replication will be able take place at any time during the day. The drug regimen of 200mg FTC daily is sufficient to suppress the viral life cycle and the likelihood of resistant strains emerging.

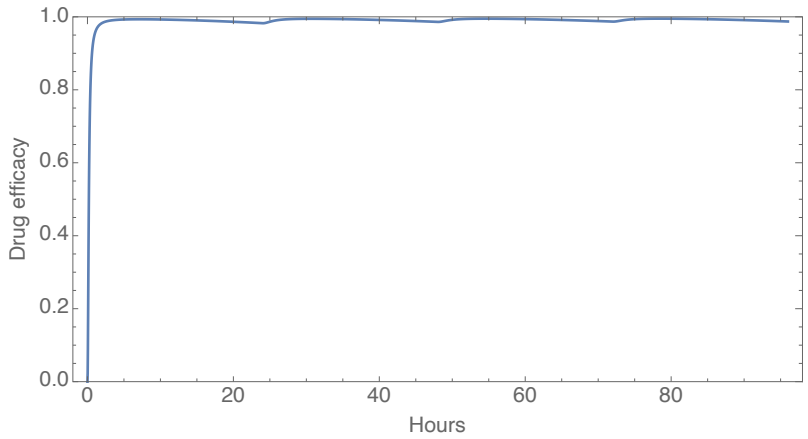

Figure 4.23: *Drug efficacy of FTC.* By using a pharmacodynamic model linked to the drug concentration profile of FTC, a prediction can be made in terms of the efficacy of the drug over time. The PD model makes use of the IC_{50} value for the drug to calculate the drug efficacy at a given drug concentration. Drug efficacy ranges from 0-1, where 0 means no inhibition and 1 means complete inhibition of viral reproduction. The graph indicates the efficacy of FTC over four days following daily drug administration.

4.3 Combined PKPD-disease models

Constructing the combined PKPD-disease models was accomplished by linking each of the HIV models to the PKPD models of the ARVs. This was achieved through the use of the drug efficacy parameters, which were implemented as reducing the viral replication and/or infection of healthy cells by a factor ranging between 0 and 1. The HIV disease models were originally published with a constant ϵ value, often 0.8 or 0.9. The combined PKPD-disease models allow for the value of ϵ to vary over time as the drug concentration varies over time, as shown for the ARV models in Figure 4.11, 4.15, 4.20 and 4.23. As discussed in Chapter 3, a drug concentration profile is determined by the relevant PK model. The drug concentration influencedsthe efficacy parameter as determined by the relevant PD model. The constant drug efficacy parameters in the disease models are then replaced by these time-varying efficacies.

As shown in the previous section, regular drug dosing leads to sustained efficacies that are similar to the published constant values of the efficacies in the disease models and one

can therefore expect the disease model to behave in a similar way under these conditions. However, a disease model with a constant efficacy cannot be used to evaluate the effect of incomplete adherence, time-dynamics related to dosing and the effect of heterogeneity on drug response and treatment outcome. The PKPD and HIV models all include measures of heterogeneity as described for the models in the previous chapter. Values for parameter distributions for the HIV models can be found in Table 3.3, 3.1, 3.2 and for the ARV PKPD models in Table 3.4, 3.5, 3.6 and 3.7. Patient heterogeneity in the PKPD models result in variation of ϵ and thus also in the efficacy of the drug blocking viral replication. For simulations, parameter values were sampled from their associated distributions. This was done for all the varied parameters, from both HIV and PK models, allowing for numerous sets of parameters to be generated (N=10 000). These simulation results can provide a more complete picture, since they include patient variability in terms of the response to drug and in terms of the natural biological variability.

4.3.1 The effect of combination antiretroviral therapy

CD4$^+$ T-cells The effect of treatment was examined by switching on combination ART when performing the simulations. After the uninfected steady state is reached, virus is introduced before treatment was initiated. All models start with a T-cell count in the normal healthy range between 1000-1500 cells/mm^3. In Figure 4.24 there is an initial drop in the T-cell count when virus is introduced. Treatment is initiated after 200 days and there is an increase and recovery in the T-cell count. Kamboj1 is the model which recovers the fastest back to the normal healthy level of T-cells. Wang1 has a slower rate of recovery due to the presence of latently infected cells, which remain difficult to target with drug therapy. Rong1 does not recover to normal levels due to the formation of drug resistant strains which cannot be eradicated. For these models, both classes of ARVs and combination treatment result in similar outcomes.

Viral load Continuing in Figure 4.24, as expected there is an initial spike in the viral load when virus is introduced to healthy individuals. This is accompanied by the initial drop seen in the CD4$^+$ T-cell count. Viral load is suppressed to below detectable limits at day 200 when treatment is switched on for the Kamboj1 and Wang1 models. However, the Rong1 model continues to harbour low levels of viral replication. This is due to the presence of drug resistant viral strains which are able to escape treatment due to

mutation which has taken place. For these models, both classes of ARVs and combination treatment result in similar outcomes. The simulation was also performed by selectively switching on only PI or RTI to examine their effects independently and the results can be found in the Appendix, sections A.1.1 and A.1.2 respectively.

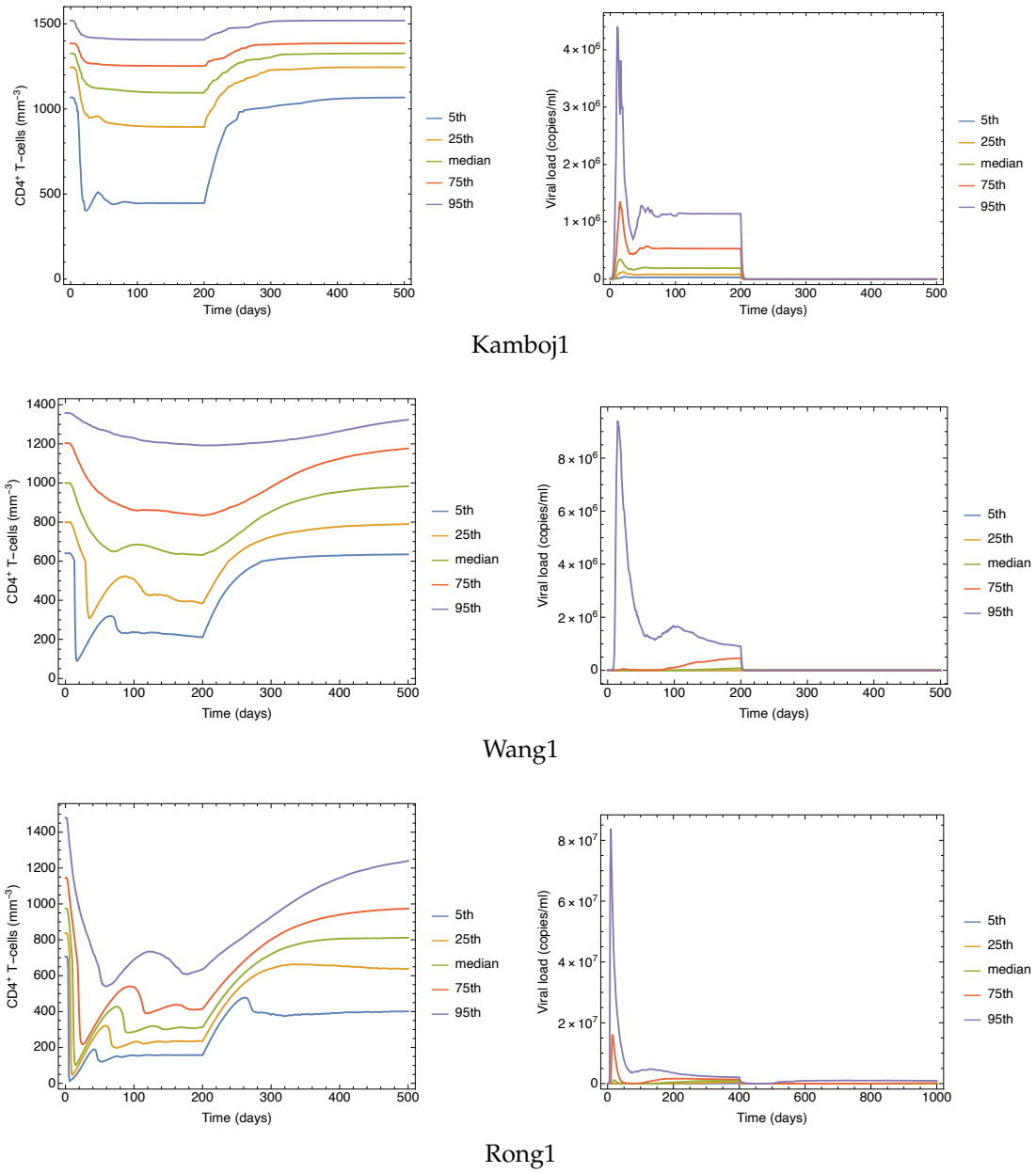

Figure 4.24: *The effect of combination ART on CD4⁺ T-cells and viral load.* Monte Carlo simulations were performed on three HIV models to determine the effect of combination RTI and PI treatment on disease progression for Kamboj1, Rong1 and Wang1. The simulation starts at the uninfected equilibrium state. Virus is then introduced and allowed to approach a steady state with a simulation time of 200 days. RTI and PI treatment is then switched on. Percentile results were generated from 10 000 parameters sets sampled from the distributions for both the HIV disease models and the PKPD models of the ARVs.

4.4 Treatment initiation and comparison to clinical data

The combined PKPD-disease models were analysed to examine the effect of treatment initiation time on patient recovery. During these simulations, treatment start day ranged from 0 - 3000 days after infection had taken place. This was done to span the range of days reported in the patient data [84, 86]. Results are compared to viral load and $CD4^+$ T-cell count data. $CD4^+$ counts and viral load measurements were determined using fasted venous blood samples as described in [84, 86].

During model simulations, it was assumed that patients are fully adherent and that the same prescribed dosage is taken every day. Days since infection and day of treatment initiation were obtained from the self-reported patient information.

4.4.1 $CD4^+$ T-cell count simulation and comparison with clinical data

The effect of different classes of ARV were examined by selectively switching on RTI, PI or combination ART when performing the simulation. Data points from the study were also selected according to the drug regimen that each patient was following. In Figure 4.25 before virus is introduced, all three models have T-cell counts in healthy expected ranges. In the plots the green surface represents the maximum values of all simulations, the blue surface represents the median values and the orange surface represents the minimum values. When virus is introduced, there is an immediate drop in the T-cell count. If treatment is started shortly after infection, recovery is rapid and happens within the first 5 days of infection according to model prediction. If treatment is only started once steady state of infection is reached, the rate of recovery will be independent of when treatment is started. In all cases recovery is complete, the viral load becomes undetectable and T-cell counts return to healthy levels.

The Kamboj1 model performs the worst in containing all the data points within its simulated ranges of T-cell counts in Figure 4.25. Only one of the data points falls near the median, with the rest of the data points falling below the minimum. This result is because of the structure of the Kamboj1 model as it does not include latency or drug-resistance. This model is unable to explain this data, if we assume that strict adherence to the prescribed regimens were followed, that there were no additional biological features present in the patients (e.g. latency, resistance), and that patient parameters remained constant

for the duration of the simulation. Wang1 performs better than Kamboj1 and many of the clinical data points fall closer to the minimum, whereas Rong1 performs the best in simulating T-cell counts which are also reflected by the clinical data. This model includes the effect that drug-resistance has on T-cell health and many of the data points fall close to the median. The simulation was also performed by selectively switching on only PI or RTI to examine their effects independently and the results can be found in the Appendix in Figure A.3 and A.4.

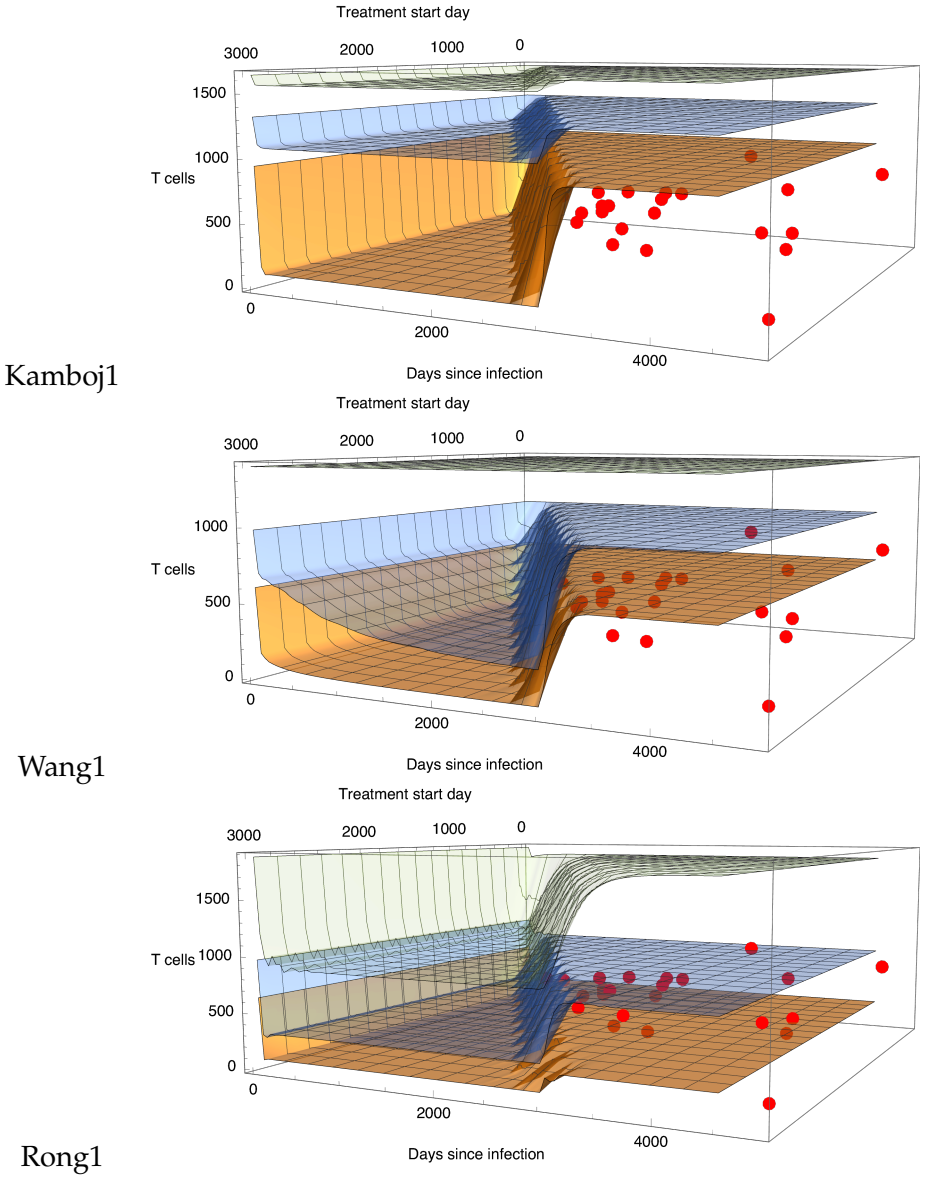

Figure 4.25: *The effect of combination ARV treatment on CD4$^+$ T-cells with clinical data.* A Monte Carlo simulation was performed on the model to examine the effect of treatment start day on recovery. From 1000 simulations, the surfaces represent the following: orange=minimum; blue=median; green=maximum. The region between the orange and the green surface therefore represent the whole range of model predictions given the parameter distributions. The simulation starts at the uninfected equilibrium state. Virus is introduced with a treatment start day ranging from 0-3000 days after infection. Results were generated from 1000 parameters sets sampled from the distributions for both the HIV disease models and the PKPD models of the ARVs. The simulation results are plotted with patient data (red dots) from [86].

4.4.2 Viral load simulation and comparison with clinical data

There is an initial spike in the viral load when virus is introduced which is accompanied by the initial drop seen in the $CD4^+$ T-cell count. According to model prediction in Figure 4.26 if treatment is started shortly after infection, the viral load is suppressed to below detectable limits within the first 5 days of treatment. In the plots the green surface represents the maximum values of all simulations, the blue surface represents the median values and the orange surface represents the minimum values. Similarly to the T-cells, the rate of recovery will be independent of when treatment is started. In all cases recovery is complete and the viral load becomes undetectable. The simulation results for Kamboj1 and Wang1 do not compare well to the clinical data. In both models the simulated viral load falls to very low levels, when the patient data remains at the untreated level of the simulations. The assumption that patients are adhering to treatment cannot be explained by modelling results. Rong1 performs better in being able to simulate realistic patient data. The majority of the patient data points lie within Rong1 model predictions. Rong1 performs better due to the presence of low-level drug-resistant viral replication taking place. The simulation was also performed by selectively switching on only PI or RTI to examine their effects independently and the results can be found in the Appendix in Figure A.5 and A.6.

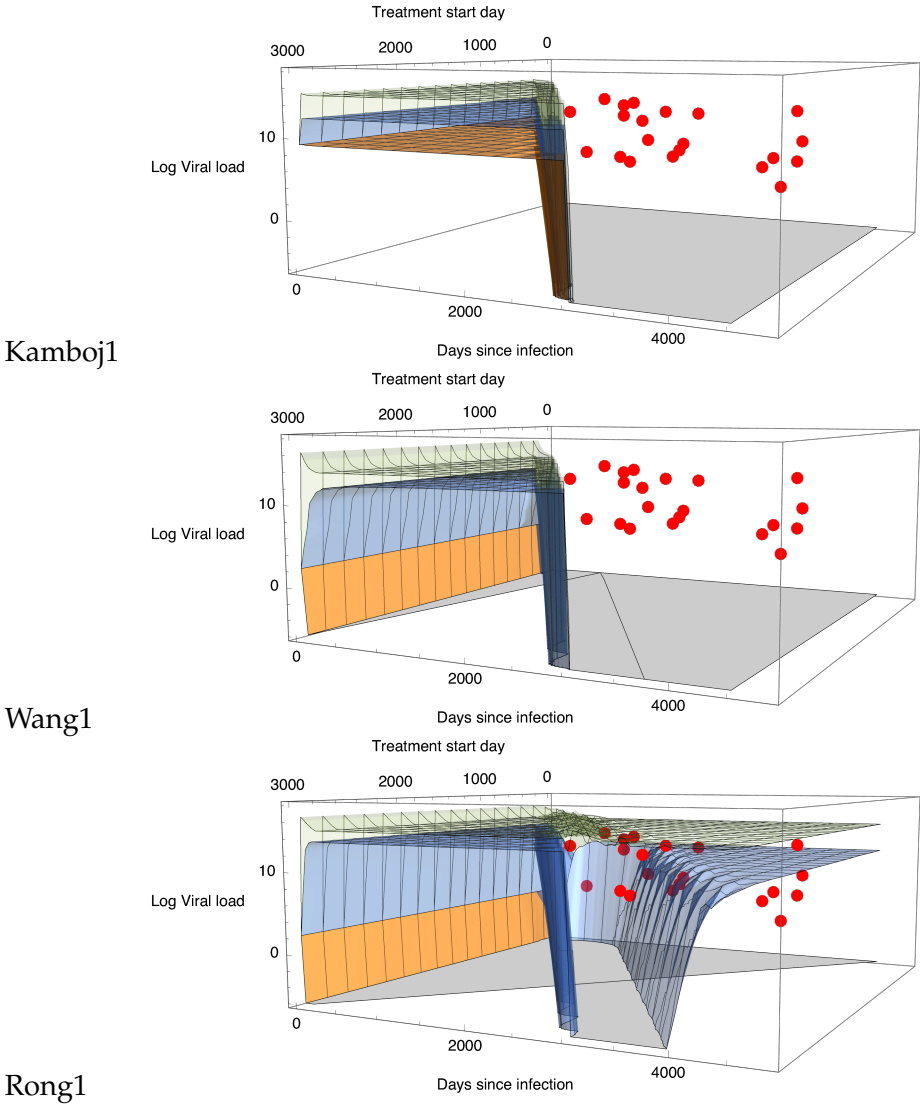

Figure 4.26: *The effect of combination ARV treatment on viral load with clinical data.* A Monte Carlo simulation was performed on the model to examine the effect of treatment start day on recovery. From 1000 simulations, the surfaces represent the following: orange=minimum; blue=median; green=maximum. The region between the orange and the green surface therefore represent the whole range of model predictions given the parameter distributions. The simulation starts at the uninfected equilibrium state. Virus is introduced with a treatment start day ranging from 0-3000 days after infection. Results were generated from 1000 parameters sets sampled from the distributions for both the HIV disease models and the PKPD models of the ARVs. The simulation results are plotted with patient data (red dots) from [86].

4.5 The effect of incomplete treatment adherence

The Wang1 combined PKPD-disease model simulation outcome was analysed to examine the effect of treatment adherence. MC simulations were performed to determine if incomplete drug adherence results are more reflective of clinical patient data when compared to the $CD4^+$ T-cell counts and for viral load measurement. The effect was examined by selectively switching on RTI, PI or combination ART when performing the simulation. Data points from the study were also selected according to the drug regimen that each patient was following. Adherence was modelled as 10% i.e. there is a 10% chance every day that the patient takes their medication.

4.5.1 $CD4^+$ T-cells

Simulations start with a T-cell count in the healthy range between 1000 - 1500 cells/mm^3. There is an initial drop in the T-cell count when virus is introduced. The green surface represents the maximum values, the blue surface represents the median values and the orange surface represents the minimum values of the MC simulations where 1000 parameter sets were randomly selected from the parameter distributions in the plot shown in Figure 4.27. Treatment start day ranges from 0 - 3000 days after infection takes place. When treatment is initiated there is an increase and recovery in the median T-cell count (blue surface) in some cases. However, in comparison to the previous Wang1 simulations in Figure A.3, A.4 and 4.25, where model adherence was assumed to be 100%, 10% adherence monotherapy with either RTI or PI results in many cases where the minimum (orange surface) does not recover back to healthy levels. When compared to clinical patient data, the weaker recovery of T-cells for RTI/PI monotherapy seem to be more reflective of the data. Simulating combination therapy with 10% results in stronger T-cell count recovery compared to monotherapy with the majority of the simulation outcomes being higher than the patient data. Although it could be that the discrepancies between modelling results and clinical patient data are exasperated by a lack of complete longitudinal data, these results indicate that the self-reported patient data could, in fact, be incorrect and that some patients were not 100% adherent to treatment.

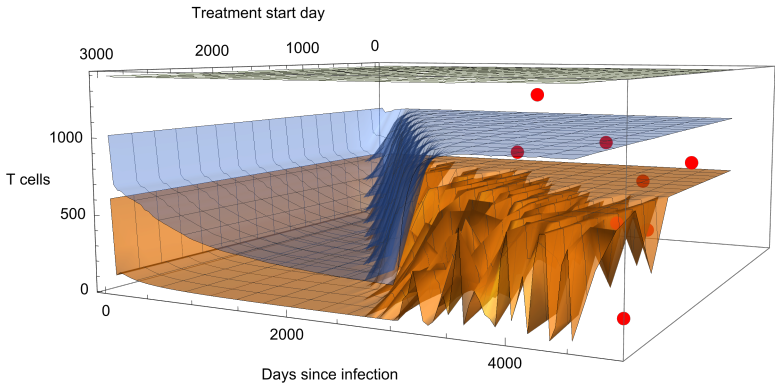

RTI

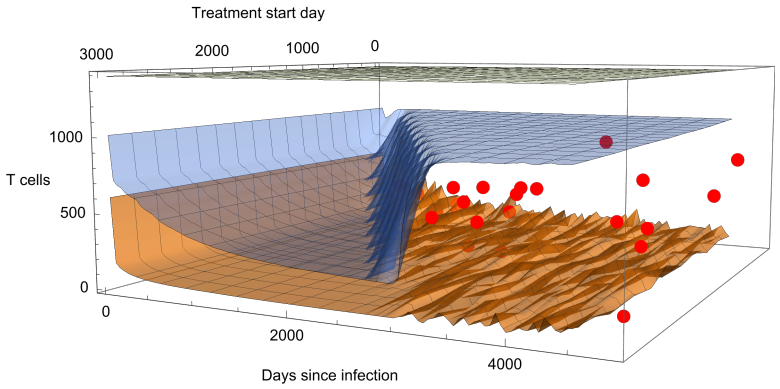

PI

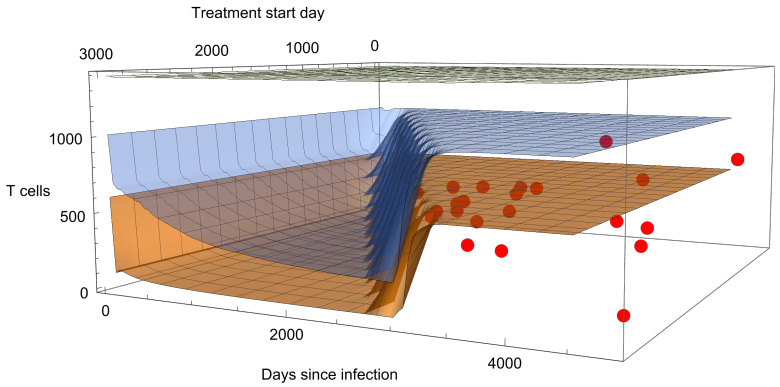

Combination

Figure 4.27: *The effect of irregular treatment adherence on CD4$^+$ T-cells.* Monte Carlo simulations were performed to determine if irregular drug adherence results in Wang1 model simulation of treatment outcomes and disease progression to be more reflective of clinical patient data. The simulation starts at the uninfected equilibrium state. Virus is then introduced and RTI, PI or combination treatment is switched on with a range of 0-3000 day after infection has taken place. Percentile results were generated from 1000 parameters sets sampled from the distributions for both the HIV disease models and the PKPD models of the ARVs. Irregular drug adherence was modelled with a probability of 10%. Simulation results are plotted with patient data (red dots) from [86]. These results are in comparison to the results for Wang1 in Figure A.3, A.4 and 4.25, where adherence was assumed to be 100%. The scalloped appearance on plot surfaces are not significant and are as a result of the scanning grid which is used to interpolate the plot surfaces.

4.5.2 Viral load

In Figure 4.28, as expected, there is a spike in the viral load when virus is introduced to healthy individuals. This is accompanied by the initial drop seen in the $CD4^+$ T-cell count when virus is introduced. The green surface represents the maximum values, the blue surface represents the median values and the orange surface represents the minimum values from the MC simulation results. Treatment start day ranges from 0 - 3000 days after infection takes place. When treatment is initiated there is a decrease in the viral load, with the median falling to below detectable limits in for all treatment options. However, 10% adherence monotherapy with either RTI or PI results in many cases where the load does not become undetectable (green surface). This is in comparison to the previous Wang1 simulations in Figure A.5 and A.6, where 100% adherence resulted in all cases becoming undetectable. When compared to clinical patient data (red dots), the high viral load for RTI/PI monotherapy seem to be more reflective of clinical data, where most data points fall between the maximum and the median. Combination therapy with both classes of drug results in all simulation outcomes with undetectable viral loads along with complete recovery of T-cells to healthy levels when adherence is 100%. Simulating combination therapy with 10% results in viral loads below those of the patient data. Similarly to the $CD4^+$ T-cell counts, the discrepancy between modelling result and clinical patient data are likely due to a lack of complete longitudinal clinical patient data or that the self-reported patient data were, in fact, not 100% adherent to treatment. Combination ART provides the strongest protection and results in all cases falling to below detectable limits for full and 10% adherence. However, the long term treatment of HIV/AIDS requires at least 95% adherence as reported in [87]. If treatment adherence is not 100%, regimen failure may happen because of the emergence of drug-resistant HIV variants, which are not accounted for in this disease model.

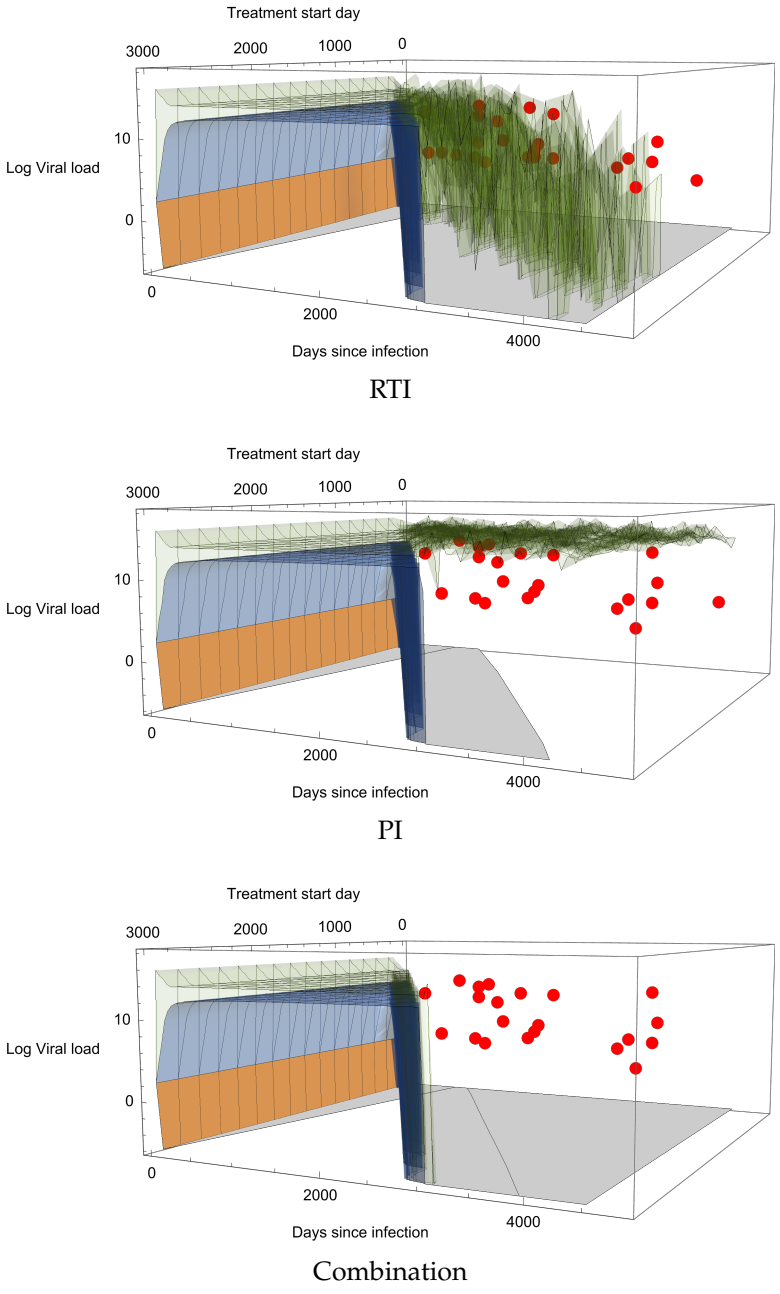

Figure 4.28: *The effect of irregular treatment adherence on viral load.* Monte Carlo simulations were performed to determine if irregular drug adherence results in Wang1 model simulation of treatment outcomes and disease progression to be more reflective of clinical patient data. The simulation starts at the uninfected equilibrium state. Virus is then introduced and RTI, PI or combination treatment is switched on with a range of 0-3000 day after infection has taken place. Percentile results were generated from 1000 parameters sets sampled from the distributions for both the HIV disease models and the PKPD models of the ARVs. Irregular drug adherence was modelled with a probability 10%. Simulation results are plotted with patient data (red dots) from [86]. These results are in comparison to the results for Wang1 in Figure A.5, A.6 and 4.26, where adherence was assumed to be 100%. The scalloped appearance on plot surfaces are not significant and are as a result of the scanning grid which is used to interpolate the plot surfaces.

Chapter 5

Conclusion

HIV infection has become a manageable disease thanks to the highly effective medications that are able to suppress viral replication. Great progress has been made by scientists and researchers in the 30 years since HIV was discovered. The current generation of ARV medications have fewer side effects than before and are able to exert prolonged control over viral replication. However, the rise in drug resistance has underlined the need for continued improvement of and research into new medications, firstly, to be able to treat drug resistant viral strains effectively and, secondly, to target the latent reservoir, which is seen as major barrier to a cure. Mathematical modelling is a valuable tool in researching and developing these new medications necessary to treat HIV.

In this study, mathematical models of HIV disease progression and pharmacological models of ARVs were selected from literature and reproduced. HIV models were chosen based on the structure and characteristics of each model. The Rong1 model includes the mutation of drug-resistant viral strains and with this the impact of drug-resistance on ARV therapy could be studied. Latently infected cells are defined in Wang1 and the model also shows more of the long-term dynamics of the immune system. Kamboj1 was most the simple model but it does well to describe the dynamics of the immune response to HIV and it also includes two stages of T-cell infection, pre-RT and post-RT. The PKPD models of the ARVs were chosen based on the currently prescribed triple-drug regimen for HIV treatment according to the South African Department of Health: two reverse transcriptase inhibitors with either a protease inhibitor or an integrase strand transfer inhibitor.

After models were reproduced, initial work included validating model simulations and analysing model performance with Monte Carlo (MC) simulations. This included a vi-

sual check of whether the reproduced model produces the same time-course plots as those in the published article. Further, the models' simulation results were compared to data ranges known from clinical research, for example, whether the model simulated T-cell counts and viral loads within expected biologically relevant ranges. PKPD model performance was validated by comparison to the results published in the original article and by comparing the predicted drug concentration for a realistic dosing regimen to the known IC_{50} value for every drug. Lastly, MC simulations were used to test the effect of patient heterogeneity in each model.

MC simulations showed that all three HIV disease models are able to encompass patient heterogeneity well and that even with variation in the parameter values, each model simulated the viral load within expected ranges. The result of the required drug efficacy scan of the HIV models showed how model structure and characteristics influence the prediction of the required drug effect for viral suppression in every model. Rong1 was the model which required the highest overall drug efficacy to bring the viral load to below detectable limits in a population, which was expected from a model that characterised the mutation of viral drug-resistance. From the MC result of the Kamboj1 model, it is apparent that the drug class also has an impact on model prediction. The Kamboj1 model, which makes provision for treatment with two different classes of ARVs indicated that a lower drug efficacy for the PI class is typically required than for the RTI class. The PKPD models of the ARVs were also analysed using MC simulations. Some faired worse at describing patient heterogeneity such as the MC simulation result of the TDF model. It is not clear if this is due to actual drug differences or differences in model structure and parameterisation. However, all PKPD models were still able to simulate a predicted plasma drug concentration which could be used with the relevant IC_{50} values to calculate the drug efficacy at different time points. Therefore, the construction of the combined PKPD-HIV disease models for the remaining research objectives could proceed.

Combined models for all combinations of disease models and treatment options were then constructed. Models of HIV disease progression were linked to the PKPD model through the used of the drug efficacy parameter ϵ. Following this, Monte Carlo simulations were performed to examine possible outcomes when taking patient heterogeneity into account. Disease progression could then be examined in a population of heterogeneous patients on different drug treatments. Lastly, these results were compared to

clinical patient data.

The combination of existing HIV disease and ARV PKPD models allowed for analyses to be performed for all the required combinations of disease models and treatment options. Whereas the initial simulations were based on the original drug effect already present in the models as published, in the subsequent simulations of combined models the drug effect parameter ϵ varied. The newly constructed combined PKPD-disease models allow for the value of ϵ to vary over time as the drug concentration varies over time. When the models of disease are linked to PKPD models of ARVs, it appears that the class of drug has a smaller impact on simulation outcome than the structure of the HIV model has. Indeed, when T-cell count and viral load time-courses for the same HIV model but different drug treatments are compared, there is little difference. However, when disease models are compared to each other, the results indicate the presence of latently infected cells and drug-resistant viral strains have an impact on T-cell health and recovery. The Rong1 model showed that drug-resistant virus was never completely suppressed. Whereas the presence of latently infected T-cells in the Wang1 model resulted in the T-cell count never fully recovering. Comparing the results to clinical data exposed shortcomings from both model simulations and a lack of complete longitudinal clinical patient data used for validation. Kamboj1 and Wang1 were unable to simulate viral loads in the same ranges as those from the patient data, whereas Rong1 simulated viral loads reflective of the data due to the presence of low level drug-resistant viral production taking place. Rong1 simulated $CD4^+$ T-cell counts containing most of the patient data points with Wang1 simulating T-cell counts higher than the majority of the patient data and Kamboj1 not simulating any T-cell counts in the range of the patient data. The simplest model, Kamboj1, faired the worst in predicting realistic disease outcomes due to its simplicity and lack of drug-resistance and latency. Following this, we examined whether altering the simulated adherence in the Wang1 model could improve its predictions.

The adherence of patients in the study was initially assumed to be 100%, since this is not accounted for in the self-reported dataset. Results show this may not be the case due to the ranges of viral load and $CD4^+$ T-cell counts that were reported and compared to model results. Including a measure of non-adherence to drug therapy improved Wang1 model predictions and made them more reflective of patient data. When comparing the results of 10% to 100% adherence in Wang1, both viral load and $CD4^+$ T-cell count simu-

lations improved and were closer to the patient data points. However, when considering the differences between the treatment options of monotherapy or combination therapy, a discrepancy between the simulation results and patient data points show that the self-reported data set is lacking completeness in terms of the reported adherence. As is also known from clinical data, if treatment adherence is not 100%, regimen failure may happen because of the emergence of drug-resistant HIV variants, which are not accounted for in the Wang1 disease model. **Overall, the results show that model structure and assumptions that are made regarding, for example, disease dynamics and treatment adherence, have a significant impact on whether a model is able to give a realistic prediction of drug response and treatment outcomes.**

The current findings rest on the following assumptions: parameters are independent of one another and covariances are accounted for in model structure; self-reported patient data was complete and accurate; patients were treatment-adherent; and biological parameters remained constant where not specified in terms of observed ranges. In terms of the clinical patient data from the HAART to HEART study, the comparison results could be improved by using a dataset which has more complete data for each patient. Longitudinal data for patients over time would greatly improve the quality of the validation as this would allow for a patient's viral load and T-cell count to be tracked over time.

The mathematical modelling of disease and drug treatment is a valuable tool often used in researching HIV and the treatment thereof. We used independent models of differing complexity without prior assumptions about the population and evaluated the predictive capability of the combined models without refitting the parameters. This is in comparison to well-controlled clinical trials where PKPD-HIV models are often constructed based on a single cohort. We showed that the structure of the disease models could have a significant impact on simulation results. It is important that the models used today are complex enough to describe the phenomena which have an effect on disease outcome. In terms of HIV, this includes the development of drug-resistant strains and the effect of long-lived latently infected cells. Disease models are often fitted with PKPD models to parameterise or determine drug effects. If model structures are not adequate (or data inappropriate), this could lead to unrealistic parametrisations for both types of models. The assumptions that are made when models are constructed and parameterised should therefore be considered carefully as they could have a significant impact on the accuracy

of the simulations. The structure of HIV models can be improved by accounting for more of the mechanisms which affect disease outcome such as drug-resistance, the latently infected reservoir of virus and how the different classes of drugs suppress different stages in the viral life cycle. PKPD models can be improved by refining the structure of the models to include compartments such as the cellular drug concentration; the process of the binding of the drug to the receptor through which it enters the cell; and importing *in vivo* IC_{50} measurements. Future work should also include improving model predictions by basing parameter values on large longitudinal data sets.

Ultimately such combined models could be used as diagnostic tools where, based on patient data, a model could suggest an optimal drug regimen according to each patient's unique characteristics. This may include suggestions of classes of drugs to use which take into account past events of drug-resistance and therapy failure. Continually improving models in this manner will result in them remaining powerful tools to be used in the era of personalised medicine.

Appendices

A.1 Additional analysis results of combined PKPD-disease models.

A.1.1 The effect of reverse transcriptase inhibitors

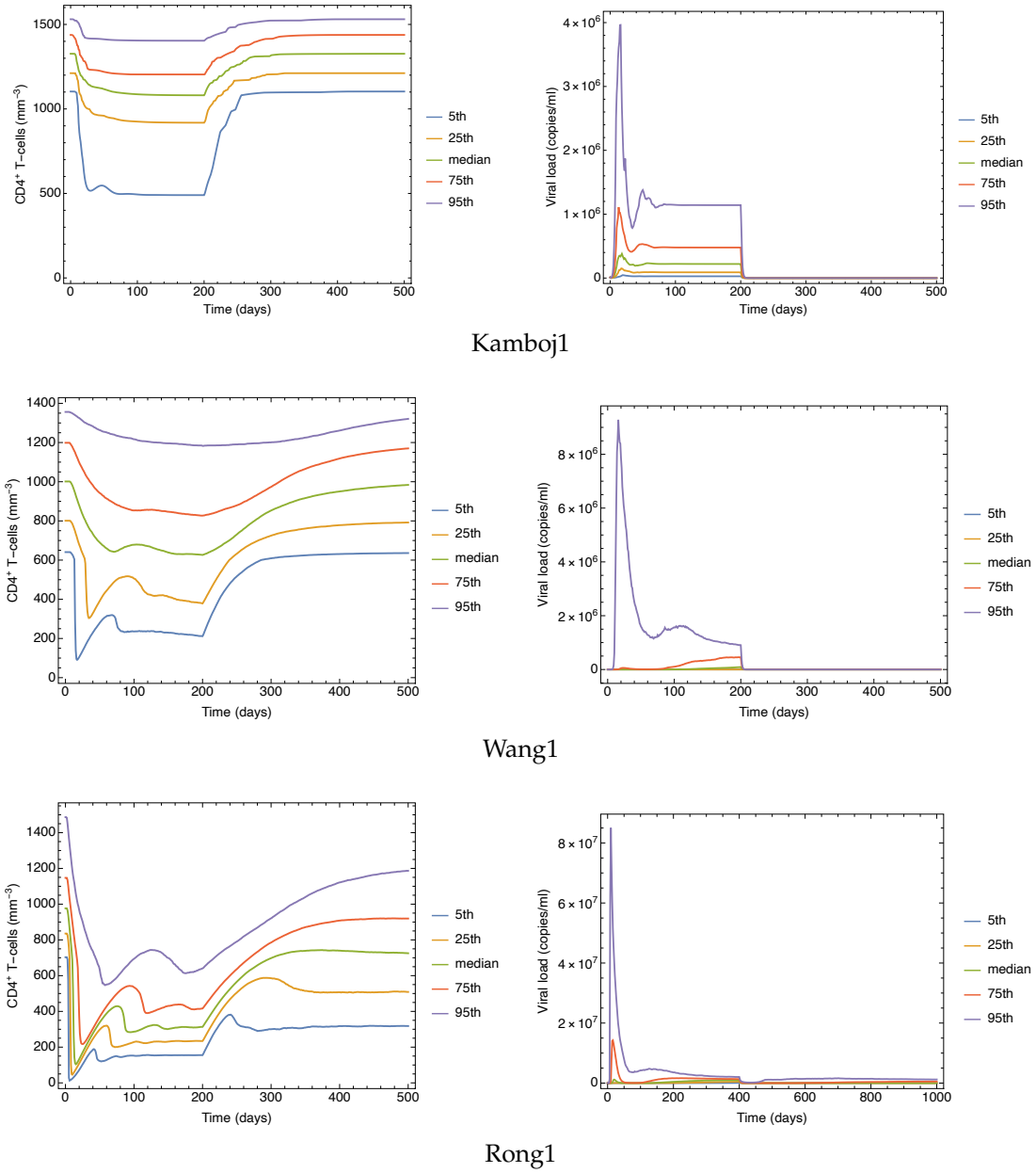

Figure A.1: *The effect of reverse transcriptase inhibitors on CD4⁺ T-cells and viral load.* Monte Carlo simulations were performed on three HIV models to determine the effect of RTI treatment on disease progression for Kamboj1, Rong1 and Wang1. The simulation starts at the uninfected equilibrium state. Virus is then introduced and allowed to approach a steady state with a simulation time of 200 days. RTI treatment is then switched on. Percentile results were generated from 10 000 parameters sets sampled from the distributions for both the HIV disease models and the PKPD models of the ARVs.

A.1.2 The effect of protease inhibitors

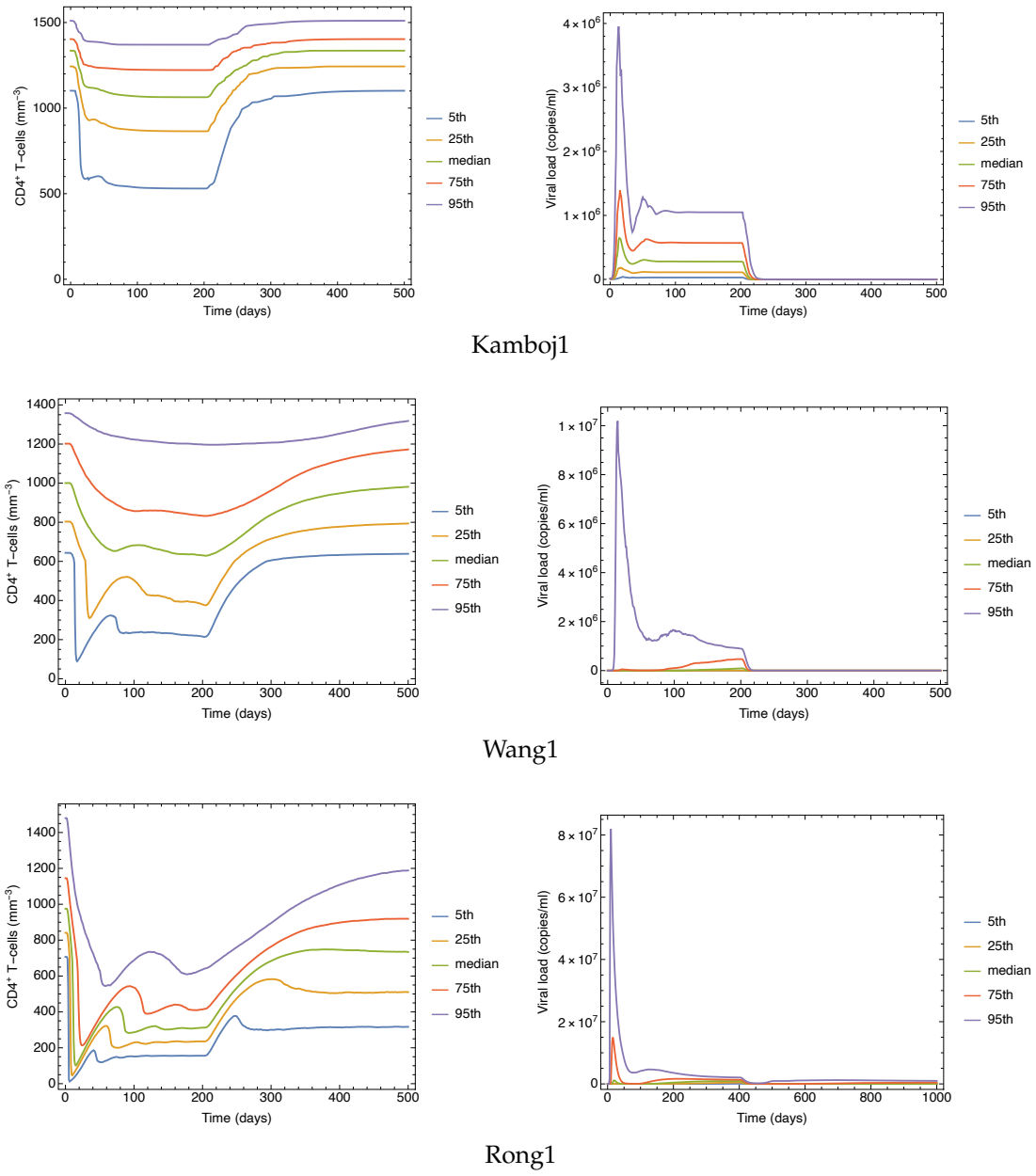

Figure A.2: *The effect of protease inhibitors on CD4⁺ T-cells and viral load.* Monte Carlo simulations were performed on three HIV models to determine the effect of PI treatment on disease progression for Kamboj1, Rong1 and Wang1. The simulation starts at the uninfected equilibrium state. Virus is then introduced and allowed to approach a steady state with a simulation time of 200 days. PI treatment is then switched on. Percentile results were generated from 10 000 parameters sets sampled from the distributions for both the HIV disease models and the PKPD models of the ARVs.

A.1.3 Treament initiation of RTI or PI respectively and comparison to clinical data for T-cells

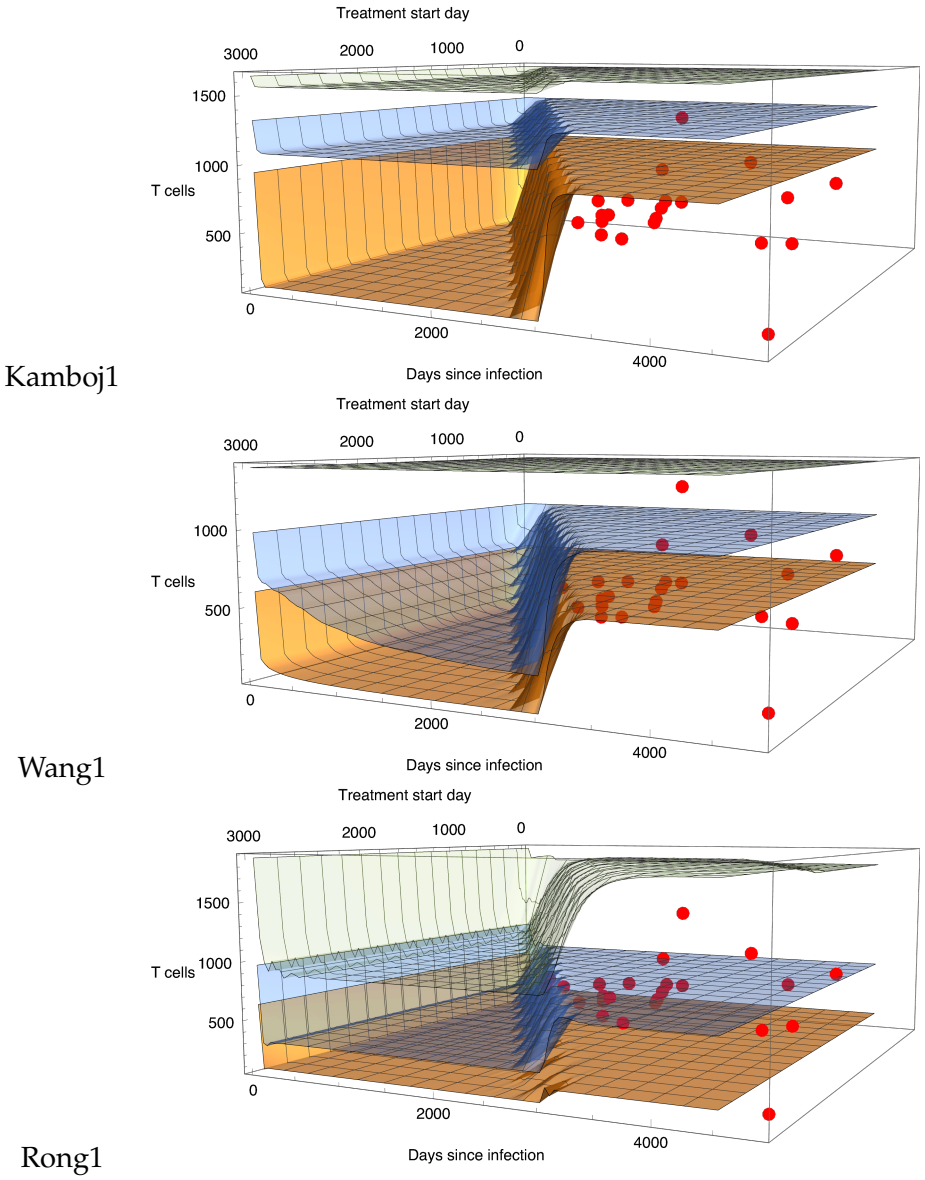

Figure A.3: *The effect of RTI treatment on CD4$^+$ T-cells with clinical data.* A Monte Carlo simulation was performed on the model to examine the effect of treatment start day on recovery. From 1000 simulations, the surfaces represent the following: orange=minimum; blue=median; green=maximum. The region between the orange and the green surface therefore represent the whole range of model predictions given the parameter distributions. The simulation starts at the uninfected equilibrium state. Virus is introduced with a treatment start day ranging from 0-3000 days after infection. Results were generated from 1000 parameters sets sampled from the distributions for both the HIV disease models and the PKPD models of the ARVs. The simulation results are plotted with patient data (red dots) from [86].

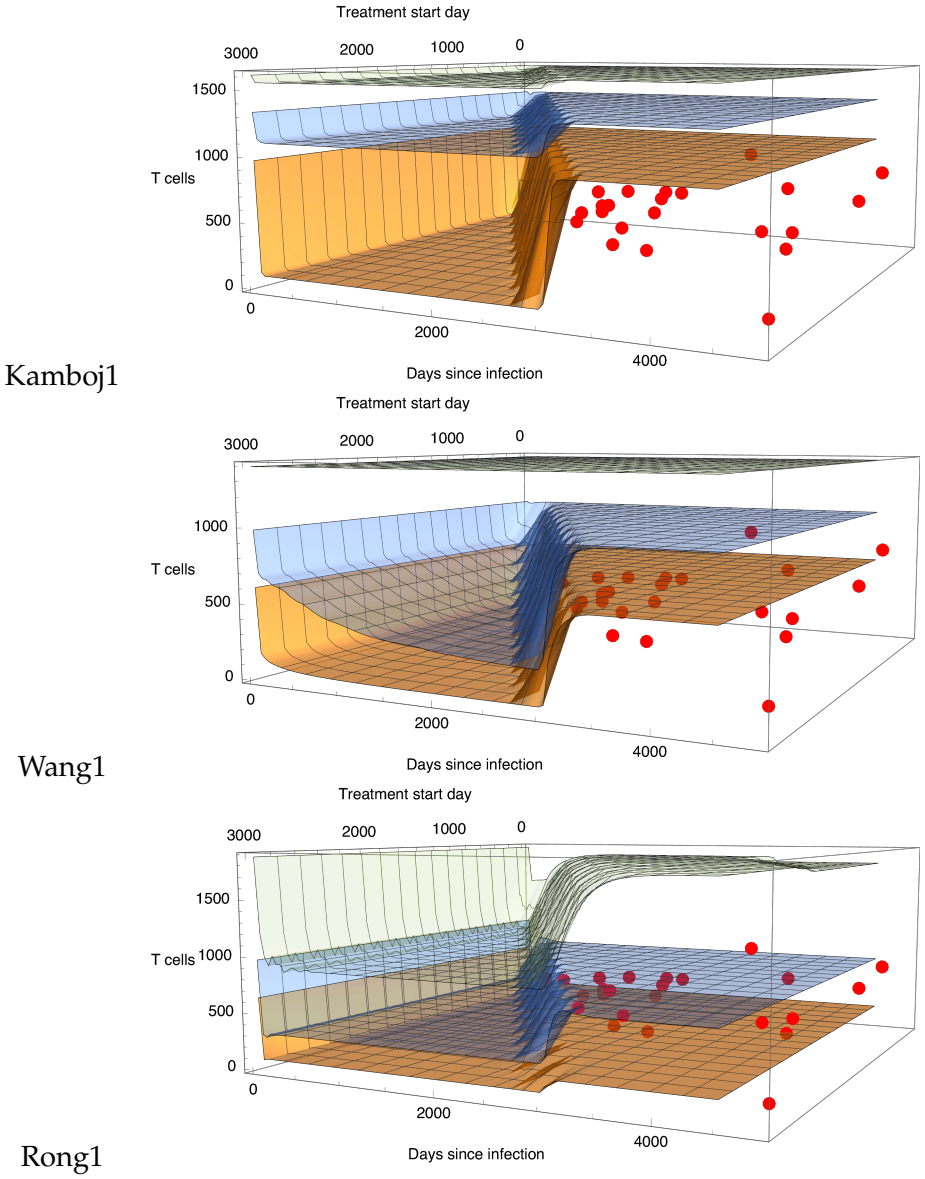

Figure A.4: *The effect of PI treatment on CD4$^+$ T-cells with clinical data.* A Monte Carlo simulation was performed on the model to examine the effect of treatment start day on recovery. From 1000 simulations, the surfaces represent the following: orange=minimum; blue=median; green=maximum. The region between the orange and the green surface therefore represent the whole range of model predictions given the parameter distributions. The simulation starts at the uninfected equilibrium state. Virus is introduced with a treatment start day ranging from 0-3000 days after infection. Results were generated from 1000 parameters sets sampled from the distributions for both the HIV disease models and the PKPD models of the ARVs. The simulation results are plotted with patient data (red dots) from [86].

A.1.4 Treament initiation of RTI or PI respectively and comparison to clinical data for viral load

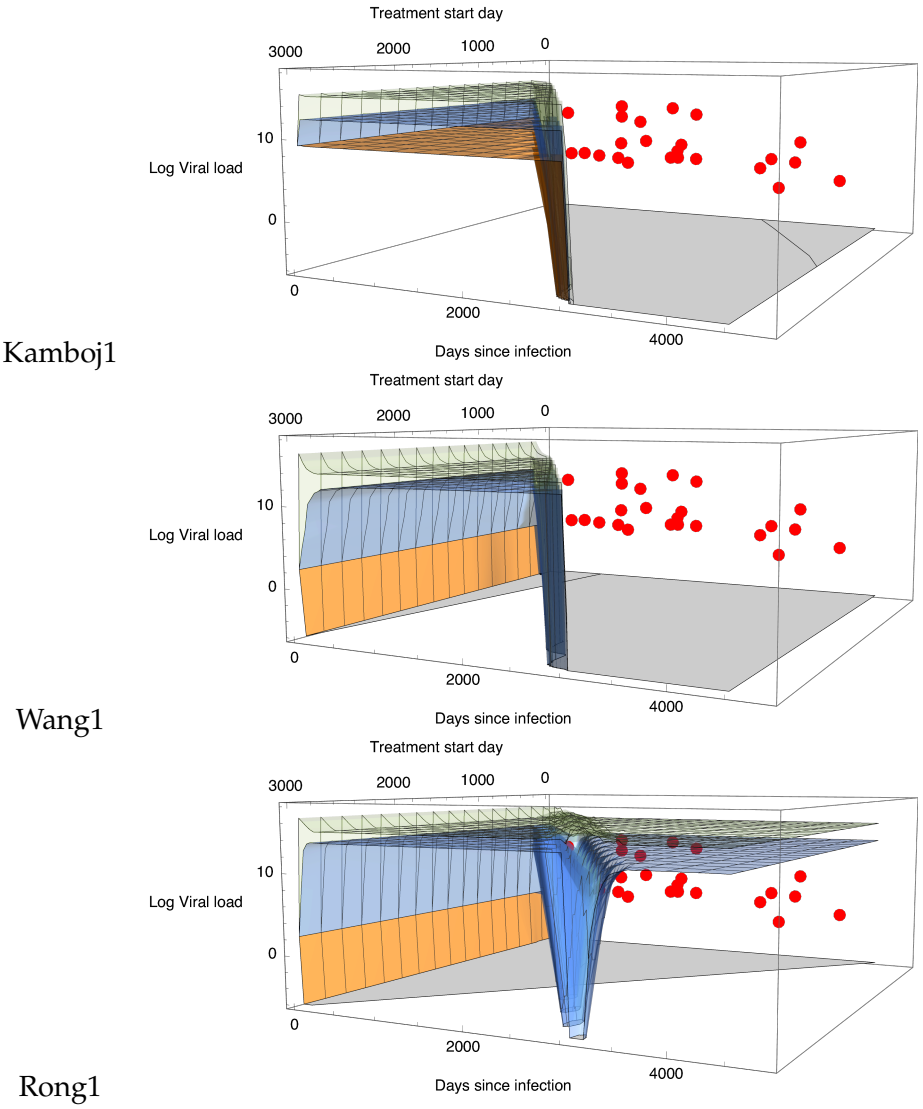

Figure A.5: *The effect of RTI treatment on viral load with clinical data.* A Monte Carlo simulation was performed on the model to examine the effect of treatment start day on recovery. From 1000 simulations, the surfaces represent the following: orange=minimum; blue=median; green=maximum. The region between the orange and the green surface therefore represent the whole range of model predictions given the parameter distributions. The simulation starts at the uninfected equilibrium state. Virus is introduced with a treatment start day ranging from 0-3000 days after infection. Results were generated from 1000 parameters sets sampled from the distributions for both the HIV disease models and the PKPD models of the ARVs. The simulation results are plotted with patient data (red dots) from [86].

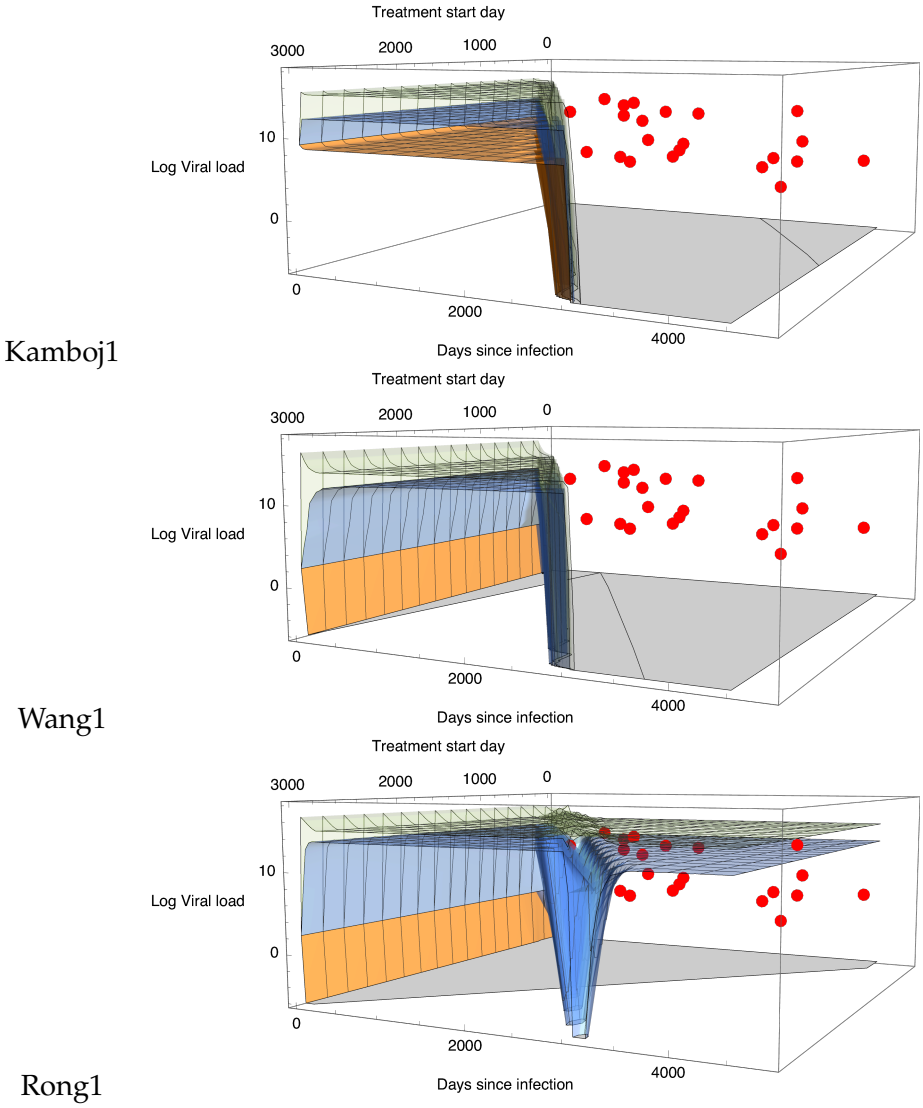

Figure A.6: *The effect of PI treatment on viral load with clinical data.* A Monte Carlo simulation was performed on the model to examine the effect of treatment start day on recovery. From 1000 simulations, the surfaces represent the following: orange=minimum; blue=median; green=maximum. The region between the orange and the green surface therefore represent the whole range of model predictions given the parameter distributions. The simulation starts at the uninfected equilibrium state. Virus is introduced with a treatment start day ranging from 0-3000 days after infection. Results were generated from 1000 parameters sets sampled from the distributions for both the HIV disease models and the PKPD models of the ARVs. The simulation results are plotted with patient data (red dots) from [86].

Bibliography

[1] Rong, L., Feng, Z., and Perelson, A. S. Emergence of hiv-1 drug resistance during antiretroviral treatment. *Bulletin of mathematical biology*, 69:2027–2060, 2007. ISSN 0092-8240. doi: 10.1007/s11538-007-9203-3.

[2] Kamboj, D. and Sharma, M. D. Multidrug therapy for HIV infection: Dynamics of immune system. *Acta Biotheoretica*, 67(2):129–147, 2018. doi: 10.1007/s10441-018-9340-0.

[3] Wang, X., Song, X., Tang, S., and Rong, L. Dynamics of an HIV model with multiple infection stages and treatment with different drug classes. *Bulletin of Mathematical Biology*, 78(2):322–349, 2016. doi: 10.1007/s11538-016-0145-5.

[4] Duwal, S., Schütte, C., and von Kleist, M. Pharmacokinetics and pharmacodynamics of the reverse transcriptase inhibitor tenofovir and prophylactic efficacy against HIV-1 infection. *PLoS ONE*, 7(7):e40382, 2012. doi: 10.1371/journal.pone.0040382.

[5] Duwal, S., Dickinson, L., Khoo, S., and von Kleist, M. Hybrid stochastic framework predicts efficacy of prophylaxis against HIV: An example with different dolutegravir prophylaxis schemes. *PLOS Computational Biology*, 14(6):e1006155, 2018. doi: 10.1371/journal.pcbi.1006155.

[6] Wang, K., D'Argenio, D. Z., Acosta, E. P., Sheth, A. N., Delille, C., Lennox, J. L., Kerstner-Wood, C., and Ofotokun, I. Integrated population pharmacokinetic/viral dynamic modelling of lopinavir/ritonavir in HIV-1 treatment-naïve patients. *Clinical Pharmacokinetics*, 53 (4):361–371, 2013. doi: 10.1007/s40262-013-0122-1.

[7] Valade, E., Tréluyer, J.-M., Illamola, S. M., Bouazza, N., Foissac, F., Mendes, M. D. S., Lui, G., Chenevier-Gobeaux, C., Suzan-Monti, M., Rouzioux, C., Assoumou, L., Viard, J.-P., Hirt, D., Urien, S., and Ghosn, J. Emtricitabine seminal plasma and blood plasma population pharmacokinetics in HIV-infected men in the EVARIST ANRS-EP 49 study. *Antimicrobial Agents and Chemotherapy*, 59(11):6800–6806, 2015. doi: 10.1128/aac.01517-15.

[8] Barre-Sinoussi, F., Chermann, J., Rey, F., Nugeyre, M., Chamaret, S., Gruest, J., Dauguet, C., Axler-Blin, C., Vezinet-Brun, F., Rouzioux, C., Rozenbaum, W., and Montagnier, L. Isolation of a t-lymphotropic retrovirus from a patient at risk for acquired immune deficiency syndrome (AIDS). *Science*, 220(4599):868–871, 1983. doi: 10.1126/science.6189183.

[9] Hill, A. L., Rosenbloom, D. I. S., Nowak, M. A., and Siliciano, R. F. Insight into treatment of HIV infection from viral dynamics models. *Immunological Reviews*, 285(1):9–25, 2018. doi: 10.1111/imr.12698.

[10] UNAIDS Data Report United Nations, 2020. URL https://www.unaids.org/sites/default/files/media_asset/2020_aids-data-book_en.pdf. Accessed 14 September 2021.

[11] Easterbrook, P. J., Doherty, M. C., Perriëns, J. H., Barcarolo, J. L., and Hirnschall, G. O. The role of mathematical modelling in the development of recommendations in the 2013 WHO consolidated antiretroviral therapy guidelines. *AIDS*, 28:S85–S92, 2014. doi: 10.1097/qad.0000000000000111.

[12] Weinstein, M. C., O'Brien, B., Hornberger, J., Jackson, J., Johannesson, M., McCabe, C., and Luce, B. R. Principles of good practice for decision analytic modeling in health-care evaluation: Report of the ISPOR task force on good research practices—modeling studies. *Value in Health*, 6(1):9–17, 2003. doi: 10.1046/j.1524-4733.2003.00234.x.

[13] Mould, D. R. and Upton, R. N. Basic concepts in population modeling, simulation, and model-based drug development. *CPT: Pharmacometrics & Systems Pharmacology*, 1(9):e6, 2012. doi: 10.1038/psp.2012.4.

[14] Page, M. and Taylor, S. Antiretroviral pharmacology. *Medicine*, 46(5):287–292, 2018. doi: 10.1016/j.mpmed.2018.02.006.

[15] WolframResearchInc. Mathematica, Version 12.0.0, 2021. URL https://www.wolfram.com/mathematica. Champaign, IL, 2021.

[16] Zhang, L., Sinha, V., Forgue, S. T., Callies, S., Ni, L., Peck, R., and Allerheiligen, S. R. B. Model-based drug development: The road to quantitative pharmacology. *Journal of Pharmacokinetics and Pharmacodynamics*, 33(3):369–393, 2006. doi: 10.1007/s10928-006-9010-8.

[17] Doekes, H. M., Fraser, C., and Lythgoe, K. A. Effect of the latent reservoir on the evolution of HIV at the within- and between-host levels. *PLOS Computational Biology*, 13(1):e1005228, 2017. doi: 10.1371/journal.pcbi.1005228.

[18] Abbas, A. K., Lichtman, A. H. H., and Pillai, S. *Basic Immunology E-Book: Functions and Disorders of the Immune System*. Saunders, 2012. ISBN 978-1-4557-0707-2.

[19] Nyamweya, S., Hegedus, A., Jaye, A., Rowland-Jones, S., Flanagan, K. L., and Macallan, D. C. Comparing HIV-1 and HIV-2 infection: Lessons for viral immunopathogenesis. *Reviews in Medical Virology*, 23(4):221–240, 2013. doi: 10.1002/rmv.1739.

[20] Faria, N. R., Rambaut, A., Suchard, M. A., Baele, G., Bedford, T., Ward, M. J., Tatem, A. J., Sousa, J. D., Arinaminpathy, N., Pépin, J., Posada, D., Peeters, M., Pybus, O. G., and Lemey, P. The early spread and epidemic ignition of HIV-1 in human populations. *Science*, 346(6205): 56–61, 2014. doi: 10.1126/science.1256739.

[21] Wikramaratna, P. S., Lourenço, J., Klenerman, P., Pybus, O. G., and Gupta, S. Effects of neutralizing antibodies on escape from CD8 t-cell responses in HIV-1 infection. *Philosophical Transactions of the Royal Society B: Biological Sciences*, 370(1675):20140290, 2015. doi: 10.1098/rstb.2014.0290.

[22] Jiang, G., Rocha, C. S., Hirao, L. A., Mendes, E. A., Tang, Y., Thompson, G. R., Wong, J. K., and Dandekar, S. HIV exploits antiviral host innate GCN2-ATF4 signaling for establishing viral replication early in infection. *mBio*, 8(3), 2017. doi: 10.1128/mbio.01518-16.

[23] Epstein, F. H., Pantaleo, G., Graziosi, C., and Fauci, A. S. The immunopathogenesis of human immunodeficiency virus infection. *New England Journal of Medicine*, 328(5):327–335, 1993. doi: 10.1056/nejm199302043280508.

[24] HIV Drug Resistance Report. World Health Organisation, 2019. URL https://apps.who.int/iris/bitstream/handle/10665/325891/WHO-CDS-HIV-19.21-eng.pdf. Accessed 14 September 2021.

[25] Kulkarni, S., Jadhav, S., Khopkar, P., Sane, S., Londhe, R., Chimanpure, V., Dhilpe, V., Ghate, M., Yelagate, R., Panchal, N., Rahane, G., Kadam, D., Gaikwad, N., Rewari, B., and Gangakhedkar, R. GeneXpert HIV-1 quant assay, a new tool for scale up of viral load monitoring in the success of ART programme in india. *BMC Infectious Diseases*, 17(1), 2017. doi: 10.1186/s12879-017-2604-5.

[26] Wilen, C. B., Tilton, J. C., and Doms, R. W. HIV: Cell binding and entry. *Cold Spring Harbor Perspectives in Medicine*, 2(8):a006866–a006866, 2012. doi: 10.1101/cshperspect.a006866.

[27] Rambaut, A., Posada, D., Crandall, K. A., and Holmes, E. C. The causes and consequences of HIV evolution. *Nature Reviews Genetics*, 5(1):52–61, 2004. doi: 10.1038/nrg1246.

[28] Varbanov, M., Espert, L., and Biard-Piechaczyk, M. Mechanisms of cd4 t-cell depletion triggered by hiv-1 viral proteins. *AIDS reviews*, 8:221–36, 2006.

[29] Pauza, C. D., Galindo, J. E., and Richman, D. D. Reinfection results in accumulation of unintegrated viral dna in cytopathic and persistent human immunodeficiency virus type 1 infection of cem cells. *The Journal of experimental medicine*, 172:1035–42, 1990.

[30] Josefsson, L., von Stockenstrom, S., Faria, N. R., Sinclair, E., Bacchetti, P., Killian, M., Epling, L., Tan, A., Ho, T., Lemey, P., Shao, W., Hunt, P. W., Somsouk, M., Wylie, W., Douek, D. C.,

Loeb, L., Custer, J., Hoh, R., Poole, L., Deeks, S. G., Hecht, F., and Palmer, S. The HIV-1 reservoir in eight patients on long-term suppressive antiretroviral therapy is stable with few genetic changes over time. *Proceedings of the National Academy of Sciences*, 110(51):E4987–E4996, 2013. doi: 10.1073/pnas.1308313110.

[31] Pantazis, N., Papastamopoulos, V., Paparizos, V., Metallidis, S., Adamis, G., Antoniadou, A., Psichogiou, M., Chini, M., Sambatakou, H., Sipsas, N. V., Gogos, C., Chrysos, G., Panagopoulos, P., Katsarou, O., Gikas, A., and Touloumi, G. Long-term evolution of CD4 cell count in patients under combined antiretroviral therapy. *AIDS*, 33(10):1645–1655, 2019. doi: 10.1097/qad.0000000000002248.

[32] Pinkevych, M., Fennessey, C. M., Cromer, D., Tolstrup, M., Søgaard, O. S., Rasmussen, T. A., Keele, B. F., and Davenport, M. P. Estimating initial viral levels during simian immunodeficiency virus/human immunodeficiency virus reactivation from latency. *Journal of Virology*, 92(2), 2017. doi: 10.1128/jvi.01667-17.

[33] Kearney, M. F., Wiegand, A., Shao, W., Coffin, J. M., Mellors, J. W., Lederman, M., Gandhi, R. T., Keele, B. F., and Li, J. Z. Origin of rebound plasma HIV includes cells with identical proviruses that are transcriptionally active before stopping of antiretroviral therapy. *Journal of Virology*, 90(3):1369–1376, 2015. doi: 10.1128/jvi.02139-15.

[34] Joos, B., Fischer, M., Kuster, H., Pillai, S. K., Wong, J. K., Boni, J., Hirschel, B., Weber, R., Trkola, A., and and, H. F. G. HIV rebounds from latently infected cells, rather than from continuing low-level replication. *Proceedings of the National Academy of Sciences*, 105(43):16725–16730, 2008. doi: 10.1073/pnas.0804192105.

[35] Rothenberger, M. K., Keele, B. F., Wietgrefe, S. W., Fletcher, C. V., Beilman, G. J., Chipman, J. G., Khoruts, A., Estes, J. D., Anderson, J., Callisto, S. P., Schmidt, T. E., Thorkelson, A., Reilly, C., Perkey, K., Reimann, T. G., Utay, N. S., Makamdop, K. N., Stevenson, M., Douek, D. C., Haase, A. T., and Schacker, T. W. Large number of rebounding/founder HIV variants emerge from multifocal infection in lymphatic tissues after treatment interruption. *Proceedings of the National Academy of Sciences*, 112(10):E1126–E1134, 2015. doi: 10.1073/pnas.1414926112.

[36] Bednar, M. M., Hauser, B. M., Zhou, S., Jacobson, J. M., Eron, J. J., Frank, I., and Swanstrom, R. Diversity and tropism of HIV-1 rebound virus populations in plasma level after treatment discontinuation. *Journal of Infectious Diseases*, 214(3):403–407, 2016. doi: 10.1093/infdis/jiw172.

[37] Palmer, S., Maldarelli, F., Wiegand, A., Bernstein, B., Hanna, G. J., Brun, S. C., Kempf, D. J., Mellors, J. W., Coffin, J. M., and King, M. S. Low-level viremia persists for at least 7 years in

patients on suppressive antiretroviral therapy. *Proceedings of the National Academy of Sciences*, 105(10):3879–3884, 2008. doi: 10.1073/pnas.0800050105.

[38] Reeves, D. B., Duke, E. R., Wagner, T. A., Palmer, S. E., Spivak, A. M., and Schiffer, J. T. A majority of HIV persistence during antiretroviral therapy is due to infected cell proliferation. *Nature Communications*, 9(1), 2018. doi: 10.1038/s41467-018-06843-5.

[39] Arts, E. J. and Hazuda, D. J. HIV-1 antiretroviral drug therapy. *Cold Spring Harbor Perspectives in Medicine*, 2(4):a007161–a007161, 2012. doi: 10.1101/cshperspect.a007161.

[40] Cahn, P., Fink, V., and Patterson, P. Fostemsavir. *Current Opinion in HIV and AIDS*, 13(4): 341–345, 2018. doi: 10.1097/coh.0000000000000469.

[41] ART Clinical Guidelines for the Management of HIV in Adults, Pregnancy, Adolescents, Children, Infants and Neonates. Republic of South Africa National Department of Health., 2019. URL http://www.health.gov.za/wp-content/uploads/2020/11/2019-art-guideline.pdf. Accessed 14 September 2021.

[42] Gibellini, D., Vitone, F., Gori, E., Placa, M. L., and Re, M. C. Quantitative detection of human immunodeficiency virus type 1 (HIV-1) viral load by SYBR green real-time RT-PCR technique in HIV-1 seropositive patients. *Journal of Virological Methods*, 115(2):183–189, 2004. doi: 10.1016/j.jviromet.2003.09.030.

[43] Haering, M., Hördt, A., Meyer-Hermann, M., and Hernandez-Vargas, E. A. Computational study to determine when to initiate and alternate therapy in HIV infection. *BioMed Research International*, 2014:1–9, 2014. doi: 10.1155/2014/472869.

[44] Tilton, J. C. and Doms, R. W. Entry inhibitors in the treatment of hiv-1 infection. *Antiviral Research*, 85(1):91 – 100, 2010. ISSN 0166-3542. doi: https://doi.org/10.1016/j.antiviral.2009.07.022.

[45] Esté, J. A. and Telenti, A. Hiv entry inhibitors. *The Lancet*, 370(9581):81 – 88, 2007. ISSN 0140-6736. doi: https://doi.org/10.1016/S0140-6736(07)61052-6.

[46] Hu, W.-S. and Hughes, S. H. Hiv-1 reverse transcription. *Cold Spring Harbor perspectives in medicine*, 2, 2012. ISSN 2157-1422. doi: 10.1101/cshperspect.a006882.

[47] Engelman, A. and Cherepanov, P. Retroviral integrase structure and DNA recombination mechanism. *Microbiology Spectrum*, 2(6), 2014. doi: 10.1128/microbiolspec.mdna3-0024-2014.

[48] Adamson, C. S. Protease-mediated maturation of HIV: Inhibitors of protease and the maturation process. *Molecular Biology International*, 2012:1–13, 2012. doi: 10.1155/2012/604261.

[49] Anderson, P. L., Kiser, J. J., Gardner, E. M., Rower, J. E., Meditz, A., and Grant, R. M. Pharmacological considerations for tenofovir and emtricitabine to prevent HIV infection. *Journal of Antimicrobial Chemotherapy*, 66(2):240–250, 2010. doi: 10.1093/jac/dkq447.

[50] Frampton, J. E. and Perry, C. M. Emtricitabine. *Drugs*, 65(10):1427–1448, 2005. doi: 10.2165/00003495-200565100-00008.

[51] Yadav, G., Kumar, P., Kumar, Y., and Singh, P. K. Dolutegravir, second generation integrase inhibitor: A new hope for HIV patient. *European Journal of Molecular and Clinical Medicine*, 5 (1):20–29, 2018. doi: 10.5334/ejmcm.252.

[52] Cvetkovic, R. S. and Goa, K. L. Lopinavir/ritonavir. *Drugs*, 63(8):769–802, 2003. doi: 10.2165/00003495-200363080-00004.

[53] Fan, J. and de Lannoy, I. A. Pharmacokinetics. *Biochemical Pharmacology*, 87(1):93–120, 2014. doi: 10.1016/j.bcp.2013.09.007.

[54] Hodgson, J. ADMET—turning chemicals into drugs. *Nature Biotechnology*, 19(8):722–726, 2001. doi: 10.1038/90761.

[55] Ciupe, S. M. and Heffernan, J. M. In-host modeling. *Infectious Disease Modelling*, 2(2):188–202, 2017. doi: 10.1016/j.idm.2017.04.002.

[56] Wang, S., Hottz, P., Schechter, M., and Rong, L. Modeling the slow cd4 t cell decline in hiv-infected individuals. *PLOS Computational Biology*, 11(12):e1004665, 2015. doi: 10.1371/journal.pcbi.1004665.

[57] Qesmi, R., ElSaadany, S., Heffernan, J. M., and Wu, J. A hepatitis b and c virus model with age since infection that exhibits backward bifurcation. *SIAM Journal on Applied Mathematics*, 71(4):1509–1530, 2011. doi: 10.1137/10079690x.

[58] Rong, L., Guedj, J., Dahari, H., Coffield, D. J., Levi, M., Smith, P., and Perelson, A. S. Analysis of hepatitis c virus decline during treatment with the protease inhibitor danoprevir using a multiscale model. *PLoS Computational Biology*, 9(3):e1002959, 2013. doi: 10.1371/journal.pcbi.1002959.

[59] Du, Y., Wu, J., and Heffernan, J. M. A simple in-host model for mycobacterium tuberculosis that captures all infection outcomes. *Mathematical Population Studies*, 24(1):37–63, 2017. doi: 10.1080/08898480.2015.1054220.

[60] Hadjichrysanthou, C., Cauët, E., Lawrence, E., Vegvari, C., de Wolf, F., and Anderson, R. M. Understanding the within-host dynamics of influenza a virus: from theory to clinical implications. *Journal of The Royal Society Interface*, 13(119):20160289, 2016. doi: 10.1098/rsif.2016.0289.

[61] Nikin-Beers, R. and Ciupe, S. M. The role of antibody in enhancing dengue virus infection. *Mathematical Biosciences*, 263:83–92, 2015. doi: 10.1016/j.mbs.2015.02.004.

[62] Penkler, G., du Toit, F., Adams, W., Rautenbach, M., Palm, D. C., van Niekerk, D. D., and Snoep, J. L. Construction and validation of a detailed kinetic model of glycolysis inPlasmodium falciparum. *FEBS Journal*, 282(8):1481–1511, 2015. doi: 10.1111/febs.13237.

[63] Dietz, K. The estimation of the basic reproduction number for infectious diseases. *Statistical Methods in Medical Research*, 2(1):23–41, 1993. doi: 10.1177/096228029300200103.

[64] Ribeiro, R. M., Qin, L., Chavez, L. L., Li, D., Self, S. G., and Perelson, A. S. Estimation of the initial viral growth rate and basic reproductive number during acute HIV-1 infection. *Journal of Virology*, 84(12):6096–6102, 2010. doi: 10.1128/jvi.00127-10.

[65] Lloyd, A. L. The dependence of viral parameter estimates on the assumed viral life cycle: limitations of studies of viral load data. *Proceedings of the Royal Society of London. Series B: Biological Sciences*, 268(1469):847–854, 2001. doi: 10.1098/rspb.2000.1572.

[66] Perelson, A. S., Neumann, A. U., Markowitz, M., Leonard, J. M., and Ho, D. D. HIV-1 dynamics in vivo: Virion clearance rate, infected cell life-span, and viral generation time. *Science*, 271(5255):1582–1586, 1996. doi: 10.1126/science.271.5255.1582.

[67] von Kleist, M., Menz, S., Stocker, H., Arasteh, K., Schütte, C., and Huisinga, W. HIV quasispecies dynamics during pro-active treatment switching: Impact on multi-drug resistance and resistance archiving in latent reservoirs. *PLoS ONE*, 6(3):e18204, 2011. doi: 10.1371/journal.pone.0018204.

[68] Sedaghat, A. R., Dinoso, J. B., Shen, L., Wilke, C. O., and Siliciano, R. F. Decay dynamics of HIV-1 depend on the inhibited stages of the viral life cycle. *Proceedings of the National Academy of Sciences*, 105(12):4832–4837, 2008. doi: 10.1073/pnas.0711372105.

[69] Perelson, A. S., Essunger, P., Cao, Y., Vesanen, M., Hurley, A., Saksela, K., Markowitz, M., and Ho, D. D. Decay characteristics of HIV-1-infected compartments during combination therapy. *Nature*, 387(6629):188–191, 1997. doi: 10.1038/387188a0.

[70] Abdel-Rahman, S. M. and Kauffman, R. E. The integration of pharmacokinetics and pharmacodynamics: Understanding dose-response. *Annual Review of Pharmacology and Toxicology*, 44 (1):111–136, 2004. doi: 10.1146/annurev.pharmtox.44.101802.121347.

[71] Csajka, C. and Verotta, D. Pharmacokinetic–pharmacodynamic modelling: History and perspectives. *Journal of Pharmacokinetics and Pharmacodynamics*, 33(3):227–279, 2006. doi: 10.1007/s10928-005-9002-0.

[72] Rosenbaum, S. E. *Basic Pharmacokinetics and Pharmacodynamics: An Integrated Textbook and Computer Simulations*. WILEY, 2011. ISBN 0470569069.

[73] Jusko, W. J. Moving from basic toward systems pharmacodynamic models. *Journal of Pharmaceutical Sciences*, 102(9):2930–2940, 2013. doi: 10.1002/jps.23590.

[74] Sandler, S. I. Chemical and engineering thermodynamics. 1989. *Dunn IJ, et., al.(2003). Appendix: Using the Berkeley Madonna Language, in Biological Reaction Engineering: Dynamic Modelling Fundamentals with Simulation Examples*, 2003.

[75] Holford, N. H. and Sheiner, L. B. Understanding the dose-effect relationship. *Clinical Pharmacokinetics*, 6(6):429–453, 1981. doi: 10.2165/00003088-198106060-00002.

[76] Bliss, C. I. The Toxicity of Poisons Applied Jointly. *Annals of Applied Biology*, 26(3):585–615, 1939. doi: 10.1111/j.1744-7348.1939.tb06990.x.

[77] Neubig, R. R., Spedding, M., Kenakin, T., and Christopoulos, A. International union of pharmacology committee on receptor nomenclature and drug classification. XXXVIII. update on terms and symbols in quantitative pharmacology. *Pharmacological Reviews*, 55(4):597–606, 2003. doi: 10.1124/pr.55.4.4.

[78] Jacqmin, P., McFadyen, L., and Wade, J. R. Basic PK/PD principles of drug effects in circular/proliferative systems for disease modelling. *Journal of Pharmacokinetics and Pharmacodynamics*, 37(2):157–177, 2010. doi: 10.1007/s10928-010-9151-7.

[79] Xiao, Y., Miao, H., Tang, S., and Wu, H. Modeling antiretroviral drug responses for HIV-1 infected patients using differential equation models. *Advanced Drug Delivery Reviews*, 65(7): 940–953, 2013. doi: 10.1016/j.addr.2013.04.005.

[80] Wu, H., Huang, Y., Acosta, E. P., Rosenkranz, S. L., Kuritzkes, D. R., Eron, J. J., Perelson, A. S., and Gerber, J. G. Modeling long-term HIV dynamics and antiretroviral response. *JAIDS Journal of Acquired Immune Deficiency Syndromes*, 39(3):272–283, 2005. doi: 10.1097/01.qai.0000165907.04710.da.

[81] Rosario, M., Jacqmin, P., Dorr, P., Vanderryst, E., and Hitchcock, C. A pharmacokinetic-pharmacodynamic disease model to predict in vivo antiviral activity of maraviroc. *Clinical Pharmacology & Therapeutics*, 78(5):508–519, 2005. doi: 10.1016/j.clpt.2005.07.010.

[82] Rosario, M. C., Jacqmin, P., Dorr, P., James, I., Jenkins, T. M., Abel, S., and van der Ryst, E. Population pharmacokinetic/ pharmacodynamic analysis of CCR5 receptor occupancy by maraviroc in healthy subjects and HIV-positive patients. *British Journal of Clinical Pharmacology*, 65(s1):86–94, 2008. doi: 10.1111/j.1365-2125.2008.03140.x.

[83] Perelson, A. S., Kirschner, D. E., and Boer, R. D. Dynamics of HIV infection of CD4 t cells. *Mathematical Biosciences*, 114(1):81–125, 1993. doi: 10.1016/0025-5564(93)90043-a.

[84] Teer, E., Joseph, D. E., Driescher, N., Nell, T. A., Dominick, L., Midgley, N., Deshpande, G., Page, M. J., Pretorius, E., Woudberg, N. J., Lecour, S., Glashoff, R. H., and Essop, M. F. HIV and cardiovascular diseases risk: exploring the interplay between t-cell activation, coagulation, monocyte subsets, and lipid subclass alterations. *American Journal of Physiology-Heart and Circulatory Physiology*, 316(5):H1146–H1157, 2019. doi: 10.1152/ajpheart.00797.2018.

[85] Phillips, A. N. HIV viral load response to antiretroviral therapy according to the baseline CD4 cell count and viral load. *JAMA*, 286(20):2560, 2001. doi: 10.1001/jama.286.20.2560.

[86] Teer, E. A. *Immune Activation in HIV-Positive Patients on Combined Antiretroviral Treatment (cART) As a High Risk Group for the Development of Cardiovascular Diseases*. PhD thesis, University of Stellenbosch, 2016.

[87] Chesney, M. Adherence to HAART regimens. *AIDS Patient Care and STDs*, 17(4):169–177, 2003. doi: 10.1089/108729103321619773.